International Journal of Modern Physics A

Review of the Properties of the W Boson at LEP, and the Precision Determination of its Mass

Raimund Ströhmer

Lehrstuhl Schaile, Ludwig-Maximilans Universität München, Am Coulombwall 1, D-85748 Garching, Germany.

Received (Day Month Year)
Revised (Day Month Year)

We review the precision measurement of the mass and couplings of the W Boson at LEP. The total and differential W^+W^- cross section is used to extract the WWZ and WWγ couplings. We discuss the techniques used by the four LEP experiments to determine the W mass in different decay channels, and present the details of methods used to evaluate the sources of systematic uncertainty.

1. Introduction

Our current understanding of the fundamental forces is contained in the description of the gravitational, the strong, the weak and the electromagnetic interactions among elementary particles. In the 1960s, Glashow, Salam and Weinberg unified the electromagnetic and weak interaction into the electroweak theory,[1] which, together with QCD (the theory of the strong interaction), forms the Standard Model of particle physics. The electroweak interaction among particles takes place through the exchange of four bosons, namely, the massless photon, and the massive Z^0, W^+ and W^- bosons. In 1983, the UA1 and UA2 experiments at the CERN proton-antiproton collider ($Sp\bar{p}S$) were first to directly observe the Z^0 and W bosons.[2]

The electron-positron collider LEP at CERN provided the possibility of precise studies of the properties of the Z^0 and W. Unlike proton-proton or proton-antiproton colliders, where quarks or gluons carry an a priori unknown fraction of the hadron momentum, the well defined initial state in electron-positron collisions is well suited for such precision measurements In its first phase (LEP-I), LEP operated at center-of-mass energies near the Z^0 resonance of about 91 GeV. In the second phase (LEP-II), the center-of-mass energy was increased above the threshold of twice the W mass (M_W), which made it possible to produce pairs of W bosons in e^+e^- collisions, and thus offered the opportunity for a precision determination of the W mass, its couplings, and decay branching ratios. The precision measurements of the properties of the Z^0 and W boson provided stringent tests of quantum corrections to the Standard Model.

In this section, we give a general overview of the LEP collider and its four major experiments. We discuss the pair production of W bosons and the event topologies arising from different decay modes of the W. Event selection, the total cross sections, and branching fractions will be presented in Section 2. The extraction of triple and quartic gauge couplings from the total and differential cross sections will be described in Section 3. In Section 4, we describe event reconstruction and the event-by-event estimation of the mass of the W and its uncertainty. Section 5 discusses different methods used to determine the Standard-Model parameter M_W from these estimates. Possible biases in determining the mass, its statistic stability, and the estimate in its uncertainty are examined using Monte Carlo ensemble tests. Section 6 describes how the systematic uncertainties of the measurements are estimated and how the measurements can be optimized in order to reduce the sum of the statistical and systematic error. Section 7 will present the determination of the W mass for events where both W bosons decay leptonically. Section 8 will summarize measurements of the mass of the W boson mass and its width and their implications for the Standard Model.

1.1. *Motivation*

In the electroweak Standard Model, the properties of the Z^0 and W boson depend only on a few fundamental parameters. A comparison of the directly measured

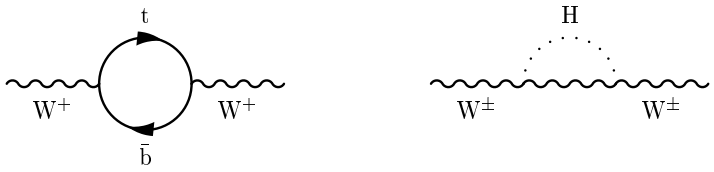

Fig. 1. Feynman diagram for 1-loop corrections to the W propagator.

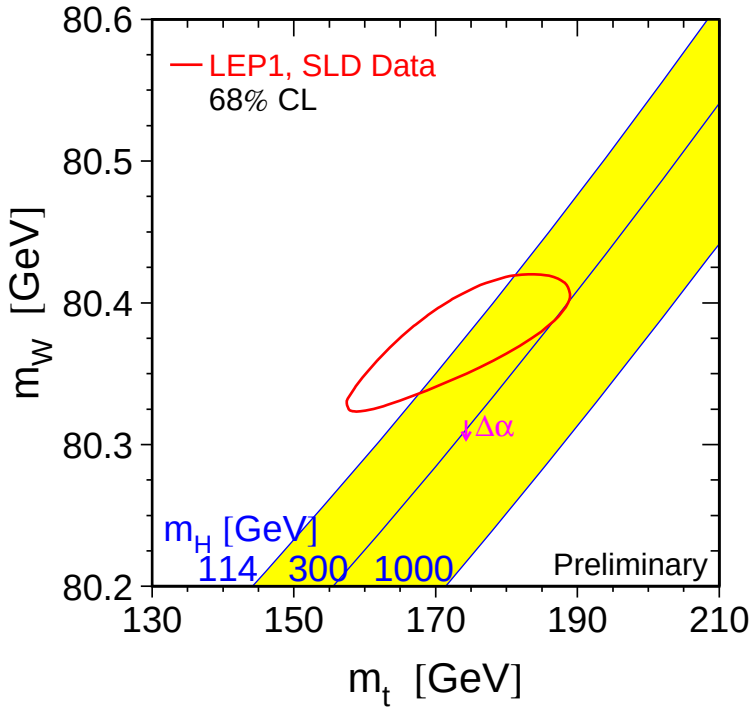

Fig. 2. Result of a fit of the electroweak data to the Standard Model, and the expected correlation between the W-boson mass and the top mass[4].

W mass with predictions based on precision measurements of properties of the Z^0 boson provides therefore an important test of the Standard Model. In the context

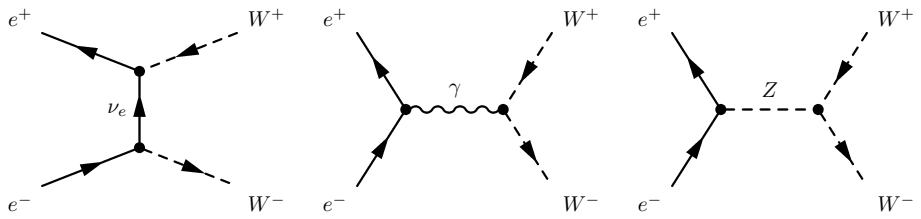

Fig. 3. Feynman diagrams for W pair production.

of LEP-I analyses, M_{W} can be determined from the relation:[3]

$$G_\mu = \frac{\alpha\pi}{\sqrt{2}M_{\mathrm{W}}^2(1 - M_{\mathrm{W}}^2/M_{\mathrm{Z}}^2)} \frac{1}{1-\Delta r}.$$

At lowest order ("tree" level), M_{W} depends only on the Fermi constant G_μ, which is known accurately from muon decay, the fine structure constant α, and the mass of the Z^0 boson (M_{Z}^0). In the above equation, loop corrections are parametrized by Δr, and lead to a quadratic dependence of M_{W}^2 on the top mass, and a logarithmic dependence on the Higgs mass. At lowest order, $\Delta r = 0$. As example, Fig. 1 shows 1-loop contributions to the W propagator, including the top quark and Higgs boson. A fit of the precision electroweak observables to the Standard Model (excluding the direct measurements of M_{top}) yields:[4]

$$M_{\mathrm{W}} = 80.373 \pm 0.033 \text{ GeV}.$$

Figure 2 shows the prediction for the W boson and top quark mass using a fit to all data, excluding the direct measurements of $\mathrm{M_W}$ and M_{top}. The figure also displays the prediction of the Standard Model for $\mathrm{M_W}$ as function of M_{top} for three values of Higgs mass. The little arrow indicates the uncertainty due to the running of α at the scale of M_{Z}^0. The comparison of these predictions with direct measurements of M_{top} and $\mathrm{M_W}$ at the LEP and TeVatron colliders are important tests of the electroweak sector of the Standard Model, which to be fully exploited require reduction of the error on the observed W mass.

Beyond just the mass, the measurement of the W pair and other four-fermion cross sections, and their angular distributions can also be used to study triple gauge-boson couplings. Any deviations from predictions of the Standard Model can then be interpreted as evidence for physics beyond the Standard Model. This issue is addressed in the next section.

1.2. W *Pair Production and Decay*

W-boson pairs can be produced in e^+e^- annihilations above the center-of-mass energy threshold of $\sqrt{s} = 2 \cdot \mathrm{M_W}$. Figure 3 shows the tree-level Feynman diagrams contributing to W pair productions. These diagrams are called CC03 diagrams. (CC refers to charged current, because W bosons are involved, and 03 to the number

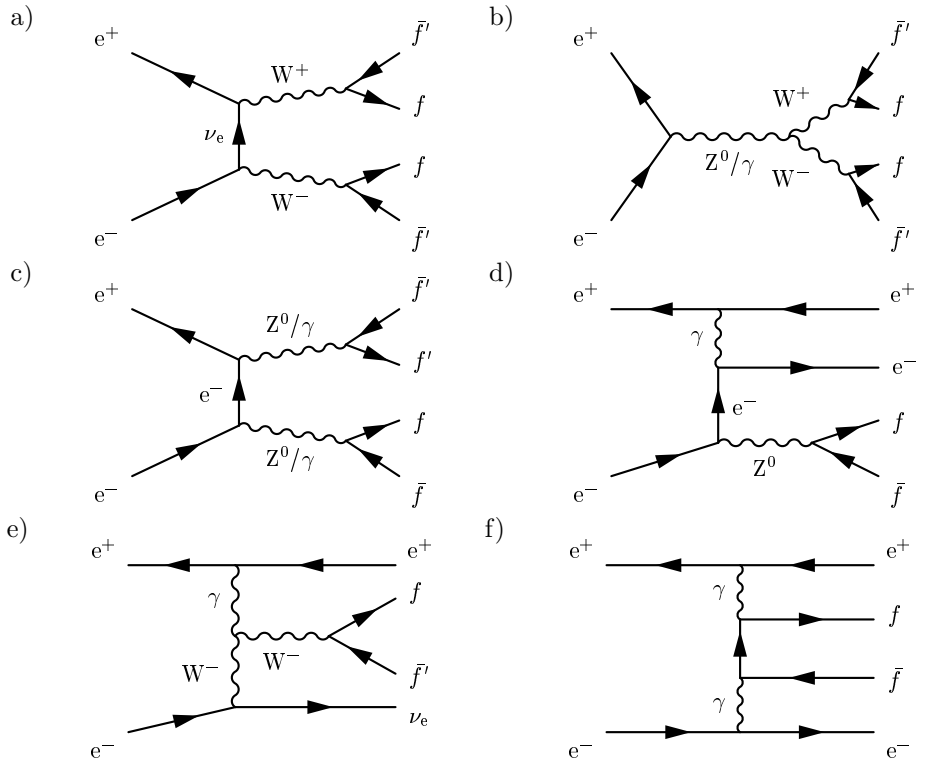

Fig. 4. Feynman diagrams leading to four-fermion final states. a) and b) display the CC03 diagrams, c) the NC02 diagrams involving Z^0 or γ-boson pairs, d),e) and f) are additional diagrams, all of which lead to a four-fermion final state.

of diagrams.) The Feynman diagrams for W pair production via a virtual Z^0 or virtual photon, contain a triple gauge-boson coupling, which can be extracted by measuring the pair-production cross section, or by studying the angular distribution of the W bosons and their decay products. The W bosons are not stable but decay within $3 \cdot 10^{-25}$s, corresponding to a decay width of about 2 GeV. Each W decays into a pair of fermions, as indicated in Fig.4 a) and b). The final state in W-boson pair production processes therefore contain four fermions. Figures 4 c)-f) show additional electroweak processes that also lead to four-fermion final states. Since these provide the same final state, their interference with W-pair production must be taken into proper account. The analysis of the W-boson cross section and mass is based on events in which the four fermions can be grouped into two pairs with invariant masses close to the W mass. In this region of phase space, the CC03 diagrams dominate the four-fermion cross section, which is of the order of 15 pb for most of the luminosity collected at LEP-II.

The W boson decays 68.5 % into a quark-antiquark pair, which is observed in

the detector as two jets, and to 31.5 % into a charged lepton and its neutrino. Consequently, the decays of the two W-bosons provide three distinct signatures. About 47 % of the time, both W bosons decay hadronically, which yields at least four jets in the final state. About 43 % of the times, one W decays hadronically and the other leptonically ("semileptonic" decay channel), leading to events with two jets, a high energetic lepton, and missing energy due to the unobserved neutrino. The remaining 10% of events, where both W bosons decay leptonically, contain two energetic leptons and a large amount of missing energy. For all these event topologies, it is important to be able to have detectors that can measure precisely the momenta and directions of the leptons and jets, and this is the subject of the next section.

1.3. *The LEP Collider and its Detectors*

LEP is an electron-positron collider with a circumference of 27 km, located at CERN near Geneva, Switzerland.[5] The electron and positron beams collide at four interaction points inside the LEP tunnel at the positions of the ALEPH,[6] DELPHI,[7] L3,[8] and OPAL [9] detectors. From 1989 until 1995, LEP was operated at center-of-mass energies near the Z^0 resonance. At the end of 1995, the center-of-energy was increased in steps, crossing the W-pair production threshold in 1996, and reaching 209 GeV for some of the data taking in the year 2000. Each LEP experiment has collected more than 700 pb^{-1} at center-of-mass energies above the W-pair production threshold, each corresponding to the production of about $10,000$ W-pair events.

All LEP detectors are cylindrically symmetric around the beam axis. The detector components most important for the study of W bosons are the inner tracking detectors, the calorimeters and the muon system. As an example of a LEP detector, Fig. 5 shows the OPAL detector.

In the inner gas-tracking detectors, the trajectory of charged particles can be observed through the ionization produced along their paths. When an electric field is applied in the gaseous volume, the created-charge drifts towards sensors, which, in the case of OPAL correspond to wires parallel to the beam axis (drift chamber), and, in the case of the other three experiments, to sensors located in a plane perpendicular to the beam, at the ends of the detectors (time-projection or time-expansion chambers). Points along the trajectory can be determined from the time it takes the charge to reach the sensor. In order to measure a particle's momentum, the track detectors are placed inside a solenoidal magnetic field, and the momentum is determined from the curvature of the track in the magnetic field. The curvature is proportional to $1/p_t$, where p_t is the component of the momentum transverse to the magnetic field. The component parallel to the magnetic field can be determined from p_t and the initial direction of the track. The sign of a particle's charge is determined by the sense of the curvature.

Electrons and photons are detected in the electromagnetic calorimeter. In mat-

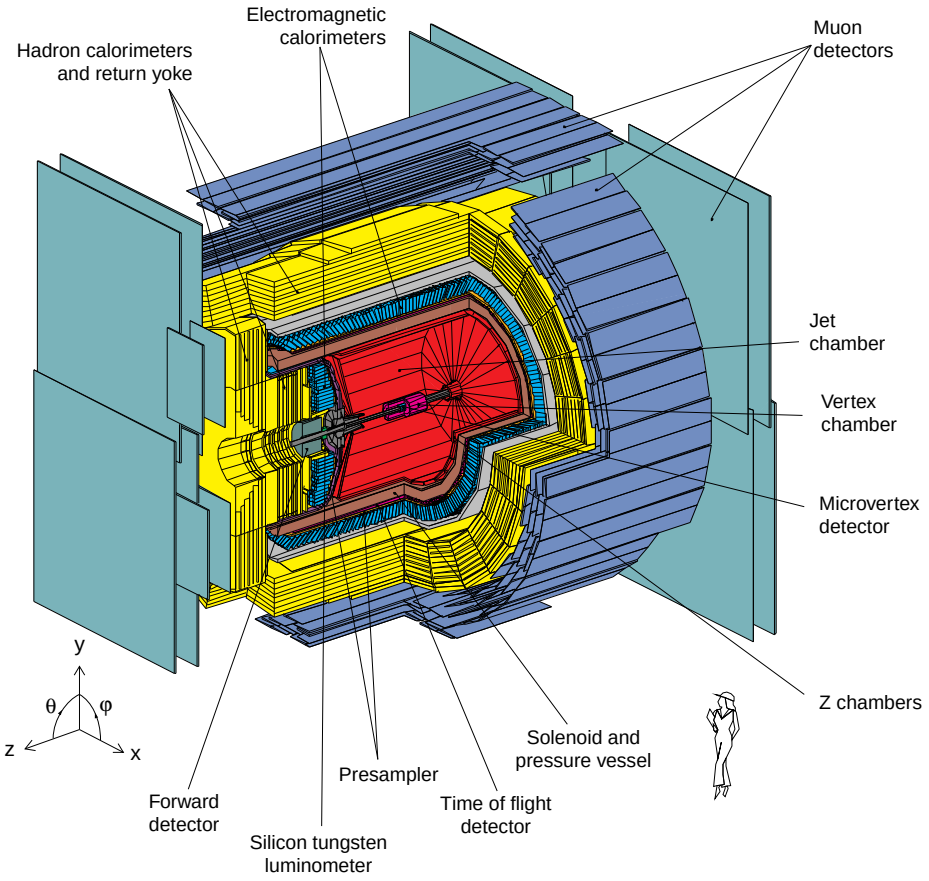

Fig. 5. The OPAL detector.

ter, electrons radiate photons through bremsstrahlung, and photons can convert into electron-positron pairs. The interplay of these two processes leads to a "shower" of electrons, positrons and photons within the calorimeter. The showering stops when the energy loss of the particles in the shower from bremsstrahlung is of the same order as the energy loss from ionization. The energy of the primary particle can be obtained from the energy deposited by the shower, which reflects the total length of the trajectories of all electrons and positrons in the shower. The effective length of the trajectory can, in turn, be determined from the amount of Çerenkov radiation produced in the detector materials (lead-glass for the OPAL detector), or the amount of light produced in scintillating material (BGO Crystal in L3), or the amount of ionization produced in gas filled detectors sandwiched between sheets of lead (sampling calorimeters of ALEPH and DELPHI).

The electromagnetic calorimeter is followed by a hadronic calorimeter, in which

energies of both charged and neutral hadrons are measured by showers they produce through strong interactions within the detector material.

The only particles that do not produce electromagnetic or hadronic showers, and are therefore not stopped within the calorimeters, are muons and neutrinos. Muons do not interact strongly and, compared to electrons, their bremsstrahlung is greatly suppressed because of their much larger mass. Muons are identified beyond the hadron calorimeter using ionization detectors. Only the muon detectors of L3 reside within a magnetic field, and can be used to measure the muon momentum. In the other three LEP experiments, the signals in the muon detectors have to be matched with a reconstructed track in the inner tracking detectors, in order to determine the muon momentum. Neutrinos interact only weakly. Because of their extremely small scattering cross section, they leave the detector without interacting, and can therefore not be detected directly in any LEP detector.

1.4. *Monte Carlo Simulation*

An important tool in interpreting LEP data involves the comparison of measurements with predictions based on Monte Carlo simulations. Precision measurements are used typically to determine parameters of theory (e.g., the mass of the W boson) that agree best with the observed data. The theory, however, only predicts the properties of fundamental particles (e.g., the quarks and leptons from W-boson decay). Monte Carlo simulations must therefore be used to estimate the effects of the fragmentation of quarks into hadrons, and the acceptance and resolution of the detector. Well-understood processes are used to test and to calibrate such Monte Carlo simulations, which can be regarded as tools for extrapolating the effects of fragmentation and detector resolution from known test samples to events used in the precision measurement. In addition to this extrapolation, Monte Carlo studies provide an important tool for the optimization of any analysis. The statistical precision and effects of systematic uncertainties can be checked using large samples of Monte Carlo events, for which the results are already known.

The first step in the generation of a Monte Carlo event involves the simulation of the primary interaction. Several programs are usually used to simulate the process $e^+e^- \to 4f$. The KoralW program[10] provides either the CC03 diagrams, or, by interfacing with the Grace4f program,[11] the full leading-order four-fermion matrix elements. The program Excalibur [12] can also be used to calculate the four-fermion matrix elements. Both programs contain a detailed implementation of the radiation of initial-state photons, and can be used to simulate the momenta of the four final-state fermions and such photons. The programs YfsWW [13] and RacoonWW [14] can simulate the full $\mathcal{O}(\alpha)$ QED correction to the CC03 contributions in the double-pole approximation.[15]

When the final state contains quarks, the fragmentation of these colored objects into hadrons is simulated with the programs Pythia,[16] Herwig [17] or Ariadne.[18] In the first phase of the simulation, a QCD cascade is generated by simulating

the radiation of gluons and the splitting of gluons into quark anti-quark pairs. In ARIADNE, the QCD cascade is simulated by a dipole model, where quarks and gluons form color dipoles which then radiate gluons. The QCD cascade is terminated when the virtuality of the quarks and gluons falls below a cut off, of typically 1-2 GeV.

The fragmentation of quarks and gluons at the end of the QCD cascade can be simulated only phenomenologically. PYTHIA and ARIADNE use string models. A string connects partons, which form a color singlet. The string begins at a quark and connects it with a gluon. This gluon is connected by the string to other gluons, until the string ends on an antiquark. The gluons can therefore be considered as kinks in a string that connects a quark with an antiquark. The string is broken into pieces by the insertion of quark-antiquark and diquark-antidiquark pairs into the string. These pieces, which consist of short strings connecting a quark and a antiquark close in phase space, form hadrons. The fraction of string energy carried by a quark or antiquark, and the fraction of momentum perpendicular to the string axis, are generated using functions that contain free parameters of the model.

In HERWIG, all gluons split into quarks and antiquarks. Hadrons are then produced from clusters that are formed of color-neutral quark-antiquark pairs. All fragmentation models have parameters that can be adjusted to maximize agreement with data, but the fragmentation of W bosons is well described using the same parameters as determined for the Z^0 at resonance.

The decay of unstable particles is simulated with the help of decay tables. For most particles, the tables are based on their measured branching ratios in different decay channels. When branching ratios are unknown, estimates are used for which the simulated inclusive-particle-rates agree best with available measurements. For particles with sufficiently long lifetimes that interact within the detector, the decay is convoluted with the detector response. A K^0_S, for example, decays typically within the volume of the tracking detectors, creating a pair of tracks that start in the middle of the tracking chambers, while most K^0_L do not decay before they reach the calorimeters. The propagation of any particle through the detector, its interaction with the detector material, and the response of the sensors, are simulated with the GEANT program package.[19]

1.5. *Measurement of Jets*

The quarks produced in the primary weak interaction cannot be observed directly in the detector. As described in Section 1.4, they fragment into hadrons that can be observed. To estimate the energy and momentum of the primary partons (quarks or any radiated gluons), the observed detector signals are clustered into so-called jets. In general, jet algorithms make use of the fact that hadrons from any primary particle are close to each other. Most analyses of e^+e^- collider data use the JADE type of jet algorithms.[20] In this algorithm, pseudo-particles are added together iteratively to form jets. The algorithm starts with a list of pseudo-particles that consist of all considered particles or detector hit information. Based on an algorithm-dependent

measure, the two pseudo-particles that are closest to each other are merged into a new pseudo-particle. This is iterated until a prescribed cutoff criterion is reached. The remaining pseudo-particles are then called jets. Different algorithms of the JADE variety use different definitions of closeness between pseudo-particles, and calculate the four-momenta of the new pseudo-particles from the four-momenta of the two parents (pseudo-particles from which they are formed) in different ways. The DURHAM algorithm,[21] which is used by all four LEP experiments in the determination of the W mass, defines the closeness between to pseudo-particles i and j as:

$$y(i,j) = \frac{2\min(E_i^2, E_j^2)(1-\cos\theta_{ij})}{E_{vis}^2}$$

where E_i and E_j are the energies of the two pseudo-particles, and θ_{ij} is the angle between them, and E_{vis} is the sum of the energies of all initial pseudo-particles. In the DURHAM scheme, two pseudo-particles are combined into a new pseudo-particle by adding their four-momenta. The four-momentum of a jet is therefore given by the sum of the four-momenta of all particles belonging to it. The jets reconstructed using the Durham algorithm have significant masses. When the algorithm is used to reconstruct W boson pairs, it is stopped when the number of pseudo-particles equals the number of expected jets, i.e., at least four in the fully hadronic channel (or five if gluon bremsstrahlung is considered), and two in the semileptonic channel (in this channel, detector signals from the identified lepton are not considered in the initial list of pseudo-particles). The smallest value of $y(i,j)$ of n remaining pseudo-particles is called $y_{n-1,n}$. It can be used to distinguish between events with an n-jet structure and events with an $(n-1)$-jet structure. y_{34} is one of the quantities used to distinguish between signal events that have both W bosons decaying hadronically, and background from 2-quark events that contain extra gluon bremsstrahlung. In certain LEP analyses, y_{45} is used to decide whether an event should be reconstructed as a four-jet or a five-jet event.

When jets are reconstructed from data or from Monte Carlo events that include full detector simulation, the initial list of pseudo-particles consists of the charged tracks measured in the tracking devices and any clusters of energy deposition in the calorimeters. Since most charged tracks are caused by pions, the pion mass is assumed in the determination of the four-momentum of a pseudo-particle obtained from tracking. As most electromagnetic showers are due to photons (from π^0 decays), the pseudo-particles formed from calorimeter clusters are assumed massless. Charged particles produce tracks and also deposit energy in the calorimeter, which can lead to a double counting of their energy. This double counting is corrected either by estimating the average effect on jet energy, or by estimating for each cluster how much of its energy is due to charged particles already measured in the tracking detector. When jets are formed from Monte Carlo events generated without detector simulation, the four-momenta of the simulated particles are used directly as the initial pseudo-particles.

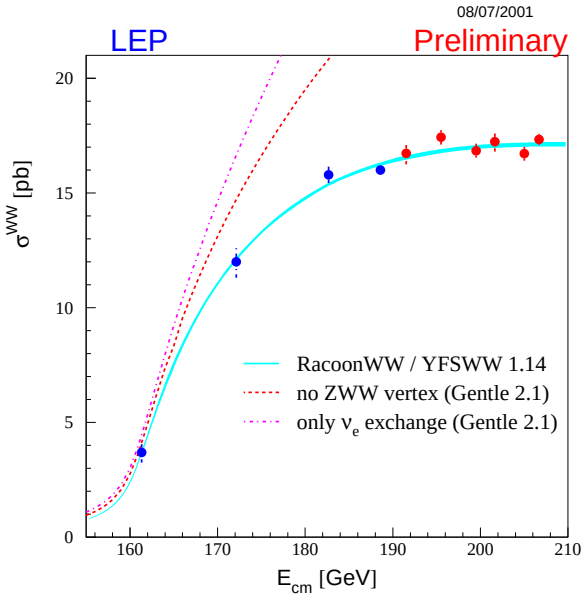

Fig. 6. Comparison of the W-pair cross section with the Standard Model, and with predictions that exclude either the WWZ coupling or use only the diagram with t-channel ν exchange. The points show preliminary results for the combination of LEP measurements.[22]

2. Measurement of the Four-Fermion Production Cross Section

As described in Section 1.2, the production cross section of four fermions in e^+e^- annihilation has contributions from Feynman diagrams containing triple gauge-boson couplings. A precise measurement of the cross section can therefore be used to extract these couplings, and test whether they are consistent with prediction. Figure 6 shows a comparison between the measured W-pair cross section and the predictions of the Standard Model,[22] as well as two other models that exclude either the WWZ coupling or use only the diagram with t-channel neutrino exchange (see Fig. 4 a). The two variants of the Standard Model lead to cross sections that increase with rising center-of-mass energies and would eventually violate the unitarity bound. The contributions to the W pair cross section from diagrams containing gauge-boson couplings provide cancellations essential to avoid this increase. Clearly, models without contributions from the omitted gauge-boson couplings are already ruled out by measurements at center-of-mass energies of about 10 to 20 GeV beyond the W-pair production threshold. As can be expected, the cross section for W-pair production near threshold is also very sensitive to the mass of the W boson and to the e^+e^- center-of-mass energy.

The Feynman diagrams discussed in Section 1.2, and shown in Figure 4, contribute in different regions of phase space of the four-fermion cross section. The

LEP experiments have therefore measured the gauge-boson cross sections in different ways. In particular, they have extracted separately the W-pair, the Z^0-pair and the inclusive single-W cross section. The W-pair cross section is defined as the contribution from the leading-order Feynman diagrams with two W bosons (the CC03 diagrams shown in Figs 4 a) and b)). The Z^0-pair cross section is defined as the contribution from the leading-order Feynman diagrams with two Z^0 bosons (the NC02 diagram are shown in Fig 4 c)). The contributions from other diagrams, or their interference terms, are small in the region of phase space used to determine the mass and cross section of the W, and are estimated by comparing Monte Carlo predictions containing all four-fermion diagrams with those containing only the CC03 or NC02 diagrams. The single-W cross section is defined as the subset of t-channel Feynman diagrams contributing to the $e\nu ff'$ final states, usually with additional selections on kinematic variables that exclude the regions of phase space dominated by "two-photon", or multi-peripheral, processes (see Fig. 4e).

2.1. *Selection of* W *Pair Events*

As mentioned before, the W boson can decay either into a lepton-neutrino pair or into a quark-antiquark pair. Consequently, different selections must be used to define the different final states. The ten experimentally distinguishable final states are: $q\bar{q}q\bar{q}$, $q\bar{q}\mu^+\nu$, $q\bar{q}e^+\nu$, $q\bar{q}\tau^+\nu$, $\mu^+\nu\tau^-\nu$, $e^+\nu\tau^-\nu$, $\tau^+\nu\tau^-\nu$, $\mu^+\nu e^-\nu$, $\mu^+\nu\mu^-\nu$ and $e^+\nu e^-\nu$. (Charge conjugation invariance is assumed throughout.) Event selections generally consist of a pre-selection, followed by the use of neural-network or likelihood discriminant to separate signal from the major backgrounds, which are dominated by $q\bar{q}\gamma$ events for the fully hadronic states, and both $q\bar{q}\gamma$ and the four-fermion backgrounds for the other channels.

The selection of fully leptonic W decays requires the event to contain exactly two jets that can be identified either as electrons or muons, or low multiplicity jets from τ-lepton decays. The two jets (which may consist of a single particles) must not be coplanar with the collision axis, and the event must contain significant missing momentum. One potential background for this class of events corresponds to leptonic Z^0 decays that contain a high momentum photon radiation in the initial state. The leptonic W-pair decays can be distinguished from such events because their missing momentum does not point preferentially along the beam direction, which means that their missing momentum has a substantial component perpendicular to the beam axis. Also, W-pairs do not contain energetic isolated photons. Neutrinos from τ decays in $e^+e^- \to \tau^+\tau^-$ events can have large missing momentum. But because of the large momentum of the $\tau^\pm$, the missing momentum from the neutrinos points along the respective τ directions. Consequently, these types of events can be distinguished from signal, for which the missing momentum is in general not parallel to the jet axis. The contribution from multi-peripheral events (Fig. 4 e) can be reduced further by requiring a minimum total visible energy, because the visible energy in these events tends to be lower than for signal. From a

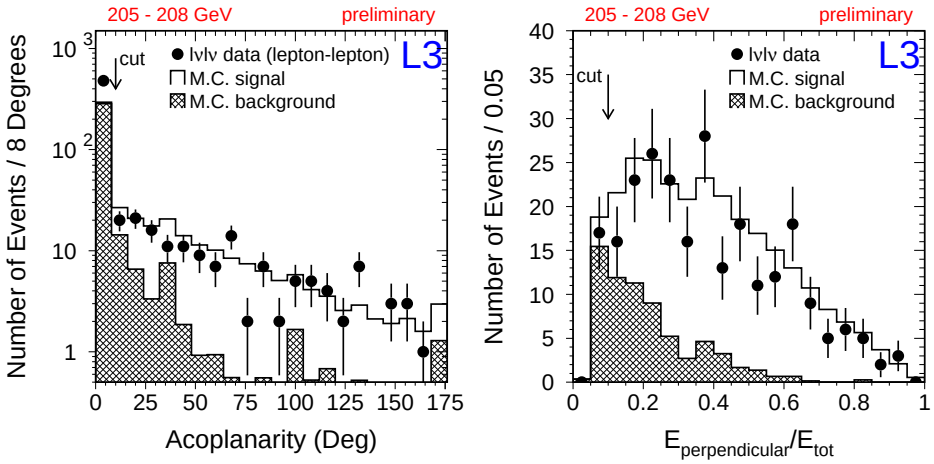

Fig. 7. Distributions in variables used to select $e^+e^- \to l\nu l\nu$ events, shown after all selections, expect on the variable in the displayed plot. Left: Acoplanarity between the two leptons. Right: Energy imbalance in the plane transverse to the beam direction (normalized to the visible energy). The results are from a preliminary analysis of the 205-208 GeV L3 data.[26]

preliminary analysis of the 205-208 GeV L3 data,[26] Fig. 7 shows the acoplanarity between the two leptons (the acoplanarity is the difference between 180° and the angle between the projection of the two leptons into the plane transverse to the beam direction), and the energy imbalance in the plane transverse to the beam direction ($E_{perpendicular}$), normalized by the total visible energy (E_{tot}) for signal and background, after applying selections on all variables expect the one displayed. The selection efficiencies for different channels depend on the details of the individual analyses and the efficiency of lepton identification. For the LEP experiments, the latter ranges from 80% (for $\mu - \mu$) to about 30 % (for $\tau - \tau$) events. The selections provide typical signal purities of about 80%-90% in all channels.

Semileptonic W-pair channels must contain two jets from one of the W bosons, and one energetic lepton and missing energy from the second W boson. Event selection is based typically on a loose pre-selection to remove events with low track multiplicity or low visible energy. For the accepted events, the most likely lepton candidate, which can contain more then one track in the case of τ-leptons, is then identified, and the remaining event information is forced into two jets. The selection likelihood or neural network output is then based on kinematic quantities such as the size and direction of the lepton momentum, the missing momentum, the angle between the two jets, the visible energy, and event-shape variables like thrust and sphericity.[27] In addition, the invariant mass of the jet pair or the lepton and the neutrino (defined by the missing momentum) can be used to improve signal/background. Alternatively, the masses can be determined in a kinematic fit,

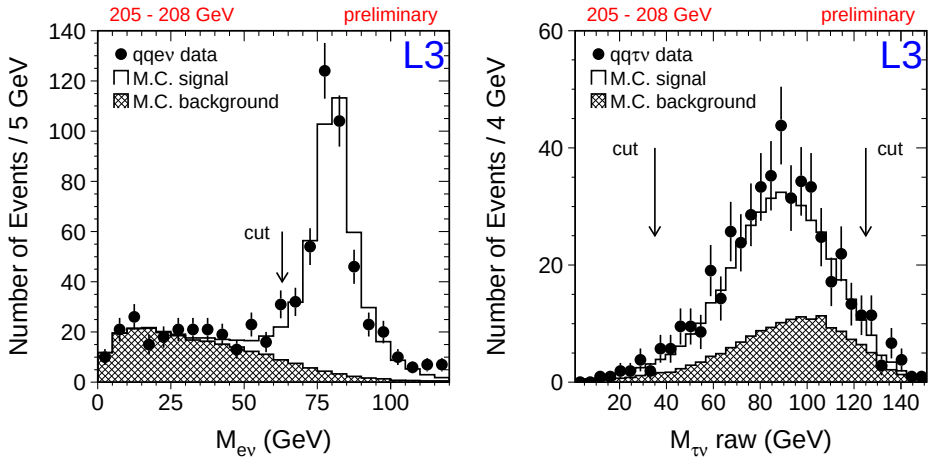

Fig. 8. Invariant mass of the lepton and neutrino in the $e^+e^- \to qql\nu$ channel, from the analysis of 205-208 GeV L3 data,[26] after all selections, expect for the $l\nu$ mass. Results for electrons are shown on the left, and for the τ channel on the right.

as will be described in Section 4. The preliminary analysis of the 205-208 GeV L3 data,[26] in Fig. 8 shows the invariant mass of the charged lepton and neutrino in the electron and τ channels. Typical efficiencies range from 70%-90% for different channels, and the purities for the electron and muon channels are about 95%, and for the τ channel about 80%.

The pre-selection for W-pair events where the W bosons yield four-jet events., includes loose requirements on the multiplicity, and a veto on events already selected as semileptonic or leptonic W-pair decays. The most important background is from quark-pair events (including events with initial state radiation) $e^+e^- \to q\bar{q}(\gamma)$, with accompanying hard-gluon radiation. In quark-pair events that contain an energetic initial-state photon, the photon is usually emitted close to the beam direction, and is therefore not observed in the detector. These types of events can be rejected by requiring a minimal visible energy, typically 70 % of the center-of-mass energy. The difference in event topology can be used to distinguish hadronic pairs from such "QCD" background. QCD events that are reconstructed as four-jet events consist of two jets from the primary quark and two jets from hard gluon radiation (in some cases these are two quark jets evolved from the splitting of a gluon into two quarks). The secondary jets are typically of lower energy, and their angles relative to the originating jets tend to be small. These features can be exploited by looking at event-shape distributions, such as the sphericity or the y_{cut} value (y_{34} where a three-jet event turns into a four-jet event or y_{45} where a four-jet event turns into a five-jet event, as mentioned Section 1.5). Another way to exploit these differences is to use the jet algorithm to reconstruct the event as a four-jet event, and then use the

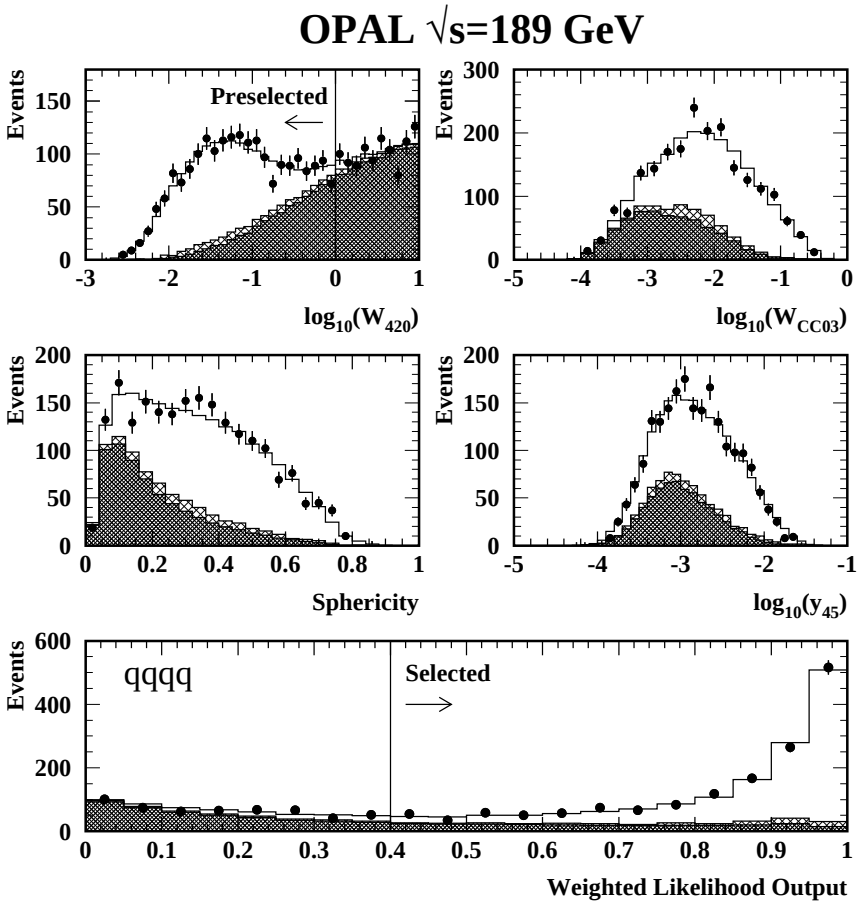

Fig. 9. Distributions used in the selection of hadronic W-pair events in the OPAL analysis of data taken at $\sqrt{s} = 189$ GeV. Also shown is the likelihood output based on these four distributions, with background peaking at ≈ 0, and signal at ≈ 1

four-momenta of the four jets to calculate the QCD matrix element "W_{420}" for four jets (defined as the sum of the $\mathcal{O}(\alpha_s^2)$ matrix elements for $e^+e^- \to q\bar{q} \to q\bar{q}gg$ and $e^+e^- \to q\bar{q} \to q\bar{q}q\bar{q}$ processes),[28] and the matrix element for the CC03 diagrams. For true hadronic W-pair events, the value of the CC03 matrix element should be larger than for QCD background and the value of the QCD matrix element should be smaller for hadronic W-pair event decays than for the QCD background. Figure 9 shows distribution in the four variables used to define the OPAL likelihood for hadronic W-pairs at a center-of-mass energy of 189 GeV.[29] The points correspond to data, the cross-hatched regions to background and the remainder to signal. The final selection efficiencies in the all-hadronic channel range from 80% to 90 %, and

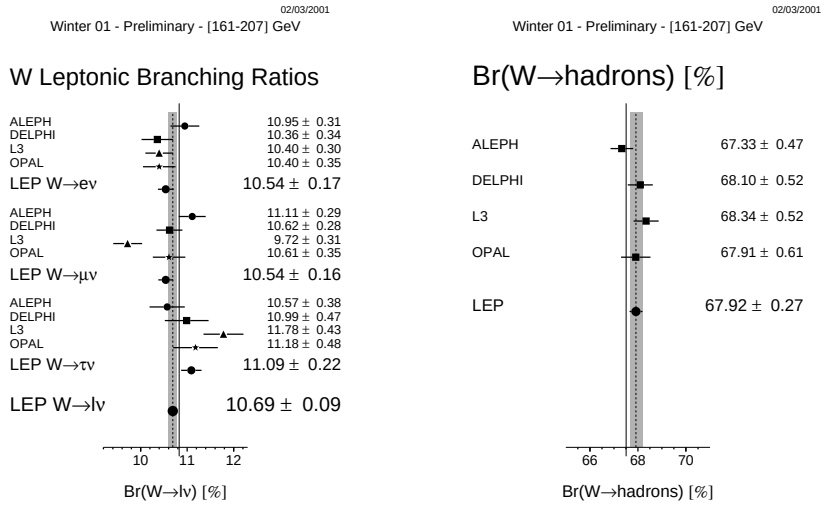

Fig. 10. Summary of the leptonic and hadronic W-decay fractions. The solid line indicates the Standard Model prediction of 10.81% and 67.51%, respectivetly.[22]. The dashed line and the gray band show the combined LEP result and its uncertainty .

the purities from 70% to 80%, for all the major LEP detectors.

2.2. *Results*

The cross sections for individual W-pair channels can be determined from neural-network or relative log-likelihood discriminants, either by counting the number of events above some cutoff, or by fitting the data to signal and background templates obtained from Monte Carlo simulations. The measurements yield the products of production cross sections and the decay branching fractions of the two W bosons in any given final state. The ratios of such results can be used to extract decay fractions for W bosons. A summary of the measurements of leptonic and hadronic W decay fractions is shown in Fig. 10. In the Standard Model, the branching fractions depend only on the six matrix elements $|V_{q\bar{q}'}|$ of the Cabibbo-Kobayashi-Maskawa (CKM) quark mixing matrix. (The CKM matrix is a unitary matrix describing the relative strength of the W coupling to different combinations of up and down types of quarks. The coupling of the W^+ to an up-quark and an anti-strange quark, for example, is proportional to V_{us}. The off-diagonal CKM matrix elements do not vanish because the eigenstates of the weak interaction are not the same as the mass eigenstates.) Leaving out the top quark because it is too heavy to be produced in W boson decays, the branching fraction of the W into any lepton flavor $\mathcal{B}(W \to l\bar{\nu})$

can be related to the CKM matrix elements as follows:[22]

$$\frac{1}{\mathcal{B}(W \to l\bar{\nu})} = 3 \left\{ 1 + \left[1 + \frac{\alpha_s(M_{\rm W}^2)}{\pi} \right] \sum_{\substack{i\,=\,(u,\,c),\\ j\,=\,(d,\,s,\,b)}} |V_{ij}|^2 \right\}$$

where $\alpha_s(M_{\rm W}^2)$ is the strong coupling constant at the scale of the W-boson mass. Taking $\alpha_s(M_{\rm W}^2) = 0.121 \pm 0.002$, and using the measured leptonic branching fractions of the W, yields:[22]

$$\sum_{\substack{i\,=\,(u,\,c),\\ j\,=\,(d,\,s,\,b)}} |V_{ij}|^2 = 2.039 \pm 0.025(\mathcal{B}_{{\rm W}\to l\bar{\nu}}) \pm 0.001(\alpha_s).$$

Using the experimental values[30] for $|V_{ud}|^2 + |V_{us}|^2 + |V_{ub}|^2 + |V_{cd}|^2 + |V_{cb}|^2 = 1.0477 \pm 0.0074$, the result can be used to extract a measurement of $|V_{cs}|$, which is the least well know of these matrix elements: $|V_{cs}| = 0.996 \pm 0.013$.

Figure 11 shows the combined LEP results for the measurement of the cross section for W-pairs (CC03 diagrams) and Z^0-pairs (NC02 diagram).[22] The W-pair cross section is compared to predictions of the Standard Model based on the programs YFSWW [13] and RACOONWW.[14] The two programs have been compared extensively, and agree at a level of < 0.5 % at LEP-II energies.[23] The calculations above 170 GeV have uncertainties decreasing from 0.7 % at 170 GeV to about 0.4 % at center-of-mass energies larger than 200 GeV. An uncertainty of 50 MeV on the W mass translates into an additional error of 0.1 % (3.0 %) on the predicted cross section at 200 GeV (161 GeV). The Z^0 pair cross section in Fig. 11 is compared with predictions based on the programs YFSZZ [24] and ZZTO.[25] The uncertainty of the theory is estimated as 2%.[23] All results up to the highest center-of-mass energies are in good agreement with the predictions.

As indicated previously, the single-W cross section is defined by the sum of all leading-order four-fermion t-channel processes contributing to the $e\bar{\nu}_e f\bar{f}$ final state, with additional selections on kinematic variables used to exclude regions of phase space dominated by multi-peripheral diagrams, where the calculation has large uncertainties. The criteria used to define signal are: $m_{q\bar{q}} > 45$ GeV/c^2 for $e\nu_e q\bar{q}$ final states, $E_l > 20$ GeV for $e\nu_e l\nu_l$ final states (with $l = \mu$ or τ); and $|cos\theta_{e^-}| > 0.95$, $|cos\theta_{e^+}| < 0.95$, and $E_{e^+} > 20$ GeV (and similar charge conjugate selections) for the $e\nu_e e\nu_e$ final states. The momentum transfer to the electron in these processes is small, and the electron is therefore often not detected (in the beam pipe). The signal therefore consists either of a single high-energy lepton, or a jet-pair with a large invariant mass and missing momentum. Figure 12 shows the combined LEP results[22] for the measurement of the single-W cross section, both for the hadronic channel alone, and for the combination of the hadronic and leptonic channels. Although the uncertainties are large, the data agree with predictions.

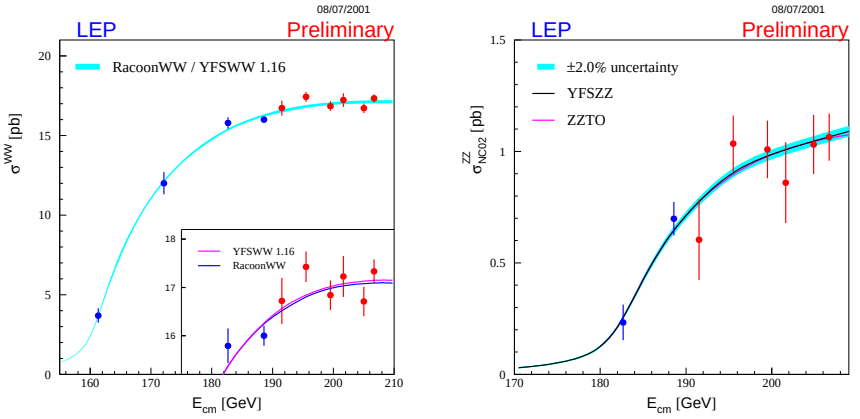

Fig. 11. The W-pair and Z^0-pair cross sections, left and right, respectively

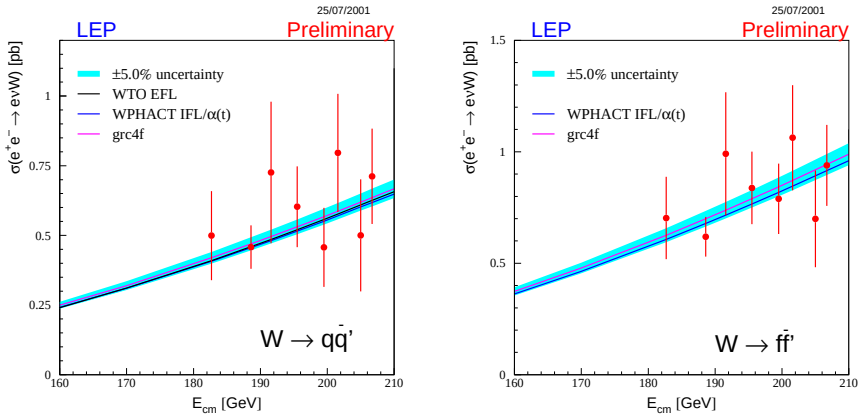

Fig. 12. The single-W cross section as function of $E_{cm} = \sqrt{s}$.

3. Gauge Boson Couplings

An essential feature of the Standard Model is the non-abelian structure of the weak interaction. The gauge-boson couplings are a consequence of this structure, and the direct observation of these couplings is therefore an important test of the non-abelian structure of the weak interaction. Any deviations from the predictions of the Standard Model would imply the presence of new physics. This could arise from a violation of the gauge invariance of the theory, or from additional particles or interactions that have yet to be observed.

Gauge-boson couplings also provide an essential contribution to the strong interaction, because QCD is a non-abelian theory, with self couplings between its gauge bosons, the gluons. These couplings are regarded as the reason for the confinement

of colored particles within objects that are neutral in color charge. Clear evidence for the triple-gluon vertex has been found in four-jet events at LEP.[31]

3.1. *Triple-Gauge Couplings of* W *Boson*

The most general Lorentz-invariant Lagrangian has seven independent couplings describing each of the WWγ and WWZ vertices.[32] By requiring electromagnetic gauge invariance, and both charge-conjugation (C) as well as parity (P) invariance, the number of parameters can be reduced to five. Thus, the parameters g_1^Z, κ_Z, κ_γ, λ_Z and λ_γ are often used to describe the WWγ and WWZ couplings.[32] The C and P conserving terms for the WWγ coupling correspond to the lowest-order multi-pole expansion of the W-photon interaction. The charge $Q_{\rm W}$, the magnetic dipole moment $\mu_{\rm W}$, and the electric quadrupole moment $q_{\rm W}$ of the $\rm W^+$, are given by:[33]

$$Q_{\rm W} = e, \qquad \mu_{\rm W} = \frac{e}{2m_{\rm W}}(g_1^Z + \kappa_Z + \lambda_\gamma), \qquad q_{\rm W} = \frac{e}{m_{\rm W}^2}(\kappa_\gamma - \lambda_\gamma).$$

The expectation for the five parameters is $g_1^Z = \kappa_Z = \kappa_\gamma = 1$, and $\lambda_Z = \lambda_\gamma = 0$. Precision measurements at the $\rm Z^0$ resonance are consistent with the following $SU(2) \times U(1)$ relations among the five couplings:[32]

$$\begin{aligned} (1 - \kappa_Z) &= -(1 - \kappa_\gamma) tan^2\theta_w + (1 - g_1^Z) \\ \lambda_Z &= \lambda_\gamma \ , \end{aligned}$$

where θ_w is the weak mixing angle. These relations leave only three independent couplings not restricted significantly[35] by existing $\rm Z^0$ data from LEP and SLD.[36] In the following, κ_γ, g_1^Z, and $\lambda = \lambda_Z = \lambda_\gamma$ will be used to check triple gauge boson couplings of the W bosons. The results will also be expressed in terms of deviations from the Standard Model, e.g., $\Delta\kappa_\gamma = \kappa_\gamma - 1$, and $\Delta g_1^Z = g_1^Z - 1$. Anomalous contributions to the couplings can yield additional contributions for different helicity states of the outgoing W bosons in W-pair events. This affects the production angular distribution of the W bosons, and, because of correlation with the W spin, it also affects the angular distribution of the decay products. Cross sections provide additional information about gauge couplings. The W pair cross section and its angular dependence, are sensitive to all three couplings. In contrast, the cross sections for single-W and single-photon production (through contributions from $e^+e^- \to \gamma\nu\nu$) are sensitive mainly to κ_γ for t-channel processes at low momentum transfers involving the WWγ vertex (see Fig. 13). Contributions from λ_γ are suppressed in this case, because, they are important only for processes involving large W momentum.

3.1.1. *Angular Distributions in Decays of* W *Pairs*

Ignoring small effects due to the finite width of the W, and the impact of initial state radiation, the production and decay of W bosons is described completely by

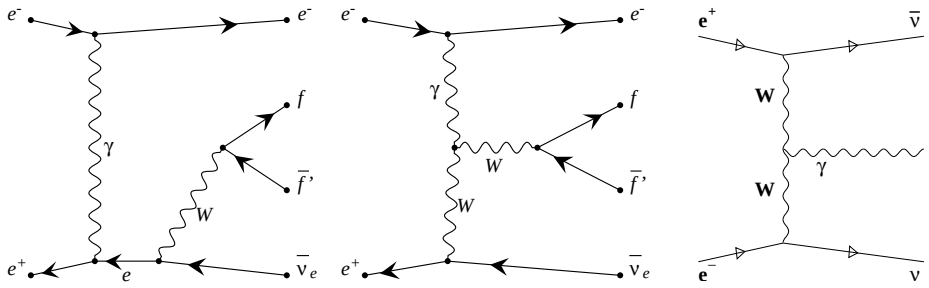

Fig. 13. Feynman diagrams for single-W and single-photon production.

five angles. Conventionally, these are taken to be:[32] the polar production angle θ_{W} defined as the angle between the incident e^- and the produced W^-, and the polar and azimuthal angles θ_1^* and ϕ_1^* of the decay fermion from the W^-, calculated in the W^- rest frame ("helicity" frame), and the analogous angles θ_2^* and ϕ_2^* for the anti-fermion for the W^+. (The axes of the right-handed coordinate system in the W rest frame are defined such that the z-axis is along the parent-W line of flight ($\vec{W}$), and the y axis is along the direction $\vec{e^-} \times \vec{W}$, where $\vec{e^-}$ is the direction of the e^- beam.) Figure 14 illustrates these definitions.

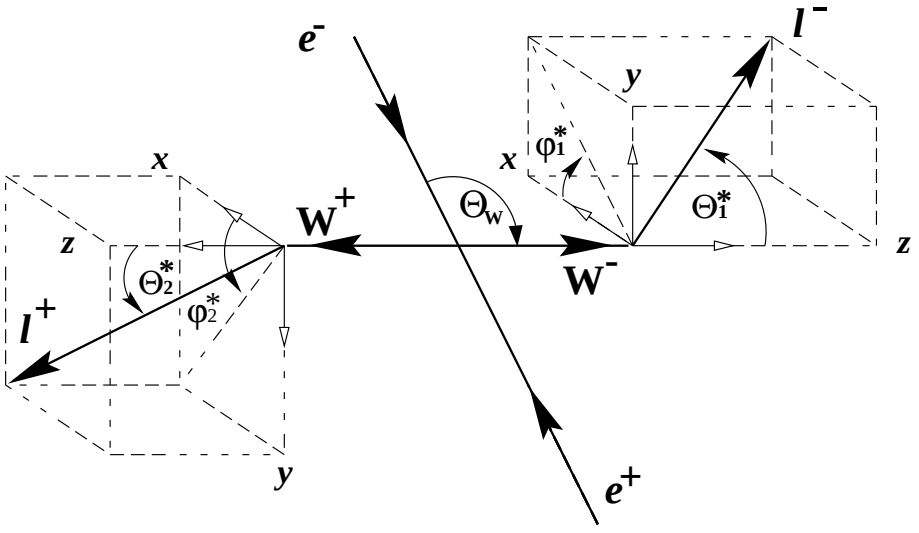

Fig. 14. Definition of the angles in leptonic W pair decay.

In most analyses using hadronic W decays, it is not possible to distinguish the quark jet from the antiquark jet. Hence, the angles in the W rest frame are defined arbitraily using the jet with the smaller azimuthal angle ϕ^*. Figure 15

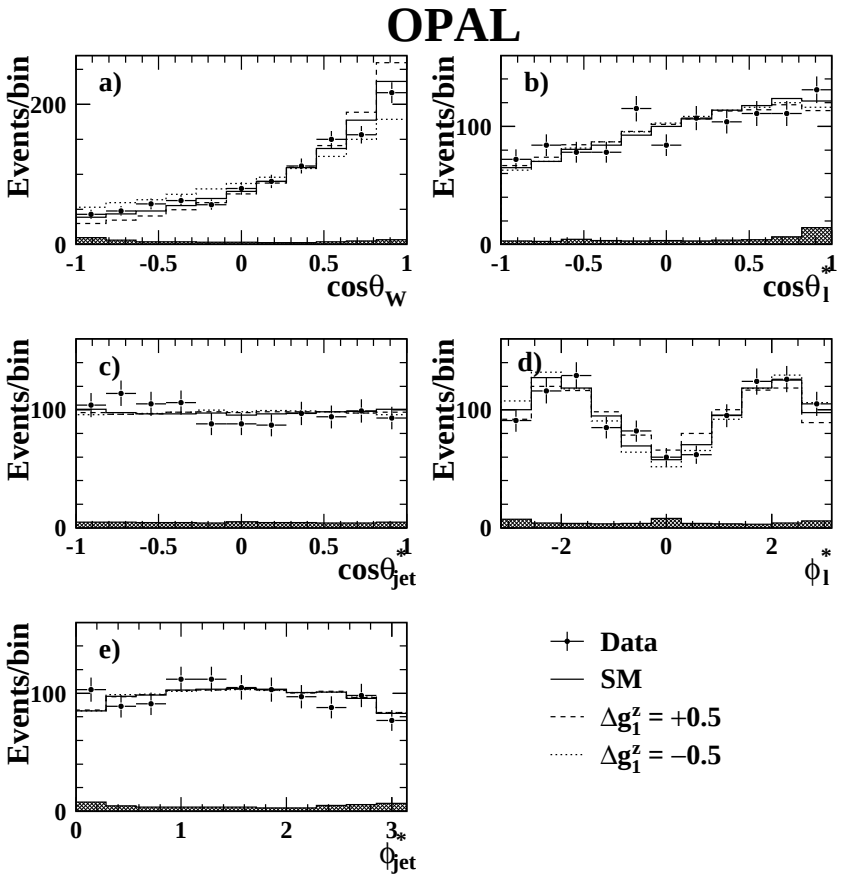

Fig. 15. Comparison of OPAL data at $\sqrt{s}$ = 189 GeV with the Standard Model and with predictions for anomalous gauge couplings $\Delta g_1^Z = \pm 0.5$. See the text for the definitions of the angles. The shaded histograms show the background from sources other than $q\bar{q}l\bar{\nu}$.

shows a comparison of OPAL data[34] for semileptonic W-pairs at $\sqrt{s} = 189$ GeV - to the Standard Model, and to predictions assuming the anomalous gauge couplings $\Delta g_1^Z = \pm 0.5$. Comparing the distributions from leptonic W decay (Figs. 15b and d) with those from hadronic decay (Figs. 15c and e), indicates the clear loss of sensitivity when the fermion cannot be distinguished from the antifermion.

The method of the "Optimal Observable" is often used to extract information about gauge couplings from the $\leq$ 5-dimensional angular distributions (for semileptonic events, some analyses use only the W^- production and lepton decay angles).[37,38] Since the Lagrangian is linear in the triple-gauge couplings, the differential cross section can be expanded in the couplings without using terms beyond

second order:

$$\frac{d\sigma}{d\Omega} = S_0(\Omega)(1 + \sum_i \mathcal{O}_i^{(1)}(\Omega)g_i + \sum_{ij} \mathcal{O}_{ij}^{(2)}(\Omega)g_i g_j),$$

where g_i denotes any type of additional coupling not included in the calculation of the differential cross section denoted by $S_0(\Omega)$, and Ω denotes the phase space variables, taking into account reconstruction ambiguities (e.g., the ambiguity between jets from quarks and antiquarks) for the individual W^+W^- channels. The functional dependence of the first-order coefficients $\mathcal{O}_i^{(1)}(\Omega)$ and of the second-order coefficients $\mathcal{O}_{ij}^{(2)}(\Omega)$ on Ω are described in terms of a phenomenological model of anomalous couplings.

Instead of the multidimensional phase space density Ω, the one dimensional projections $\mathcal{O}_i^{(1)}(\Omega)$ can be used to determine the gauge couplings. The information about the couplings g_i can be extracted from the mean values of the $\mathcal{O}_i$. This can be seen as follows: Neglecting the quadratic g terms, the value for $d\sigma/d\Omega$ increases faster with increasing g_i for events with large $\mathcal{O}_i^{(1)}(\Omega)$ than for events with smaller $\mathcal{O}_i^{(1)}(\Omega)$. Consequently, the probability for events with large $\mathcal{O}_i^{(1)}(\Omega)$ and, therefore the mean value of $\mathcal{O}_i$, increases with g_i.

Detector and hadronization effects can be included in the determination of the couplings by comparing the measured mean value $\langle \mathcal{O}_i(\Omega) \rangle$ to the mean value extracted from a full Monte Carlo simulation, where samples with different anomalous couplings are generated using a reweighting technique (see Sect. 5.2). For large values of g_i, the contribution from the quadratic terms reduces the sensitivity of an analysis based on only the mean values $\left\langle \mathcal{O}_i^{(1)} \right\rangle$ of the linear terms. This can be mitigated either by using an iterative approach, were $S_0(\Omega)$ is recalculated in each step, and the g_i reflect the additional contributions to the gauge couplings compared to the previous iteration, or by including of the mean values $\left\langle \mathcal{O}_{ij}^{(2)} \right\rangle$ of the quadratic terms. The second approach has the additional advantage that the second-order terms can be used to resolve ambiguities of an analysis based on only the first-order terms.

The OPAL [34] and ALEPH collaborations[39,40] use the mean values of the Optimal Observables to derive limits on anomalous gauge couplings. The DELPHI collaboration uses the distribution of the Optimal Observables in a likelihood approach to determine limits on the couplings.[41] The L3 collaboration determines limits on anomalous gauge couplings using a binned maximum-likelihood fit to the production and decay angles in W-pair events,[42] and a likelihood fit to the distribution of the Optimal Observables as a cross check.[43]

3.1.2. *Results*

The gauge couplings can be extracted either by fitting one of the three couplings, while keeping the other two at their Standard-Model predictions, or by simultaneously fitting two or three couplings (in the fit of two couplings, the third coupling

is fixed to the lowest-order prediction of the Standard Model). These fits include information from the total cross section, and from the angular distributions in W-pair, single-W, and single-photon events. A preliminary analysis from the ALEPH

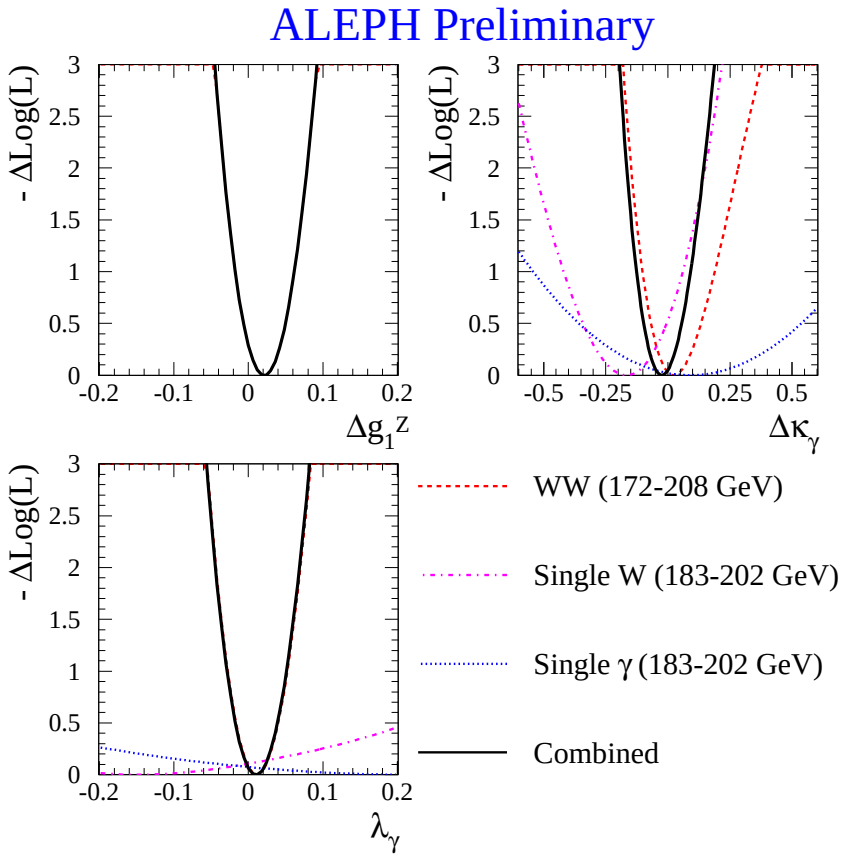

Fig. 16. Dependence of the likelihood on triple-gauge couplings of W bosons.

collaboration,[39] fitting only one coupling at a time, is given in Fig. 16 in terms of the dependence of the log-likelihood on the couplings. The plot also indicates the separate contributions of the W-pair, single-W, and single-photon components to the likelihood. The results are clearly dominated by the contribution from from W-pair events, except in the determination of $\Delta\kappa_\gamma$, where the contribution from single-W events is also important. The contribution of single-W events is especially important in the two- and three-parameter fits, where they help to reduce the correlation between parameters. Figure 17 shows the results of the two- and three-parameter fits to the same data.[39] The preliminary results from all 4 LEP collaborations, [31] and their combined one-parameter fits, are shown in Fig. 18 and

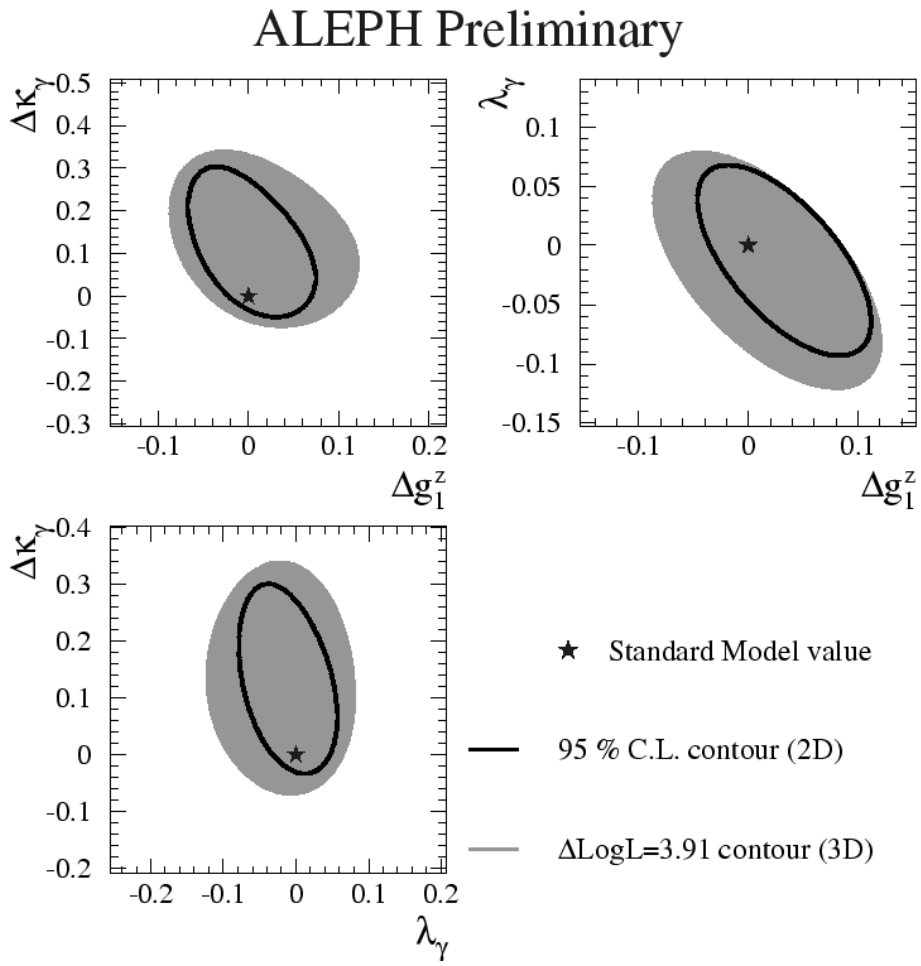

Fig. 17. Contours of 95% confidence for simultaneous fits of two gauge couplings, and projections of the 95% confidence volume for a simultaneous fit to all three parameters (shaded region).

in Table 1.

The experimental results can be compared to the Standard-Model loop corrections, to the gauge couplings, and to expectation for extensions of the Standard Model.[32] The one-loop corrections are of the order $\Delta\kappa_\gamma \simeq (4.1 - 5.7) \times 10^{-3}$.[44] In the minimal supersymmetric extensions of the Standard Model (MSSM), additional loop corrections contribute to the gauge couplings.[32] These are typically of the same size as the predictions from the Standard Model, but, for specially chosen parameters, the contributions can be enhanced and can get as large as $\Delta\kappa_\gamma \simeq 1.7 \cdot 10^{-2}$.[45] Contributions to gauge couplings from additional heavy gauge bosons (Z′) are suppressed by a factor m_W^2/Λ^2, where Λ is the scale associated with the new gauge boson. Only through delicate construction is it possible to invent

Table 1. Preliminary results of the combined LEP fits to triple gauge couplings of the W boson. Given are the 68 % and 95 % C.L. intervals. In each case, only the listed parameter is varied, while the others are kept at the Standard-Model predictions.

Parameter	68% C.L.	95 % C.L
g_1^Z	$0.990\ ^{+0.023}_{-0.024}$	$[0.944, 1.035]$
κ_γ	$0.896\ ^{+0.058}_{-0.056}$	$[0.786, 1.009]$
λ	$-0.023\ ^{+0.025}_{-0.023}$	$[-0.069, 0.026]$

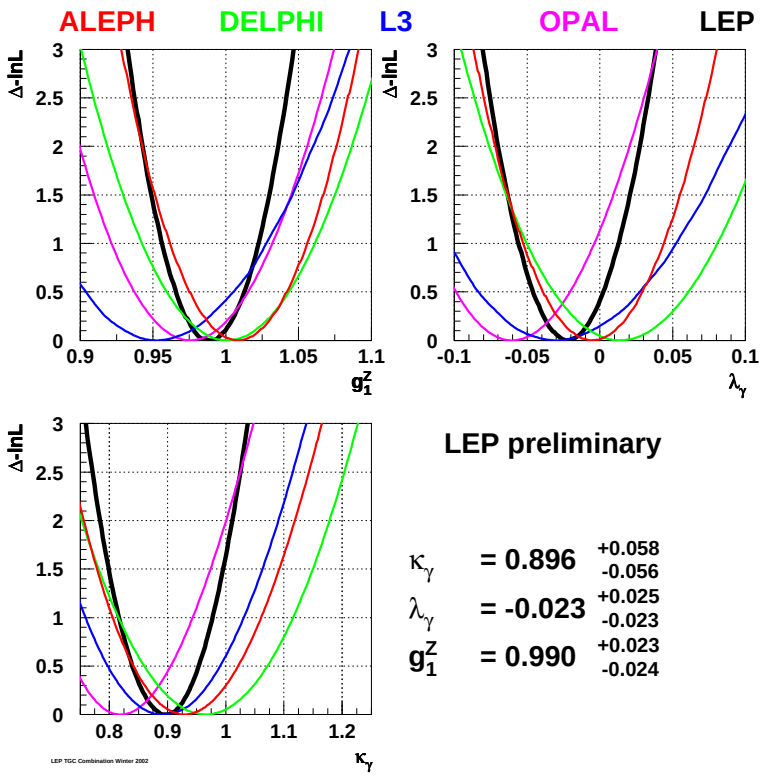

Fig. 18. The combined one-parameter fits to triple-gauge couplings of the W boson.

models with heavy gauge bosons that are consistent with LEP-I data, and have significant contributions to the gauge couplings.[32]

The gauge boson couplings influence quantities such as the partial width of the $Z^0 \to f\bar{f}$, the branching ratio $B(b \to s\gamma)$, and, through loop contributions, the anomalous magnetic-moment of the muon. The impact on the partial width of the

Table 2. Preliminary combined LEP results on neutral triple gauge-boson couplings. Shown are the 95 % C.L. limits. In each case, only the listed parameter is varied, while the others are kept at their Standard-Model values.

Parameter	95 % C.L
h_1^γ	$[-0.056, +0.055]$
h_2^γ	$[-0.045, +0.025]$
h_3^γ	$[-0.049, +0.008]$
h_4^γ	$[-0.002, +0.034]$
h_1^Z	$[-0.13, +0.13]$
h_2^Z	$[-0.078, +0.071]$
h_3^Z	$[-0.20, +0.07]$
h_4^Z	$[-0.05, +0.12]$

Parameter	95 % C.L
f_4^γ	$[-0.17, +0.19]$
f_4^Z	$[-0.31, +0.28]$
f_5^γ	$[-0.36, +0.40]$
f_5^Z	$[-0.36, +0.39]$

Z^0 can be used to determine limits on anomalous gauge-boson couplings from fits to the precision data on the Z^0. This yields:[46]

$$\Delta\kappa_\gamma = 0.016 \pm 0.019 \quad \Delta g_1^Z = -0.017 \pm 0.018.$$

In the fit gauge couplings, all but the one being fitted are set to their Standard-Model predictions. However, these indirect limits on anomalous gauge-boson couplings depend on assumptions such as scales and form factors of the processes in question. They therefore provide tests of the gauge couplings only in specific models.

3.2. *Neutral Triple-Gauge Couplings*

The triple gauge-boson couplings $Z^0\gamma Z^0$, $Z^0\gamma\gamma$ and $Z^0Z^0Z^0$ vanish at lowest-order in the Standard Model. Loop contributions to these vertices are of the order of 10^{-4}.[47] Experimentally, the existence of such gauge couplings can be inferred from the total cross section and angular distributions of Z^0Z^0 and $Z^0\gamma$ final states. The $Z^0\gamma$ final state is sensitive to the $Z^0\gamma Z^0$ and $Z^0\gamma\gamma$ vertices. The most general description of such interactions that is compatible with Lorentz and electromagnetic gauge invariance contains eight independent parameters (h_i^V, $i = 1..4$, and $V = \gamma, Z^0$). The ZZ final state is sensitive to the $Z^0Z^0Z^0$ and $Z^0Z^0\gamma$ vertices. In this case, the couplings can be parametrized using four independent parameters f_i^V, $i = 4, 5$, and $V = \gamma, Z^0$. The parameters h_i^V and f_i^V are in general independent of each other. Both t f_i^γ and h_i^Z are used to parametrize couplings at a $Z^0Z^0\gamma$ vertex, but in one case the vertex involves two real Z^0 bosons, and in the other case it involves a real Z^0 boson and a real photon.

Preliminary combined results for the h and f parameters from LEP experiments [31] are shown in Table 2 for fits to single parameters, while keeping all other parameters fixed at their Standard-Model values. Figure 19 shows examples of fits where two parameters are fitted simultaneously, while the other parameters are kept at their Standard-Model predictions. For neutral gauge-boson couplings, the precision is about an order of magnitude worse than for gauge couplings of the W.

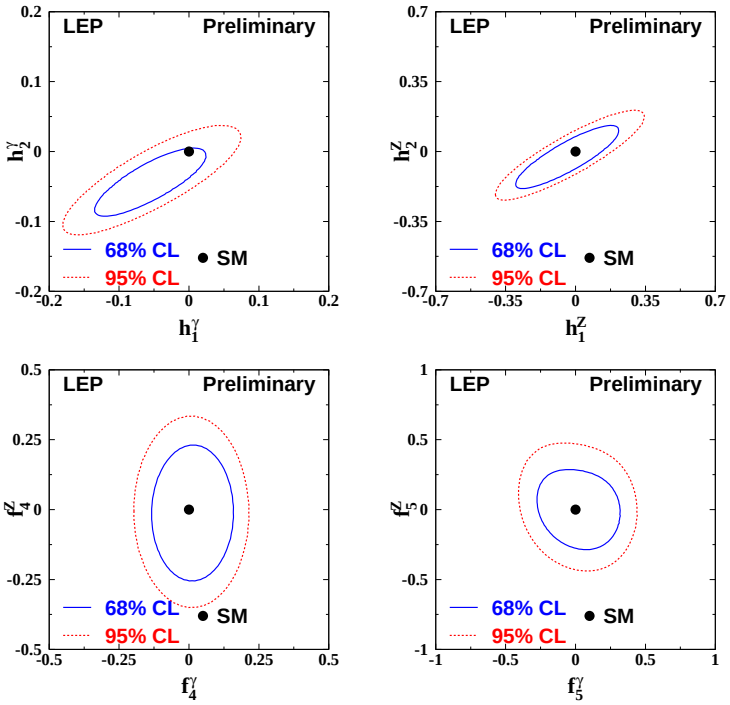

Fig. 19. Contours for 68 % and 95 % confidence regions for the simulaneous fit of the two neutral gauge couplings, while the others are kept at their Standard-Model values.

3.3. *Quartic Gauge Couplings*

Due to the non-abelian nature of the electroweak interaction, the Standard Model predicts finite quartic gauge couplings $W^+W^-W^+W^-$, $W^+W^-Z^0Z^0$, $W^+W^-Z^0\gamma$ and $W^+W^-\gamma\gamma$. These do not play a significant role at LEP energies, but will be important at the LHC[49] and at any future TeV e^+e^- linear collider.[48] At LEP-II, the study of $W^+W^-\gamma$ and $\nu\nu\gamma\gamma$ final states can be used to infer the $W^+W^-Z^0\gamma$ and $W^+W^-\gamma\gamma$ couplings. The coupling $Z^0Z^0\gamma\gamma$, which is not contained in the Standard-Model Lagrangian, can be studied in $Z^0\gamma\gamma$ events. Figure 20 shows the relevant Feynman diagrams. The observation of $W^+W^-\gamma$ events has been used to set the first direct limits on anomalous quartic gauge couplings.[50,51] However, the indirect limits on anomalous quartic couplings derived from the value of Δr obtained from the precise LEP/SLD Z^0 data[52] are significantly better than the limits from the direct measurements at LEP-II.

4. Kinematic Reconstruction of W-Pair Events

The observables in W-pair decays are the jets from hadronically decaying W bosons and the charged leptons from leptonic W-boson decays. This section describes how

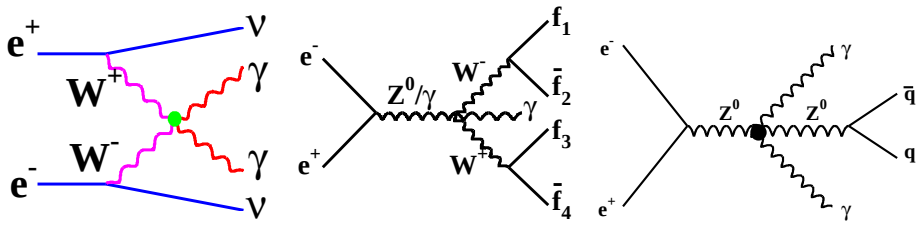

Fig. 20. Feynman diagrams for quartic gauge couplings contributing to the $\nu\nu\gamma\gamma$, $W^+W^-\gamma$ and, $Z^0\gamma\gamma$ final sates.

the data can be used most effectively to extract information on the mass of the W boson in each event. To motivate the need for kinematic reconstruction of the events, we first discuss the simpler case of semileptonic W-pair decays. In the ideal case, the mass of the hadronically decaying W in a $W^+W^-\rightarrow q\overline{q}\ell\overline{\nu}_\ell$ event can be calculated exactly from the invariant mass of all its decay products. Since the jets are formed through the addition of the four momenta of the jet fragments (see Section 1.5), the invariant mass of the two jets in the event, in principle, equals the invariant mass of all the particles from the hadronic W decay (the charged lepton and the unobserved neutrino are ignored in the reconstruction of the jet). For a real detector, however, the mass resolution is degraded, largely because of the energy resolution of jets.

Part of the resolution can be regained by imposing the constraints of energy and momentum conservation in each event. This can be done in a kinematic fit to the final state. However, the simplest approach is to scale the jet-pair mass by the ratio of the beam energy to the sum of the energies of the two jets. This is equivalent to scaling the jet energies and momenta of both jets by the same factor to make the energy of the reconstructed W equal that of the beam. However, it should be recognized that the energies of the two W bosons in an event do not exactly equal the beam energy, because of the natural width of the W, and the possibility of initial-state radiation.

Figure 21 shows the invariant mass of the jet pair in semileptonic events for a "perfect detector" (ideal process), and for the full simulation of the OPAL detector, both with and without scaling to beam energy. (For the perfect detector, it was assumed that all particles from W decay are measured correctly. The invariant mass of the two jets then equals the mass of the hadronically decaying W boson, assuming energy and momentum conservation in the hadronization process.) The line shape for the perfect detector is characterized by the natural width of the W, and reflects the ultimate mass resolution. Not surprisingly, the invariant mass determined from the two reconstructed jets has a very broad distribution, but part of the resolution is regained through a rescaling of the mass. More sophisticated approaches implement the constraints of energy and momentum conservation to improve mass resolution, and will be discussed in the following section. The distribution of the scaled mass in Fig 21 is observed to be biased towards larger masses. This is due to the mass

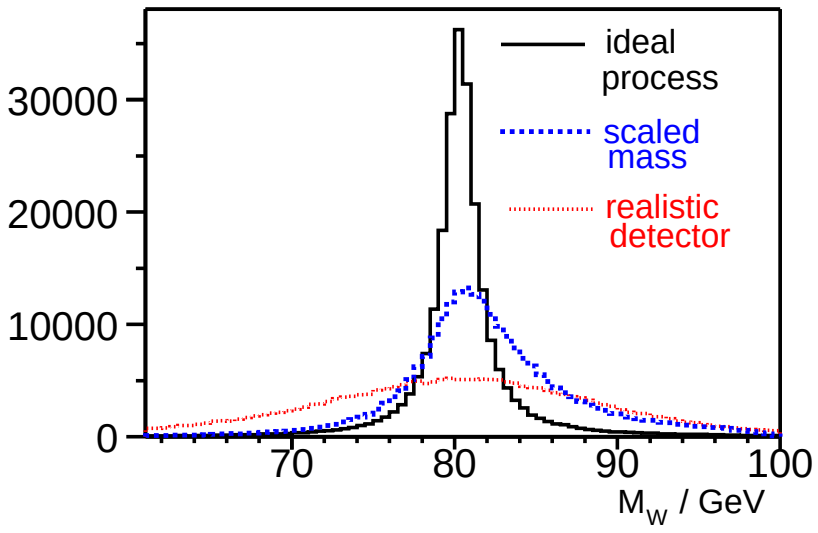

Fig. 21. Mass of the hadronically-decaying W in semileptonic events, calculated from the jets for the ideal case (all particles are measured perfectly), and for a realistic detector, both with and without rescaling to the beam energy. The Monte Carlo events were generated at a center-of-mass energy of 200 GeV.

rescaling of events that contain initial-state radiation, and will be discussed in Section 4.2.

4.1. *Kinematic Fiting*

A kinematic fit can be used to include energy-momentum constraints in any event, and thereby improve the reconstruction of the W mass. In such a fit, the values of the momenta and energies of the jets and leptons are modified within their experimental uncertainties, subject to the desired constraints. Technically, this is achieved through minimizing a $\chi^2 = \mathbf{x}\mathsf{V}\mathbf{x}^T$, where the vectors $\mathbf{x}$ contain the measured information for of the jet and lepton variables, and V is the covariant matrix for their uncertainties and correlations.[53] The constraints can be included either through Lagrange multipliers, or through "penalty" functions that add contributions to the χ^2 if the constrains are not fulfilled (e.g., $(\sum E_{fit} - E_{cm})^2/(\delta_E)^2$, where δ_E is the uncertainty in E_{fit}, and E_{cm} is the value to which the fitted energy E_{fit} should be constrained.)

Assuming a known lepton mass, the energies and momenta of the charged leptons can be described by three variables. In the case of jets, this is more complicated since the jet mass is not well defined, but has to be determined via the jet algorithm. In principle, this can be varied in the fit, but this leads to instability of the

fits. In practice, the jet mass is either fixed in the fit or the $\beta = p/E$ of the jet is kept constant. The components of the vector $\mathbf{x}$ that describe the energies and momenta of a lepton or jet are typically chosen in a way that makes it possible both to treat the errors as Gaussian, and to minimize their correlations. Reflecting the cylindrical symmetry of the detector two of the variables define the azimuthal and polar directions, and the third gives the magnitude of the momentum. The optimal choice for the third variable depends on the flavor of the particle. For electrons, for which the energy is measured in the calorimeter, the energy is most appropriate. For muons, the momentum is measured by the curvature of the trajectory in a magnetic field, making $1/p$ a better choice. For jets, the situation is less clear, and typically either p or $\ln p$ are used in the fits.

Constraints of total energy and momentum conservation are applied in all fits. These are referred to as 4C fits, because of the presence of the four kinematic constraints. In addition, the constraint that both W bosons have the same mass can be applied (5C fit). This is equivalent to requiring that each W boson has half of the center-of-mass (or beam) energy. The constraint does not reflect the exact underlying kinematics, but since the resolution of the kinematic fit is comparable to the natural width of the W boson, it is a useful constraint to impose, if there is interest only in the average W mass in the event. It is also possible to constrain both W masses to some fixed values (6C fit). This is useful for determining the χ^2 of the fit as function of the W mass, which in turn can be used to calculate the probability of observing the given event as a function of the W mass. Combining such probability distributions from many events, can provide another measure of M_{W} and its uncertainty.

Semileptonic W-pair events contain a neutrino that cannot be measured directly. The three components of the neutrino momentum can therefore be taken as free parameters, reducing the effective number of constraints of the fit to two (for the 5C fit) or one (for the 4C fit). Technically, the fits are more stable when the momentum constraint is used directly to calculate the neutrino momentum (from the missing energy), instead of leaving the neutrino momentum as a free parameter, and then imposing the constraint via a Lagrange multiplier or a penalty function. For the case of semileptonic W-pair decays into a τ, ν_τ, and two jets, the analysis is more complicated because the additional neutrino (or neutrinos if the τ decays leptonically) from the τ decay. However because of the large large momentum of the τ, the direction of the τ can be estimated simply from the direction of its decay products, but its energy has to be treated as a free parameter. It can be shown that, in this case, the 5C fit is equivalent to fitting the two jets to the constraint that the W has the beam energy. The measured direction of the τ does not affect the value of the W mass, and is used only to find the energy of the τ and the momentum of the ν_τ that fulfill all the constraints.

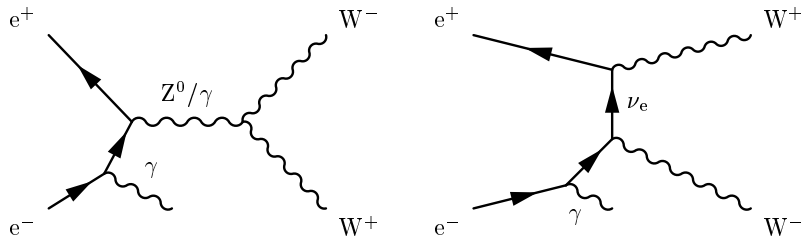

Fig. 22. Feynman diagram of an event with initial-state radiation.

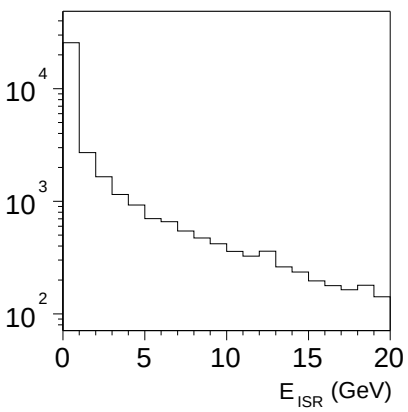

Fig. 23. Energy of the initial-state photons simulated with KoralW.

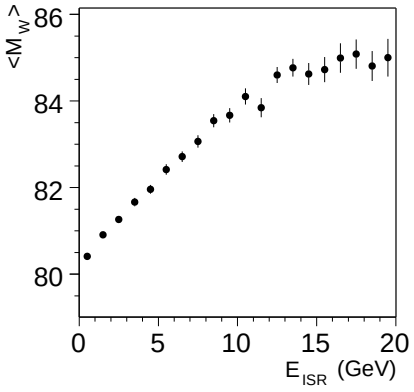

Fig. 24. Average reconstructed mass for semileptonic W-pair decays versus the energy of the initial-state photon.

4.2. *Initial-State Radiation*

The kinematic fit assumes that the sum of energies of the W-pair decay products is equal to the center-of-mass energy. Of course, this is not true when a photon is radiated by the electron or positron prior to the creation of the W pair (see Fig. 22). The energy distribution of such initial-state photons (E_{ISR}), simulated with the KoralW program, is shown in Fig. 23. In the fit, the center-of-mass energy is assumed to be the same as the energy of the W^+W^- system, which means that the reconstructed energy of the jets (and of the lepton) will tend to be biased to larger values. As shown in Fig. 24, this causes an overestimation of the W mass by about 0.5 GeV, and must be taken into proper account. Because the initial-state photons are radiated mainly at small angles (along the beam pipe), and are therefore not observed in the detector, the effect of such ISR on the mass reconstruction can be considered in a relatively straightforward statistical manner in the determination

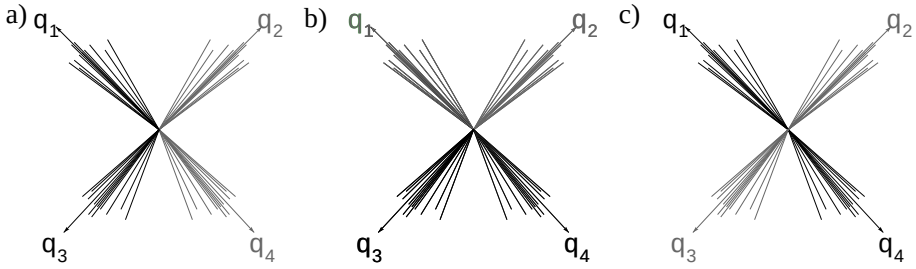

Fig. 25. Possible ways to combine four jets into two W bosons. The two corresponding to each W are marked by the same shading.

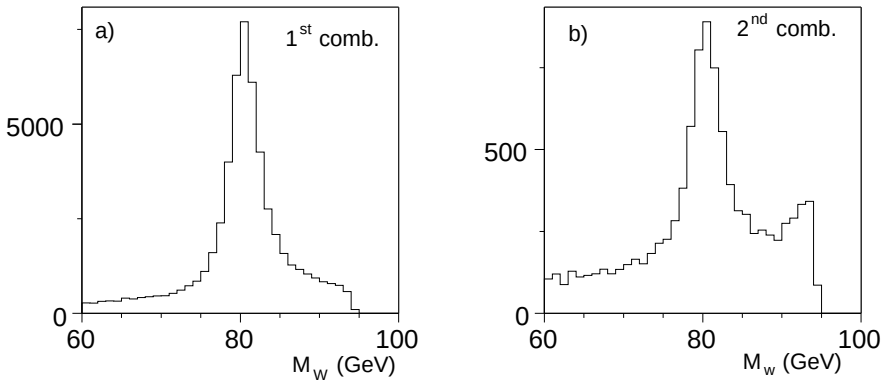

Fig. 26. Mass distribution for the combination with the highest fit probability, and the next highest probability if $P_2 > 1/3 \times P_1$.

the W mass, and will be discussed in Section 5.

4.3. *Jet Pairing*

In all-hadronic W-pair decays, there are three possible ways to combine the four jets into two W bosons. Figure 25 illustrates the three combinations. One way to decide which of the combinations is best for determining the mass is to convert the 5C kinematic χ^2 fits into fit probabilities. The combination with the highest probability is most likely to be the correct combination. But the fit with the next highest fit probability often carries useful information about the W mass. Figure 26 shows the mass distribution from the 5C fit for the combination with the highest fit probability, and for the combination with the next highest fit probability, provided it has at least 1/3 of the probability of the best fit. To ensure a reliable result, only fits with $P > 0.01$ are used for reconstructing the mass. Monte Carlo simulations indicate that 90 % of the events yield the correct combination among those chosen

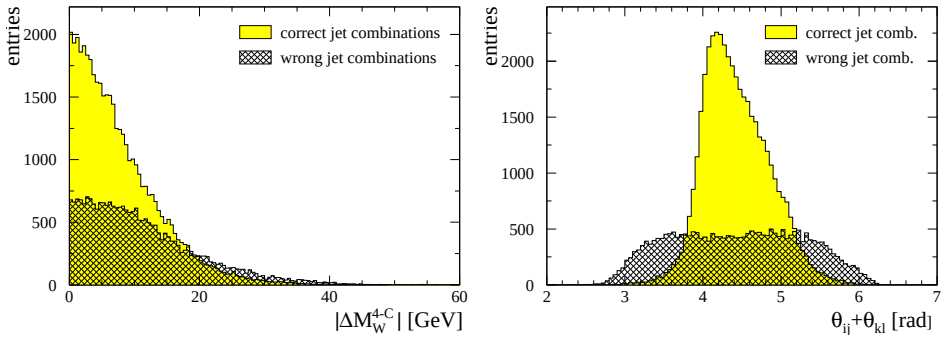

Fig. 27. Distributions used to distinguish between the right and wrong jet combination in four-jet events.

in Fig 26.

Other techniques can be used to improve the probability of finding the correct jet pairing. For the analysis of the data at $\sqrt{s} = 189$ GeV, the OPAL collaboration, for example, used a likelihood discriminator based on:

- The difference between the two W masses (ΔM_W^{4C}) obtained in 4C fits that used only energy and momentum conservation but not the equal mass constraint.
- The sum of the two dijet opening angles $\theta_{ij} + \theta_{kl}$ in the laboratory frame.

Only combinations that had a 5C fit probability greater than 0.01, and a fitted mass in the range 65 GeV $< M_W^{5C} <$ 90 GeV, were considered in the analysis. Figure 27 shows the value of ΔM_W^{4C} and $\theta_{ij} + \theta_{kl}$ for the right and the wrong combinations. The plot contains more right than wrong combinations because most wrong combination do not fulfill the requirement on fit probability and fitted mass (M_W^{5C}). The combination with the highest likelihood is correct in 89 % of the cases. The output of the jet-pairing likelihood is correlated with the mass resolution. Figure 28 shows the mass distribution for the published OPAL data and the Monte Carlo prediction in bins of jet-pairing likelihood.[54] Clearly, both the mass resolution and background fraction improve with increasing values of the jet-pairing likelihood. This information can also be used to strengthen the statistical power of the final mass determination.

The information from the angles between jets is also correlated with the W mass, and it can therefore bias events with a high jet-pairing likelihood towards the reference mass used in the construction of that likelihood. To illustrate this effect, Fig. 29 shows the truncated mean of the difference of the reconstructed W mass (M_{rec}) and the two-parton mass (M_{part}) for events with $\log y_{45} < -6$ and a jet-pairing likelihood greater than 0.6, as a function of the W mass used to generate the Monte Carlo sample (M_{gen}). The truncated mean was calculated only for events in which the parton and reconstructed W mass agreed within 5 GeV.

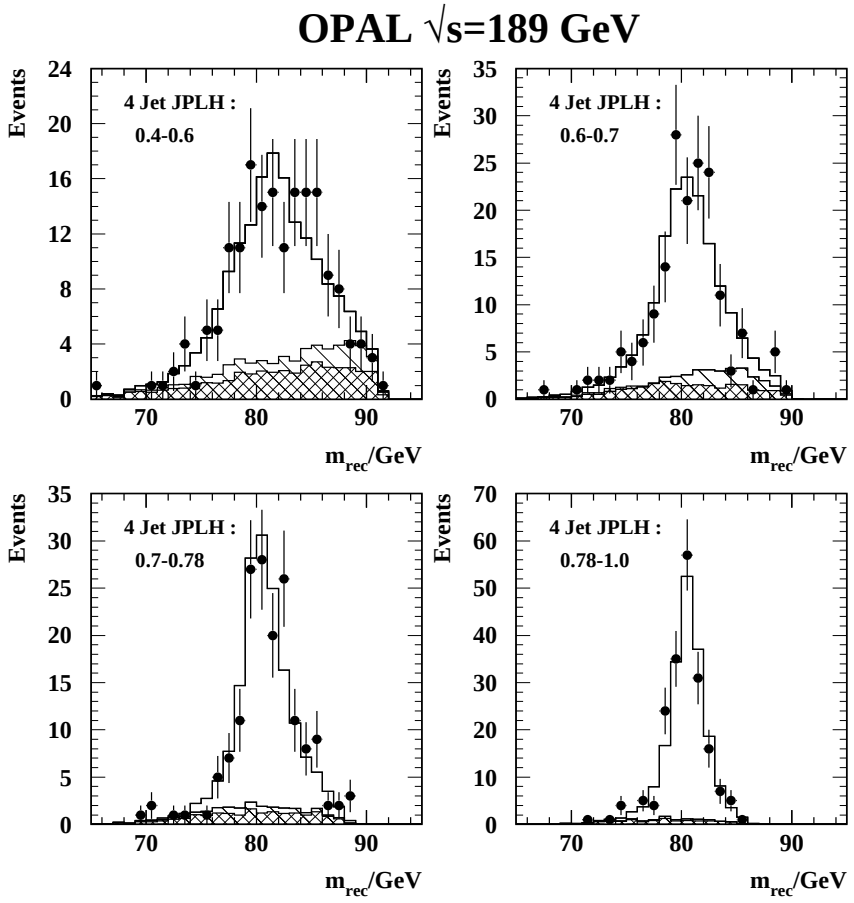

Fig. 28. Fitted W mass in bins of the jet-pairing likelihood (JPLH). The points are the OPAL results for a center-of-mass energy of 189 GeV, and the solid lines show the prediction from Monte Carlo. The contribution from background (other than W-pairs) corresponds to the cross-hashed histograms, and the contribution from wrong jet pairing as singly-hashed histograms.

From the slope of the linear fit, it can be seen that the mean reconstructed mass (for the selected jet combination) is biased towards the mass used to construct the reference distributions in the jet-pairing likelihood (about 70 MeV per GeV). Biases of this type have to be accounted for in the final extraction of the mass, and, in general, reduce the sensitivity of the analysis. In the extreme circumstance when the fit always returns the reference mass, the analysis would, of course, have no sensitivity.

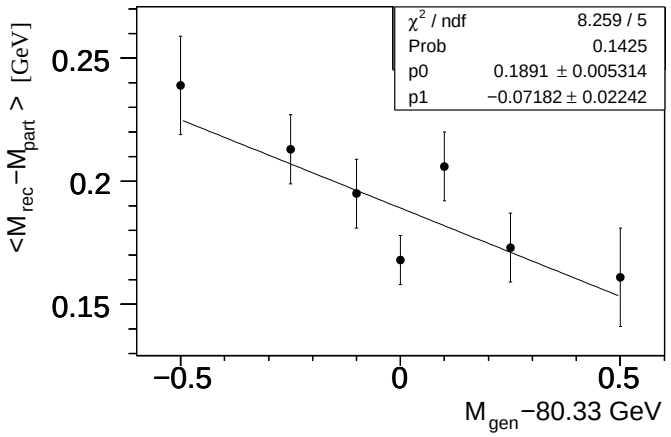

Fig. 29. Truncated mean of the difference between the reconstructed W mass and the two-parton mass for events with $\log y_{45} < -6$, and a jet pairing likelihood greater than 0.6, as function of the W mass used to generate the Monte Carlo sample. The function $< M_{rec} - M_{part} >= P_0 + P_1(M_{gen} - 80.33\ \text{GeV})$ was fitted to the points. A horizontal line ($P_1 = 0$) would correspond to a lack of dependence on M_{gen}. The overall shift is due to the bias from events with initial-state radiation.

4.4. *Five-Jet versus Four-Jet Events*

In the reconstruction of all-hadronic W pairs, it is not possible to know which hadron originates from which W. Consequently, jets often contain hadrons from both W bosons, and, even for the "correct" jet pairing, the reconstructed W will therefore contain energy from both W bosons. (This can be confirmed using Monte Carlo events, where it is possible to match the reconstructed jets to the closest initial quark. The correct jet pairing is then defined as the pairing for which the matched quarks originated from the same W.) In events where a quark radiates an energetic gluon at large angle, the jet algorithm can sometimes assign the hadrons from gluon fragmentation to those from a quark originating from the other W boson. In this kind of event, the reconstructed W mass is unreliable, and produces large uncertainties. Some of these events can be recovered if the jet algorithm is used to reconstruct five instead of four jets. In this case, the hadrons from the gluon can form a separate jet, leading to a clarification of the kinematics.

When hadrons from the two W-decays are associated to the same jet, then even the correct jet pairing will have a fraction of the measured energy assigned to the wrong W boson. For the correct jet combination, Fig. 30 a) shows the fraction of events in which more than 10 GeV of energy is assigned to the wrong W, as function of $\ln y_{45}$ (events with larger $\ln y_{45}$ are more five-jet like, as discussed in Section 1.5). This fraction is shown both for the case when the event is reconstructed as a four-jet and as a five-jet event. Figure 30 b) shows the distribution of incorrectly

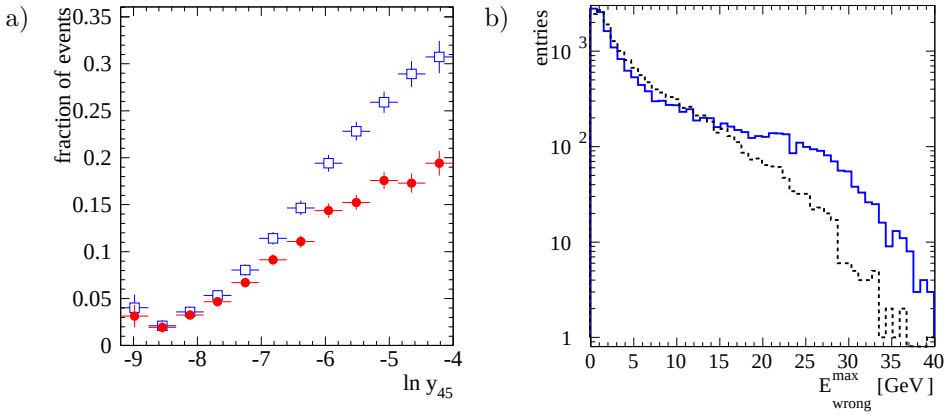

Fig. 30. a) Fraction of events with more than 10 GeV energy assigned to the wrong W boson (for correct jet pairing) as function of $\ln y_{45}$ for four jets (empty boxes) and 5 jets (solid circles). b) Distribution of incorrectly associated energy for events with $\ln y_{45} > -6.8$, for four jets (solid) and five jets (dashed) .

associated energy for events with $\ln y_{45} > -6.8$ (five-jet like events), when these are reconstructed as four-jet and as five-jet events. Clearly, the fraction of events with a large amount of wrongly associated energy is expected to be greater for five-jet like events. This effect is less pronounced if the event is reconstructed as a five-jet instead of a four-jet event. Thus, as stated previously,the problem of wrongly associated energy can be reduced by reconstructing the event as having five jets. There are ten ways to combine five jets into two W bosons, in contrast to only three possibilities for 4 jets. Thus, in selecting the best strategy, the advantage of having less wrongly associated energy in the correct jet pairing has to be weighed against the increased difficulty of finding the right jet combinations.

For five-jet like events with $\ln y_{45} > -6.5$, the OPAL analysis of the 189 GeV data used a different likelihood discriminator to find the right jet combination. This was based on the mass in the 5-C fit, the difference between the two masses in the 4-C fits, the smallest opening angle among two jets associated with the W reconstructed from three jets, and the production angle of the W reconstructed from three jets (relative to the beam axis). The probability of finding the correct jet pairing is $\approx 70\%$. Because the mass from the 5-C fit is used in the jet-pairing likelihood, the mean reconstructed mass of the selected jet pairings is more biased to M_{gen} than in the case of four-jet events. This is shown in Fig. 31.

The question, for which values of $\ln y_{45}$ the event should be reconstructed as a four-jet rather than a five-jet event, and how to pick the right combinations, depends critically on the technique used to calculate the W mass from the specific event information (this will be discussed in Section 5). If the analysis had, for example, only little sensitivity to wrong jet combinations, it would then be possible to reconstruct all events as five-jet events, and to use more than just the “best”

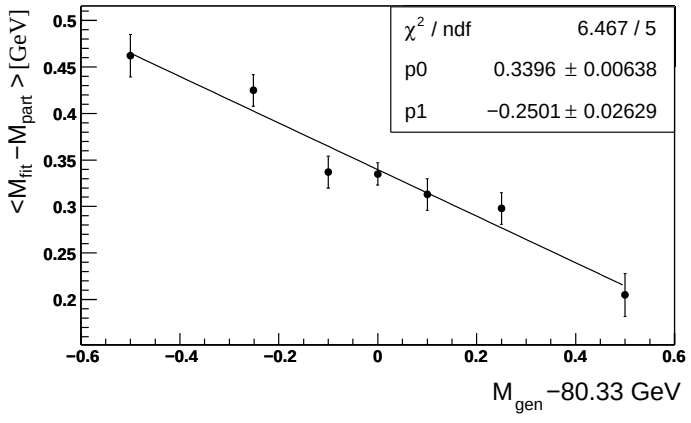

Fig. 31. Truncated mean of the difference between the reconstructed W mass from five jets and the two-parton mass for events with $\log y_{45} > -6$, and a jet pairing likelihoods greater than 0.4, as a function of the W mass used to generate the Monte Carlo sample. The function $< M_{fit} - M_{part}. = P_0 + P_1(M_{gen} - 80.33\ \text{GeV})$ was fitted to the points. A horizontal line ($P_1 = 0$) would correspond to a lack of dependence on M_{gen}.

combination in any event.

5. Determination of the Mass of the W Boson

This section will focus on how the information described previously can be used to determine the value of the mass of the W boson. For the ideal case, namely a perfect detector and exact association of all emitted particles to their respective W bosons, the mass of the W boson and its width can be determined through a fit of the distribution in reconstructed mass to a Breit Wigner function. However, as emphasized previously, quark fragmentation, detector resolution, initial state radiation, event selection, and backgrounds have pronounced impact on M_{W} and Γ_{W}. These effects can be estimated through Monte Carlo calculations that include full detector simulation. The methods used to determine the mass of the W boson can be grouped into three classes, all of which will be discussed in this section. In order to calibrate or to check any specific procedure, the method is applied to many Monte Carlo samples that are of the same size as the data samples, and generated for different values of the W-boson mass.

5.1. *Fitting with an Analytic Function*

On way to calculate the W mass from the reconstructed mass distribution is to fit that distribution with some analytic function. The chosen parametrization must agree with the Monte Carlo predictions for different values of the W mass, if the

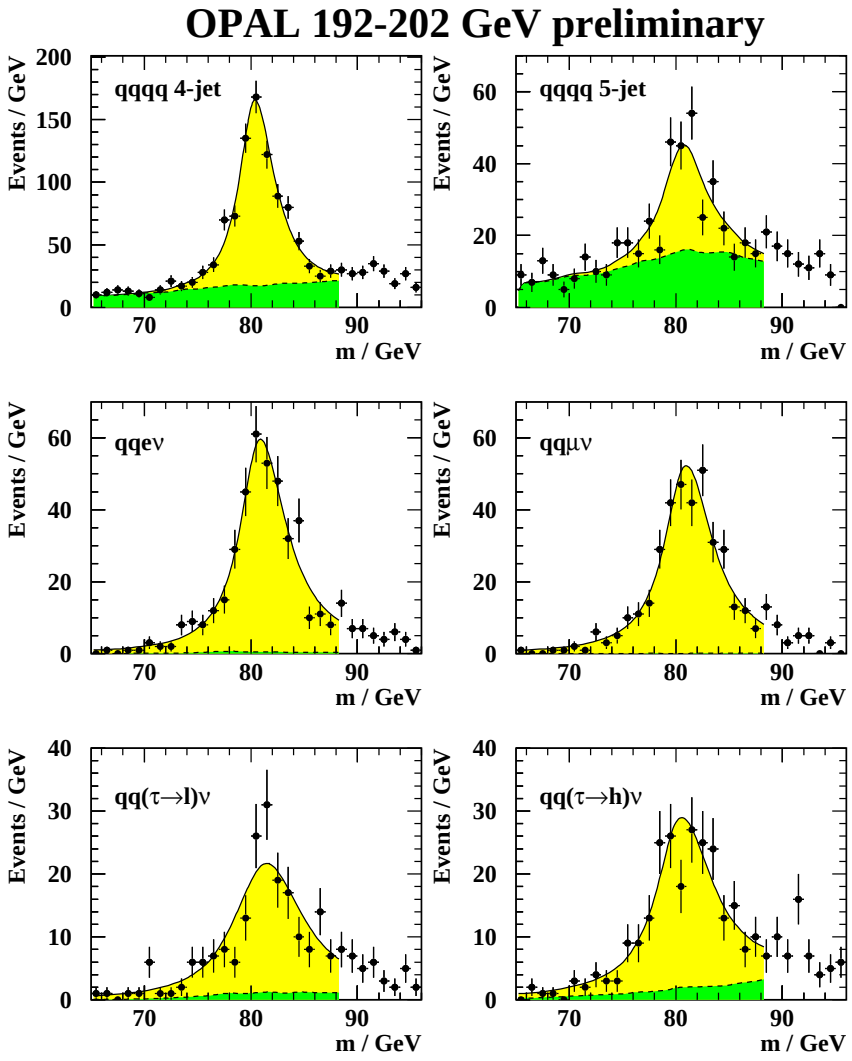

Fig. 32. Comparison of the reconstructed mass (points) with the result of the fits. The dark area indicates the background contribution, which includes for the case of hadronic W-pair decays the impact of wrong jet combinations.

extracted mass is to be reliable. The OPAL collaboration, in a preliminary analysis of the 192-202 GeV data,[55] used a Breit Wigner function for semileptonic W-pair decays, with a maximum at m_0 and, different widths below (Γ_-) and above the

maximum (Γ_+), to fit the distribution in reconstructed mass M_{rec}:

$$S(M_{rec}) = A\frac{M_{rec}^2\Gamma_{+(-)}^2}{(M_{rec}^2 - m_0^2)^2 + M_{rec}^2\Gamma_{+(-)}^2}.$$

where A is a normalization constant. The reason for using a different width above and below the maximum is that the asymmetry from initial state radiation biases the reconstructed mass towards larger values (see Section 4.2). The values of $\Gamma_{+(-)}$ depend on the resolution, and are determined from Monte Carlo for the different lepton channels. The data is fitted with the sum of this (pseudo) Breit-Wigner function and a contribution from background. The background terms are obtained from Monte Carlo, and include the contribution from wrong jet combinations in W^+W^- events when $> 10\%$ of the hadronic energy is assigned incorrectly. Ignoring the normalization, the only free parameter is the maximum M_0 of the Breit-Wigner function. This parameter is closely related to the W mass. Monte Carlo samples generated with different values of the W mass are used to determine a calibration that is used to convert the fitted value of M_0 into a true W mass ($M_{\rm W}$).

In the hadronic channel, the fitting function is a product of $S(M_{rec})$) and a Gaussian $G(M_{rec}) = \exp[-(M_0 - M_{rec})^2/2\sigma^2]$. The width σ of the Gaussian is determined from Monte Carlo simulations that are used to optimize agreement between the analytic function and the Monte Carlo distribution in the reconstructed mass. Figure 32 displays the bests fit to the data for different hadronic and semileptonic channels.

5.2. *Comparison with Monte Carlo Spectra—Reweighting*

The W mass can also be determined by searching for the value of the W mass that provides best agreement between data and Monte Carlo for any variables that are sensitive to the W mass. A direct comparison of data with Monte Carlo includes automatically all effects present in the mass distribution, which are, after all, part of the Monte Carlo simulation, e.g., detector resolution, hadronization, initial-state radiation, background, biases due to jet pairing, etc. It is not possible, however, to generate a set of fully simulated events for each W-mass point used in such a comparison. It is not even feasible to produce a very fine grid (say, 0.02 GeV) of mass points to provide templates as a function of W mass. However, with the help of a weighting procedure described below, it is possible to produce distributions in any observables for arbitrary values of W mass, from just a single sample of Monte Carlo events generated at $M_{\rm W}^{gen}$. This method is particularly valuable for small excursions from $M_{\rm W} = M_{\rm W}^{gen}$. The probability p_i that some observable falls into bin i of a distribution can be estimated from N Monte Carlo events generated at $M_{\rm W}^{gen}$ as:

$$p_i = N_i/\sum_j N_j. = N_i/N$$

where N_j is the number of generated Monte Carlo events falling into bin j. The uncertainty on p_i from the statistics of Monte Carlo is given by

$$\sqrt{\frac{N_i((\sum_j N_j) - N_i)}{\sum_j N_j}} \frac{1}{\sum_j N_j} \approx \frac{\sqrt{N_i}}{\sum_j N_j} = \frac{\sqrt{N_i}}{N}.$$

In any simulation of W-pair events, there is some probability to produce two W bosons that have masses m_1 and m_2. This probability will, of course, depend on the input value M_{W} in the simulation. In the following, we will call $p(\mathbf{x}|M_{\mathrm{W}})$ the probability density for generating an event with a four-fermion configuration $\mathbf{x}$ in a Monte Carlo simulation that uses a value of M_{W} for the W mass. The four-fermion configuration $\mathbf{x}$ can be specified, for example, by the two masses m_1 and m_2 of the W pair. In the most general case, however, $\mathbf{x}$ is given by the four-momenta of the four fermions. The reweighting technique is based on the fact that the difference between Monte Carlo simulations that correspond to different W masses is given by the probability $p(\mathbf{x}|M_{\mathrm{W}})$. We can define a weight function

$$w(\mathbf{x}, M_{\mathrm{W}}^{gen}, M_{\mathrm{W}}^{rew}) = p(\mathbf{x}|M_{\mathrm{W}}^{rew})/p(\mathbf{x}|M_{\mathrm{W}}^{gen})$$

which can be used to obtain a distribution that corresponds to a W mass M_{W}^{rew}, by taking events generated with M_{W}^{gen} and multiplying each by this weight. Basically, this means that the probability to simulate a configuration $\mathbf{x}$ (i.e., W masses m_1, m_2), for a $M_{\mathrm{W}}^{rew} \neq M_{\mathrm{W}}^{gen}$, is obtained through a weighting by w of Monte Carlo events generated at a mass M_{W}^{gen}, thereby generating a distribution for a new mass M_{W}^{rew}. More formally, this can be seen from the fraction of $N_i(M_{\mathrm{W}}^{gen})$ weighted entries in a bin i of any distribution B_i:

$$\frac{1}{N} \sum_{n=1}^{N_i(M_{\mathrm{W}}^{gen})} w(\mathbf{x}_n, M_{\mathrm{W}}^{gen}, M_{\mathrm{W}}^{rew}) = \int p(i, \mathbf{x}, |M_{\mathrm{W}}^{gen}) w(\mathbf{x}, M_{\mathrm{W}}^{gen}, M_{\mathrm{W}}^{rew}) d\mathbf{x} =$$

$$\int p(i|\mathbf{x}) p(\mathbf{x}|M_{\mathrm{W}}^{gen}) \frac{p(\mathbf{x}|M_{\mathrm{W}}^{rew})}{p(\mathbf{x}|M_{\mathrm{W}}^{gen})} d\mathbf{x} = \int p(i|\mathbf{x}) p(\mathbf{x}|M_{\mathrm{W}}^{rew}) d\mathbf{x} = p(i|M_w^{rew}),$$

which is indeed the probability $p(i|M_w^{rew})$ to find an event in bin i for Monte Carlo events generated at M_{W}^{rew}. Here $p(i|\mathbf{x})$ is the probability for an event with a parton configuration $\mathbf{x}$ (generated at M_{W}^{gen}) to fall into bin i, and $p(i, \mathbf{x}|M_{\mathrm{W}})$ is the probability to find an event with a parton configuration $\mathbf{x}$ falling into bin i for Monte Carlo events generated at a mass M_{W}. Using the reweighting ansatz, the number of events in any bin j is given by:

$$N_j(M_{\mathrm{W}}^{rew}) = \sum_{n=1}^{n=N_j(M_{\mathrm{W}}^{gen})} w(\mathbf{x}_n, M_{\mathrm{W}}^{gen}, M_{\mathrm{W}}^{rew})$$

and its error is given by:

$$\Delta N_j(M_{\mathrm{W}}^{rew}) = \sqrt{\sum_n w^2(\mathbf{x}_n, M_{\mathrm{W}}^{gen}, M_{\mathrm{W}}^{rew})}.$$

Using the above, we can define a probability density $p_i(M_{\rm W}^{gen}, M_{\rm W}^{rew})$ of finding a contribution in bin i for mass $M_{\rm W}^{rew}$, based on a Monte Carlo sample generated at a W mass $M_{\rm W}^{gen}$, as follows:

$$p_i(M_{\rm W}^{gen}, M_{\rm W}^{rew}) = \frac{N_i(M_{\rm W}^{rew})}{\sum_j N_j(M_{\rm W}^{rew})} = \frac{\sum_{n=1}^{N_i(M_{\rm W}^{gen})} w(\mathbf{x}_n, M_{\rm W}^{gen}, M_{\rm W}^{rew})}{\sum_j \sum_{n=1}^{N_j(M_{\rm W}^{gen})} w(\mathbf{x}_n, M_{\rm W}^{gen}, M_{\rm W}^{rew})}$$

The reweighting ansatz, can be extended to change both the generated W mass and its width. The parton configuration $\mathbf{x}$ can be described by the two W masses m_1 and m_2. The probability to have an event with W masses m_1 and m_2 at a center-of-mass energy $\sqrt{s'}$ of the W pair, can be approximated by:

$$\mathcal{BW}(M_{\rm W}, \Gamma_{\rm W}, m_1)\mathcal{BW}(M_{\rm W}, \Gamma_{\rm W}, m_2)PS(s', m_1, m_2)ISR(s, s')$$

where $M_{\rm W}$ and $\Gamma_{\rm W}$ are the mass and width of the W boson, and $\mathcal{BW}$ is the Breit-Wigner function:

$$\mathcal{BW}(M_{\rm W}, \Gamma_{\rm W}, m_{\rm W}) = \frac{\Gamma_{\rm W}}{\pi \cdot M_{\rm W}} \frac{m_{\rm W}^2}{(m_{\rm W}^2 - M_{\rm W}^2)^2 + (m_{\rm W}^2 \cdot \Gamma_{\rm W}/M_{\rm W})^2}$$

PS is a factor leading to a decreased probability when the sum $m_1 + m_2$ gets close to the phase space limit of $\sqrt{s'}$. $ISR(s, s')$ gives the probability for radiating an initial-state photon, which leads to the center-of-mass energy $\sqrt{s'}$ of the W pair for an e^+e^- center-of-mass energy of $\sqrt{s}$. The ISR and PS functions do not depend on $M_{\rm W}$, and will therefore cancel in the calculation of any weight. Thus, the relative weight w that we seek can be given by the ratio of the product of two Breit-Wigner functions:

$$w(m_1, m_2, M_{\rm W}^{gen}, \Gamma_{\rm W}^{gen}, M_{\rm W}^{ref}, \Gamma_{\rm W}^{ref}) = \frac{\mathcal{BW}(M_{\rm W}^{rew}, \Gamma_{\rm W}^{rew}, m_1)\mathcal{BW}(M_{\rm W}^{rew}, \Gamma_{\rm W}^{rew}, m_2)}{\mathcal{BW}(M_{\rm W}^{gen}, \Gamma_{\rm W}^{gen}, m_1)\mathcal{BW}(M_{\rm W}^{gen}, \Gamma_{\rm W}^{gen}, m_2)}$$

The L3 collaboration uses the four-momenta of the partons to define the parton configuration $\mathbf{x}$ to calculate the following weights in their analysis of data taken at $\sqrt{s} = 183$ GeV:[56]

$$w(p_1, p_2, p_3, p_4, M_{\rm W}^{rew}, \Gamma_{\rm W}^{rew}, M_{\rm W}^{gen}, \Gamma_{\rm W}^{gen}, s') = \frac{\mathcal{M}^{4F}(p_1, p_2, p_3, p_4, \Gamma_{\rm W}^{rew}, M_{\rm W}^{rew}, \Gamma_{\rm W}^{gen}, s')}{\mathcal{M}^{CC03}(p_1, p_2, p_3, p_4, \Gamma_{\rm W}^{gen}, M_{\rm W}^{gen}, \Gamma_{\rm W}^{gen}, s')}.$$

where $\mathcal{M}^{4F}$ and $\mathcal{M}^{CC03}$ are the the matrix element for producing four partons with four-momenta p_i at a center-of-mass energy $\sqrt{s'}$. $\mathcal{M}^{4F}$ is calculated using the full set of four-fermion diagrams, while $\mathcal{M}^{CC03}$ is calculated from the CC03 diagrams. Here, the reweighting also corrects for the fact that the reference Monte Carlos are generated using a CC03 matrix element.

Figure 33 shows the ratio of two Breit Wigner functions for $M_{\rm W} = 80.0$ GeV and $M_{\rm W} = 80.5$ GeV, as a function of $m_{\rm W}$. In the tails of the Breit Wigner functions, the weights stay close to unity, as long as the difference between $M_{\rm W}^{gen}$ and $M_{\rm W}^{rew}$ is small compared to the width of the W boson. For larger differences between $M_{\rm W}^{gen}$ and $M_{\rm W}^{rew}$, the increase in uncertainty from large weights can be reduced by using Monte-Carlo samples generated at other values of the W mass $M_{{\rm W},k}^{gen}$. Under such

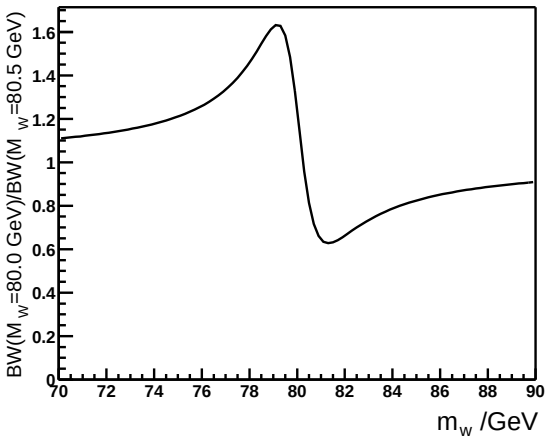

Fig. 33. Ratio of two Breit Wigner functions for $M_{\mathrm{W}} = 80.0$ GeV and $M_{\mathrm{W}} = 80.5$ GeV, as a function of m_{W}.

circumstances, the error on the probability for an entry in bin i for a W mass M_{W}^{rew} can be minimized by using a weighted average of the probabilities calculated from different $M_{\mathrm{W},k}^{gen}$.

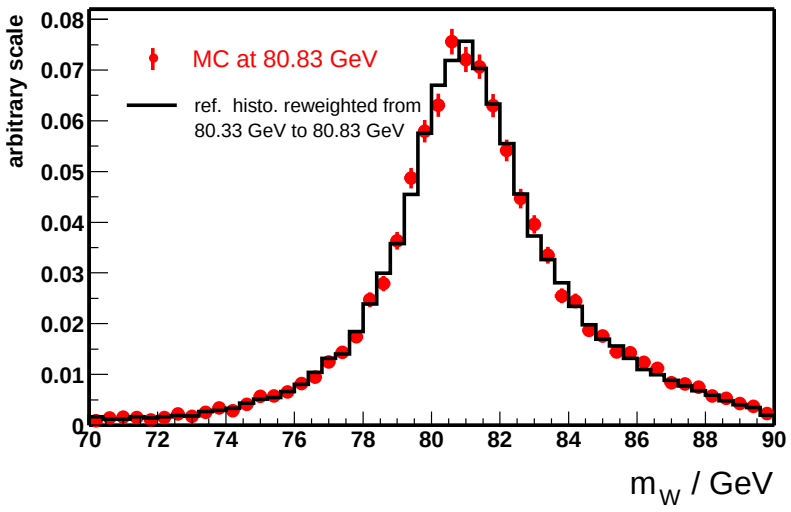

Fig. 34. Comparison of the reconstructed W mass from a Monte Carlo generated at M_{W} =80.83 GeV (points with error bars) with the corresponding distribution from a Monte Carlo generated at M_{W}^{gen} =80.33 GeV and reweighted to M_{W}^{rew} =80.83 GeV (histogram).

Figure 34 shows a comparison of the reconstructed W mass for a Monte Carlo sample generated at $M_{\rm W}$ =80.83 GeV with the corresponding distribution generated from Monte Carlo at $M_{\rm W}^{gen}$ =80.33 GeV, but then reweighted to $M_{\rm W}^{rew}$ =80.83 GeV. Clearly, the reweighted distribution is in excellent agreement with the direct Monte Carlo.

The reweighted distribution can be used in a likelihood fit to extract the mass and width of the W boson. If there is interest only in the mass, the width can be defined using the value from the Standard Model, i.e., $\Gamma_{\rm W} = 3G_F M_{\rm W}^3/(2\sqrt{2}\pi)(1 + 2\alpha_s/(3\pi))$.[3] The simplest approach for a fit is to use a bin size such that the bin to bin fluctuations of the reweighted reference histograms are sufficiently small that they do not affect the significance of the fit. However, this approach uses only the finite bin into which the observable (e.g., the reconstructed mass) falls, and not its exact value, and may thereby limit the statistical power of the data. In their analysis of the 183 GeV data, the L3 collaboration compares two approaches that minimize this effect: [56] In the "box method", the likelihood of observing a given event is calculated using 1000 Monte Carlo events that fall into a box centered around the data point. The box size at the peak of the distribution is typically $\pm$35 MeV. In the tails, it is limited to a maximum value of $\pm$250 MeV, even if the box contains less than 1000 events. In a second approach, a fine binning is chosen, and the histograms are then smoothed with a cubic spline fit. The results from these two methods agree within 15% of their statistical errors.

The ALEPH collaboration uses multi-dimensional distributions in their analysis of $\sqrt{s} = 189$ GeV data.[59] In the four-quark channel, they use the two masses from the 4C fit (requiring energy and momentum conservation, as discussed Section 4.1). In the $qqe\nu$ and $qq\mu\nu$ channels, they use the single mass from a 5C fit (energy and momentum conservation and equal-mass constraint – see Section 4.1), the fitted error on that mass, and the mass of the di-jet system from a 4C fit. (There is a 43% correlation between the mass from the 4C and the 5C fit). Using this 3-dimensional distribution reduces the statistical uncertainty by 14 ± 1% relative to a one-dimensional mass analysis in the $qql\nu$ channel.

The OPAL collaboration separates its 189 GeV data into subsets of different resolution or background fractions.[54] The semileptonic data is analyzed in bins that correspond to the fitted uncertainty. In the four-quark channel, four-jet and five-jet events are treated separately, and the four-jet data is analyzed in terms of bins of different jet-pairing likelihood (see Section 4.3). Figure 35 shows the dependence of the results on the value of y_{45}^{cut}, which determines whether events are treated as four-jet or as five-jet events.[60] Figure 35 a) shows the remaining fraction of four-jet events when all events with $y_{45} > y_{45}^{cut}$ are treated as four-jet events. The expected uncertainty on the mass ($\delta M_{\rm W}$), shown in Fig. 35 b) is based on an integrated luminosity of 183 pb^{-1} for a center-of-mass energy of 189 GeV. The solid circles represent an analysis where the reweighting is done in two classes, one for four-jet events and one for only five-jet events. The stars represent an analysis where the fit for reweighted four jets is done in four bins of

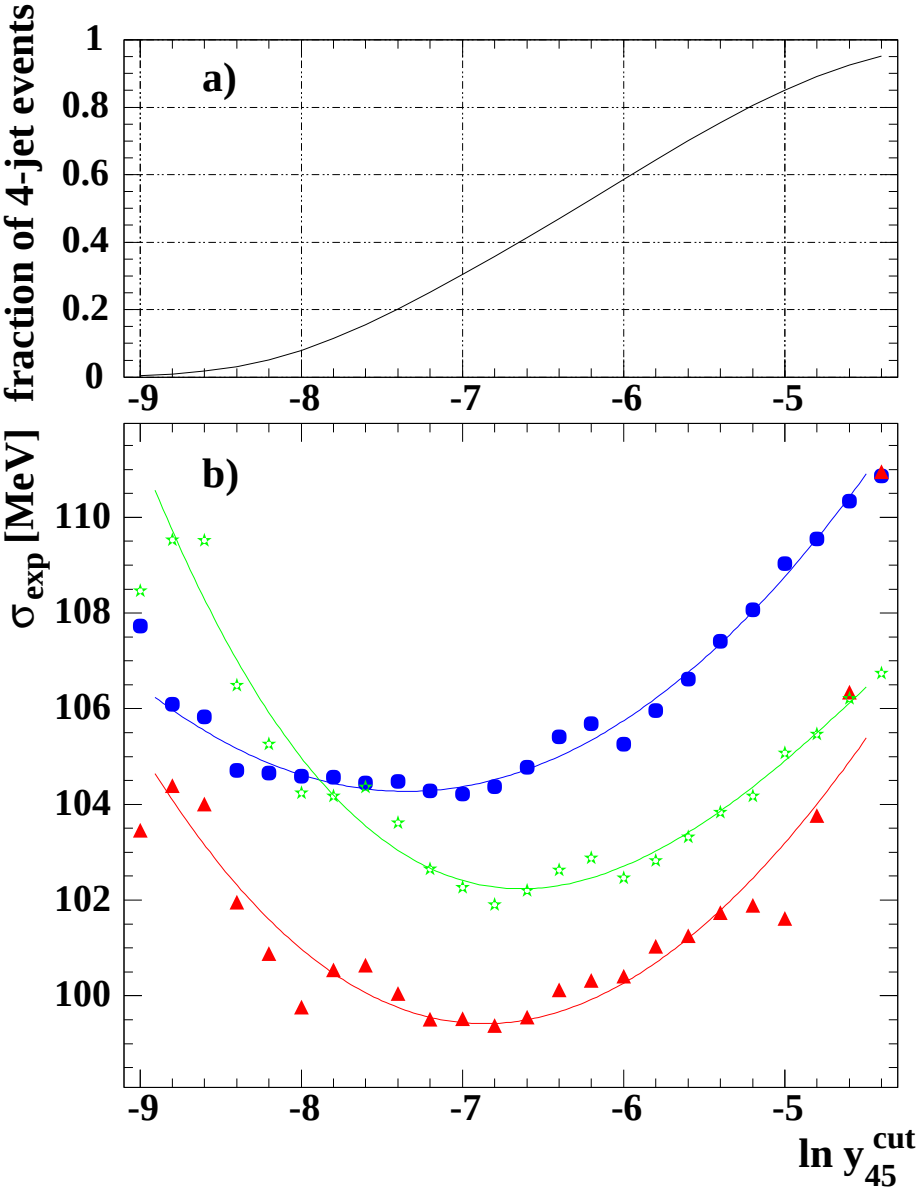

Fig. 35. The dependence of a) fraction of 4-jet events and, b) the statistical uncertainty on the W mass, on y_{45}^{cut}, for the 4-quark analysis described in the text. The solid circles represent an analysis for which the reweighting is done for two classes of events, one for four-jet events and one for five-jet events. The stars represent an analysis where the fit for reweighted four-jets is done in four bins of the jet-pairing likelihood. (Events in different bins have different resolutions and different background fractions.) The triangles indicate the improvement achieved if the jet combination with the second-highest jet-pairing likelihood (Section 4.3) is used as an additional class of events when the fit probability of this combination is greater than 1/3 of the fit with highest probability.

the jet-pairing likelihood. As discussed in Section 4.3, events in different bins have different resolutions and different background fractions. The triangles indicate the additional improvement gained when the jet combination with the second-highest jet-pairing likelihood (see Section 4.3) is used to define an additional class of events for which the fit probability of that combination is greater than 1/3 of the best-fit probability. All distributions have a broad minimum in the range $-8 < \ln y_{45}^{cut} < -6$. The sharper increase at small four-jet fraction, especially for the analysis using four bins for the four-jet events, is due to the fact that the reweighted reference histograms have poor statistics for small four-jet fractions. One can clearly see the improvement in the expected statistical error when the four-jet events are split into more bins, and also when the second-best jet combination is used.

The mass determination at DELPHI is based on a convolution fit, which is described in the following section.

5.3. *Determination of the Event Likelihood—Convolution Analysis*

The mass of the W boson can also be determined from an overall minimization of a product of individual event likelihoods that are calculated from a convolution of a "physics", or signal function, with a resolution function. Here, the total probability to observe a given event is split into two parts: One reflects the probability to observe the quantities derived from some kinematic fit (e.g., the two masses from a 4C fit) when W bosons of mass m_1 and m_2 are produced in an event. This part is given by a resolution function. The other part of the probability, namely that the specified masses m_1 and m_2 are produced in the e^+e^- collision, depends on the mass and width of the W boson (the dynamics). This part of the probability is called the physics function.

The simplest ansatz is that the physics function is given by a Breit-Wigner function in one or two variables, multiplied by a phase space factor, and the resolution function is given by a Gaussian with a central value and width determined from the kinematic fit.

The importance of taking the background into proper account in the event likelihood is crucial, as can be seen by the following example: A single event with a reconstructed mass of 60 GeV can change the log-likelihood by 0.15, if the assumed W boson mass is changed from 80 GeV to 81 GeV, and can therefore affect significantly the final fit. However, the most likely explanation for such an event is that it is due to background, for which the likelihood should not depend at all, or, in the case of a wrong jet pairing in a $\mathrm{W^+W^-}$ event, only weakly, on the assumed mass of the W boson. In the convolution analysis, this option can be implemented by adding a term that does not depend on the W mass, but describes the background.

As discussed in Section 4.2, initial-state radiation shifts the reconstructed mass by a factor $\sqrt{s/s'}$. Since s' is not known on an event-by-event basis, any initial-state radiation can be taken into account through a convolution of a shifted physics

function with the spectrum for initial-state radiation:

$$f(m_w|M_{\mathrm{W}},\Gamma_{\mathrm{W}},s) = \int_0^s f_{noISR}(m_w \cdot \sqrt{s'/s}; M_{\mathrm{W}},\Gamma_{\mathrm{W}},s')ISR(s,s')ds'.$$

where f_{noISR} refers to the physics function before considering the initial-state radiation, and $ISR(s,s')$ is the probability for emitting radiation in the initial state, which reduces the center-of-mass energy of the W-boson pair from $\sqrt{s}$ to $\sqrt{s'}$. Figure 36 shows the dependence of the physics function on M_{W}, before and after

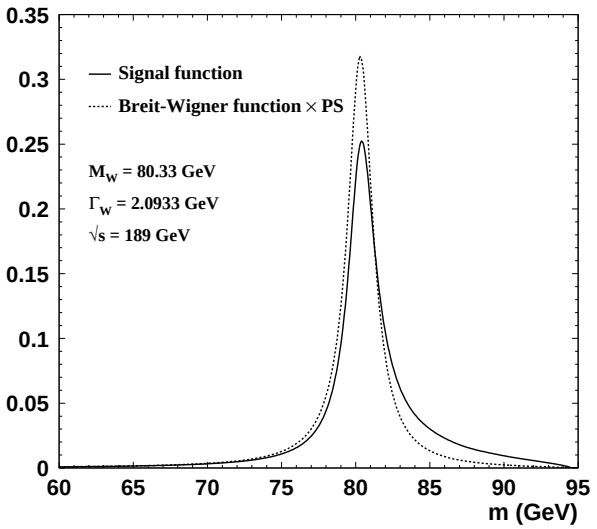

Fig. 36. Physics function before (dotted) and after (continuous) the convolution with initial-state radiation.[61]

the convolution with initial-state radiation. The shift to higher masses as a result of initial-state radiation is visible in Fig. 36. A more natural way to include the effect of initial-state radiation is to convolute the ISR spectrum with a scaled resolution function instead of the physics function, but this is very difficult for an analysis in which the resolution function is calculated separately for each event, basically because of the required computing time.

It is also possible to neglect initial-state radiation at the first stage of analysis, and to correct for the bias at a later step. The DELPHI collaboration followed this approach in their analysis of semileptonic data taken at $\sqrt{s} = 183$ GeV.[57] For the data sample at $\sqrt{s} = 189$ GeV,[58] DELPHI included an ISR correction in their physics function, which resulted in a reduction of ≈ 400 MeV in the bias of the fitted mass.

The uncertainties on reconstructed mass in 5C fits in the $qql\nu$ channel, can be quite asymmetric. For such events, information would be lost if purely Gaussian

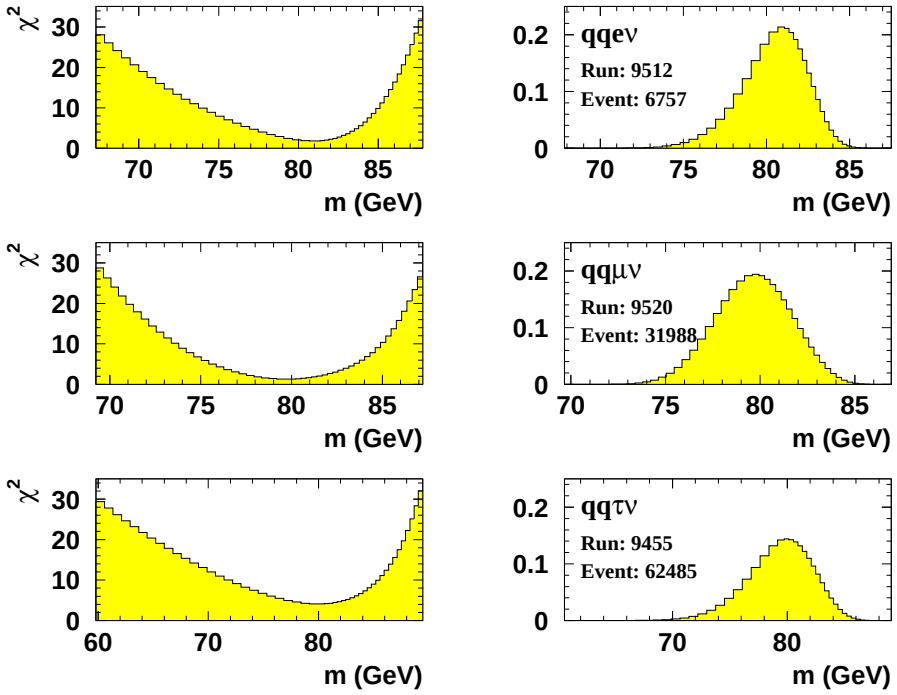

Fig. 37. χ^2 distribution and resolution function as functions of average W mass for three events from the OPAL detector. [61]

errors were assumed for the resolution. In order to treat these kinds of events more correctly, the resolution function can be determined using the dependence of the χ^2 of Sect. 4.1 on m_{W}. This χ^2 dependence is obtained from the 6C fit, in which, in addition to energy and momentum conservation, both W masses are fixed to a specific value. Figure 37 shows examples of the χ^2 dependence and the resolution functions for three $qql\nu$ events in a one-dimensional analysis,[61] where both W masses are fixed and sampled at the same average mass. For these events, one can see the asymmetric nature of the χ^2 dependence.

The contours of equal χ^2 for two events, as a function of the W masses assumed in a scan of 6C fits, are shown in Fig. 38. Clearly, a Gaussian error (determined by a 4C fit) would not be appropriate for describing these events.

The problem of finding the correct jet pairing in the four-quark channel (see Sect. 4.3) can be avoided in a two-dimensional convolution analysis. In this case, the resolution function, which yields the probability that the observed event originates from two W bosons with masses m_1 and m_2, can be calculated from the sum of probabilities for the different jet combinations. From the three possible combi-

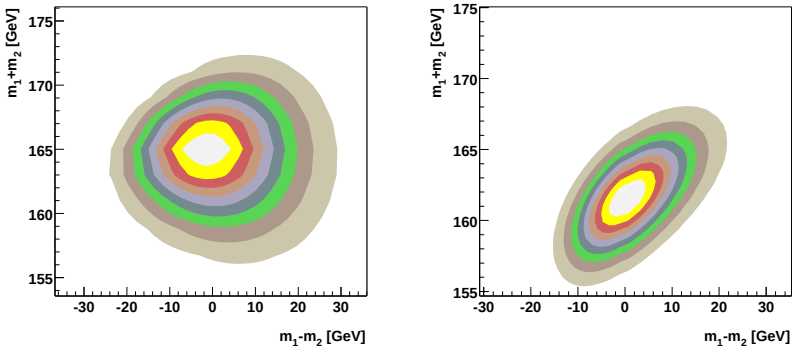

Fig. 38. Two examples of contours of equal χ^2 for the sum and difference of the two masses determined by a scan of 6C fits in semileptonic W pair decays (m_1 is the mass of the hadronically decaying W boson).

nations in four-jet events (and the ten possible combinations in five-jet events), typically, only the right combination contributes significantly to the sum in the region of $m_1 \approx m_2$. Since the convolution of the resolution function with the physics function (a two-dimensional Breit-Wigner function, with a maximum at $m_1 = m_2 = M_{\mathrm{W}}$) dominates this region, and the contribution to the probability from wrong combinations is quite small.

The DELPHI collaboration uses three different jet algorithms (DURHAM, DCLUS and CAMJET) in the analysis of their $\sqrt{s} = 189$ GeV all-jet data[58] to select the jets in a 4C fit. Events for which the DURHAM algorithm gives a value of $y_{45} > 0.002$ (see Section 1.5) are reconstructed as five-jet instead of four-jet events. The resolution function is then determined through a sum over all jet combinations and all jet algorithms, with relative weights reflecting the probability of correct jet pairing. This probability is determined from the jet charge and, in the case of five-jet events, from the transverse momentum of the gluon candidate. The possibility that an event contains initial-state photon radiation along the beam pipe is considered by repeating the kinematic fit using a modified energy and momentum constraint:[58]

$$\sum_i (E, p_x, p_y, p_z)_i = (|p_z^{fit}|, 0, 0, p_z^{fit}).$$

For 16% of the events, such a fit favors a solution with significant momentum emitted along the beam pipe ($|p_z^{fit}|/\sigma_{p_z^{fit}} > 1.5$). For these events, an additional term, using jets from the modified fit, is then included in the calculation of the resolution function. The relative weight of this term is based on the probability for the ISR hypothesis. The inclusion of this extra term improves the expected uncertainty on the mass for these events by 15%. Figure 39 shows the contours of the resolution function for a four-jet event with and without the additional ISR term in the fit. The diagrams show the contours from the two wrong jet combinations at

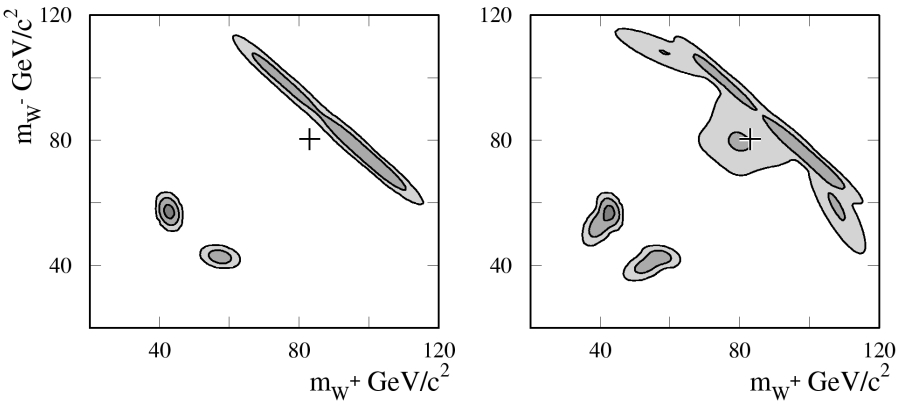

Fig. 39. Contours of the resolution function for a four-jet event without (left) and with (right) the additional term from the fit of the ISR hypothesis .

low mass and away from $m_{\mathrm{W}_+} = m_{\mathrm{W}_-}$, and the contour from the correct solution at $(m_{\mathrm{W}_+} + m_{\mathrm{W}_-})/2 \geq 80$ GeV, which has a significant contribution at $m_{\mathrm{W}_+} = m_{\mathrm{W}_-}$. Due to the initial-state radiation, the correct jet combination favors mass values above 80 GeV, while the inclusion of the additional ISR term gives an additional contribution at $m_{\mathrm{W}_+} = m_{\mathrm{W}_-} \approx 80$ to the physics function.

In a 2-dimensional convolution analysis of hadronic W pairs at $\sqrt{s} = 189$ GeV,[54] the OPAL collaboration uses a slightly different approach: All events are reconstructed as five-jet events using the DURHAM algorithm, independent of their value of y_{45}. As discussed above, jet combinations with large differences between the two reconstructed masses do not have a large effect on the probability in a two-dimensional convolution analysis. However, if an event is reconstructed as a five jet-event, the jet combination where only the gluon is associated wrongly can have contributions to the resolution function close to the diagonal $m_1 = m_2$, when the gluon energy is sufficiently small. The gluon jet is most likely to be combined with another jet in the reduction of five jets to four. All possible jet pairings that differ only in the association of these two jets to the W bosons are grouped together. By construction, the group containing the correct jet combination also contains the combination where only the gluon is associated to the wrong W boson. A special jet-pairing selection was developed using the information from all the jet combinations within a group of jets to suppress the jet combination where only the gluon is associated incorrectly.[54] On average, three combinations are selected, which include the correct combination 92% of the time. A good feature of treating all events as five-jet events is that it avoids the necessity of choosing a value of y_{45} to decide whether an event is treated as a four or a five-jet event.

All convolution analyses use approximations in their estimation of the physics

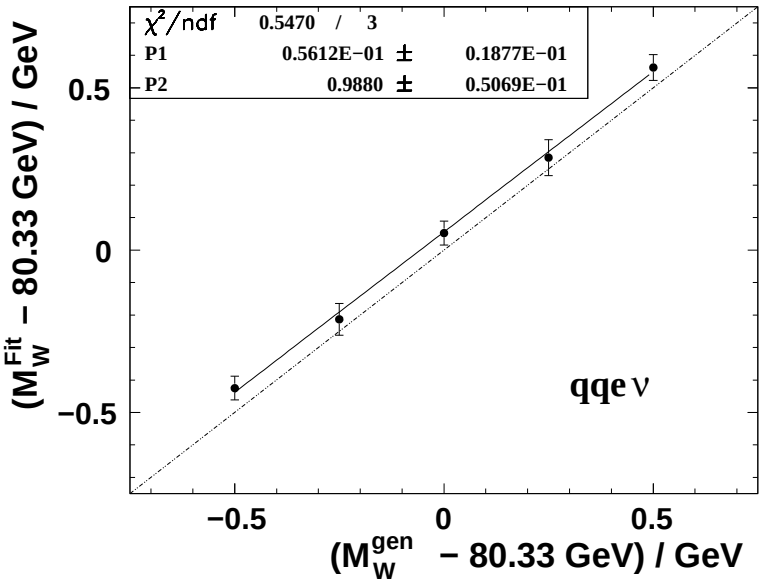

Fig. 40. The extracted mass (M_{W}^{Fit}) as function of the input mass (M_{W}^{gen}) for the convolution fit to semileptonic W-pair decays at $\sqrt{s} = 189$ GeV from OPAL.[54,61]

and resolution functions: The errors on the input variables are treated as uncorrelated Gaussian errors. The jet masses are either fixed in the fit to some initial input values, or they are calculated assuming a constant $\beta = p/E$ given by the initial values of the jet energy and momenta. In reality, both the jet masses and β have uncertainties and complicated correlations with the measured jet energies. Because of this and other approximations (e.g., the complete neglect of ISR in the 183 GeV DELPHI analysis[57]), biases are expected in the extraction of the W mass, and these have to be corrected with the help of some calibration procedure based on Monte-Carlo events.

In comparison with other techniques, the convolution method has the advantage of a more complete treatment of the fit errors on an event-by-event basis. The two-dimensional convolution analyses in the four-quark channel also make it possible to include more jet pairings.

5.4. *Ensemble Tests*

The different techniques to determine the W mass are calibrated and tested using Monte-Carlo event samples. The treatment includes full detector simulation, and uses subsamples comparable in size to those in the data. The calibration response, which is defined by the generated (input) W mass as a function of the extracted mass, is determined from the analysis of such Monte Carlo samples generated at different W-boson masses. As example, Fig. 40 shows the mass correction for the

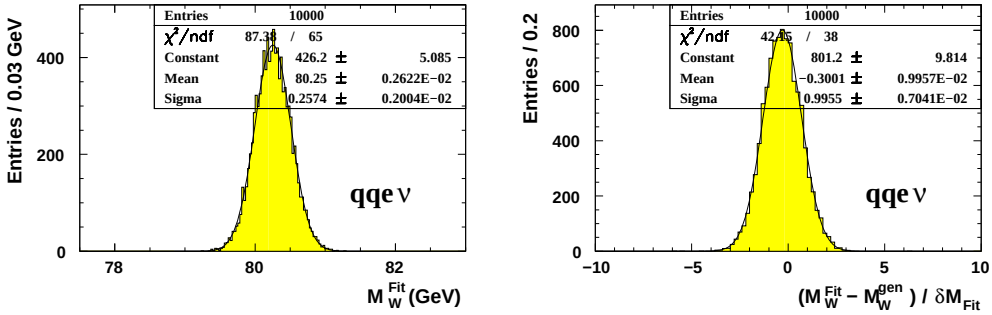

Fig. 41. Example of an ensemble test for the convolution analysis of semileptonic W-pair decays at $\sqrt{s} = 189$ GeV.[61]

convolution analysis in the $W^+W^- \to q\overline{q}e\overline{\nu}_e$ channel (in fact, this is used only as a cross check in the analysis of the OPAL data at $\sqrt{s} = 189$ GeV [54,61]). The masses were determined from the mean value of the results of statistically independent data-sized subsamples generated with a W-boson mass given by M_W^{gen}. The error bars indicate the uncertainty on the mean value. Since the points are consistent with a linear dependence, they were fitted to the function $M_W^{Fit} - 80.33$ GeV $= P_1 + P_2 \cdot (M_W^{gen} - 80.33$ GeV). (The average value of M_W^{gen} was subtracted both from M_W^{gen} and from M_W^{Fit}.) The result is used to correct the extracted value (M_W^{Fit}) to an unbiased measurement. The statistical error on the extracted mass has to be scaled by the inverse slope of the response function to account for the fact that a change in ΔM_W^{Fit} corresponds to a change of $\Delta M_W^{gen} = 1/P_1 \cdot \Delta M_W^{Fit}$.

In mass extraction techniques that use a bias correction to determine the final result, the uncertainty of the correction from limited Monte Carlo statistics has to be taken as an additional source of error. In the case of the reweighting analyses, this kind of bias study is used only as a cross check, and if the result is consistent with no bias, no further correction is required. Nevertheless, in this case, an error of similar size, from statistical uncertainty of the reference distributions used for the reweighting, has to be taken into account.

Monte-Carlo ensembles can also be used to estimate the expected statistical error, and to check whether the error returned in the analysis is a good estimator of statistical uncertainty. Figure 41 shows the distribution of the result of 10,000 data-size Monte Carlo samples and their pull distribution $(M_W^{Fit} - M_W^{gen})/\delta M_W^{Fit}$ from OPAL.[61] The RMS of the distribution of the extracted mass, or the width of a Gaussian fitted to the distribution, can be used as an estimate of the expected statistical error of the measurement. For data samples with low statistics, the error returned for different samples often shows large variations. The precision of the fit fluctuates because different samples contain events with different sensitivity to the measurement. However, the pull distribution can be used to check whether the fitted uncertainty is reasonable. When the uncertainty is estimated correctly, the

pull distribution is a Gaussian centered at zero, with a width of unity. A different central value indicates a bias, while a larger (or smaller) width indicates a under- (or over) estimation of statistical uncertainty on the extracted mass.

The subsamples of events used in Fig. 41 were sampled from a Monte-Carlo pool of events only a factor of 90 larger than the data sample. Any given Monte Carlo event is therefore used multiple times in different subsamples. The uncertainty on the RMS of a Gaussian distribution with N uncorrelated entries is given by $RMS/\sqrt{2N}$. For 100 subsamples, this would lead to an uncertainty on the expected error of about 7 %. This is not sufficiently precise to compare the statistical power of different methods used to determine the W mass. Since it is not technically feasible to produce Monte-Carlo samples with enough statistics for such a comparison, alternative techniques, involving multiple use of the same event in different samples, have been tried.

However, multiple use of the same events affects the statistical precision of the ensemble test, both in the determination of any possible bias in the W mass, as well as in the determination of the expected uncertainty from the RMS of the results. In addition, using the same events in different subsamples can decrease the RMS of any result from such correlated subsamples, and therefore lead to an underestimation of the expected error. This issue was tested using a simple "toy" Monte-Carlo simulation.

In such a toy Monte Carlo, the parton-level W masses are generated using a random number generator that provides a Breit-Wigner distribution. The usual result from some kinematic fit is replaced by the average of the two W masses, and a random term generated with a Gaussian distribution with a width of 2 GeV (a width that corresponds to the resolution of the kinematic fit). The ensemble test of the toy Monte Carlo is based on subsamples of 1000 events in which the individual masses are determined from reweighting analyses. The procedure has a statistical precision that is of the same order as the mass determination of hadronic or semileptonic data collected in a single LEP experiment at a center-of-mass energy of 189 GeV. Ensemble tests are performed using total Monte Carlo samples consisting of $N_{sam} = 10,000$ to $100,000$ events, from which subsamples of an average of 1000 events are formed by selecting any given event with a probability of $1000/N_{sam}$. Since the probability to be selected in any sample is identical for all events, the multiple use of events should not introduce a systematic bias to the measurement. The size of the total pool of Monte-Carlo events, corresponding to 10 to 100 times the data sample, are typical for Monte Carlo studies with full detector simulation. In order to check the veracity of the more detailed ensemble studies, the tests were repeated, but using 500 statistically independent sets of $100,000$ toy Monte-Carlo events, which were used in different ways to check for the presence of any bias and its expected uncertainty.

Figure 42a) shows the RMS of the bias, as determined from the toy ensemble tests, as a function of the number of subsamples chosen from a fixed total of events. It is clear that the RMS decreases as the size of the Monte Carlo sample increases.

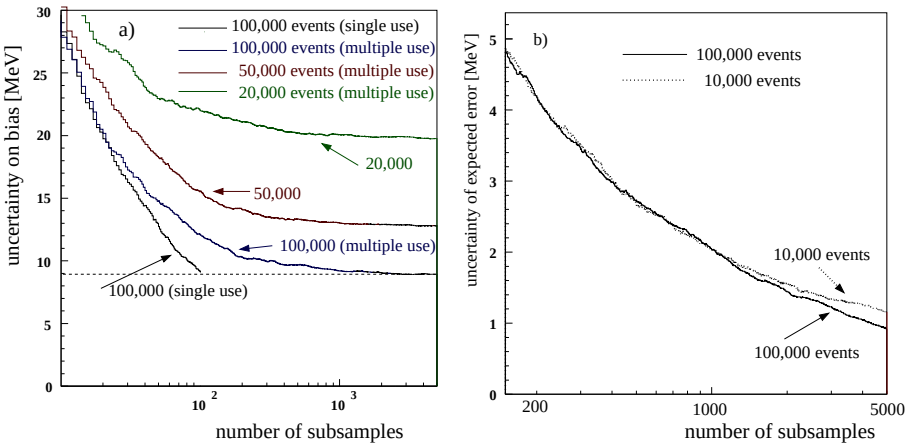

Fig. 42. Test of the multiple use of the same Monte Carlo events in subsamples of 1000 events based on total Monte-Carlo samples of 10,000 to 100,000 events. a) Statistical uncertainty on the bias determined in the subsample tests. b) Statistical uncertainty on the expected error on the W mass.

This can be inferred from the drop in the uncertainty as the number of subsamples increases (especially for the case when no events are ever used more than one time), and in the scaling of the uncertainties with total number of events, when events are used a large multiple number of times. But it also seems that the multiple use of events does not improve the ultimate precision achieved on the bias, compared to when the events are used just once. The dotted horizontal line indicates the result for the case when any of the 100,000 events is used only once (this provides a maximum of 100 independent samples). The additional uncertainty from using an event several times appears to decrease, and approach the statistical power of the total sample, in the limit of a large number of subsamples.

Figure 42b) shows the reduction in the statistical uncertainty on the expected error on the W mass with increasing number of samples. For more than 1000 subsamples, the decrease is slower when 10,000 independent events are used (this is only 10 times the size of a subsample) rather than 100,000 events, but, even for a total sample of 10,000 events, statistical uncertainties of about 1 MeV can still be reached.

From Figure 42b), one might be tempted to conclude that it is possible to measure the expected error on the W mass ($\approx$ 50 MeV) with a relative precision of a few percent, even with total Monte-Carlo samples that are only 10 times larger than data. But, in addition to the statistical uncertainty on the expected error, corrections for systematic underestimation of the expected error from the multiple use of the same events must also be considered. This is because the analysis of the subsamples are not independent, and the RMS of any results therefore tends to be smaller than for independent subsamples. In particular, Table 3 gives the

Table 3. Expected error on the W mass (in MeV), calculated using 5000 subsamples, for different total-sample and subsample sizes.

	Events per subsample		
Total Events in MC	1000	500	250
50,000,000	89	126	179
100,000	88	125	178
50,000	88	124	175
20,000	87	123	172
10,000	84	118	166

expected error on the W mass, calculated from 5000 subsamples, based on the total 50,000,000 independent Monte Carlo events, with prediction for smaller batches of Monte Carlo events and for different number of events per subsample. The impact on the uncertainty becomes more pronounced as the number of events per subsample is reduced. Nevertheless, as seen from Table 3 and Fig. 42b), it is still possible to estimate the expected error on the W mass with a precision of the order of 1% using Monte-Carlo samples of about 100 times the data sample of ≈ 1000 events.

6. Systematic Uncertainties

As described in Section 5, the determination of the mass of the W boson is based on a comparison of data with a prediction from Monte Carlo. This can be done either by using any reference distributions (templates) from the Monte Carlo simulations, or through direct comparison of the mass determined from data with that from Monte-Carlo samples (with bias correction).

As discussed previously, the modeling of W-pair production has uncertainties due to contributions from the four-fermion diagrams, initial-state radiation, and general QED corrections. Simulation of the hadronization and of detector response contributes major sources of systematic uncertainties, but the reliability of many features of the Monte-Carlo simulation can be checked using the large amount of data that is available at center-of-mass energies close to the Z^0 mass (Z^0 data), where the cross section for $e^+e^- \to f\bar{f}$ is very large due to the Z^0 resonance. Nevertheless, when both W bosons in W^+W^- production decay hadronically, final-state interactions between their decay products provide an additional source of systematic uncertainty that cannot be studied with Z^0 data. These final-state interactions can be classified into two groups: Bose-Einstein correlations between identical particles from different W bosons, and color-reconnecting effects caused by interactions between the decay products of the two W bosons that can lead to an the exchange of color. In addition, from the assumption of energy conservation, any uncertainty on the beam energy causes a corresponding uncertainty in the reconstructed W mass. All these issues are discussed below in greater detail.

6.1. *Uncertainties from QED and Four-Fermion Processes*

The largest QED correction to the reconstructed W mass is due to initial state radiation (ISR). As mentioned before, neglecting this effect would result in a shift of the reconstructed mass of about 0.5 GeV. The Monte-Carlo generator KoralW [10] describes the ISR up to $\mathcal{O}(\alpha^3)$. Multiple low-energy or collinear photon radiation is taken into account through exponentiation in the leading-log or next-to-leading-log approximation. The uncertainty due to ISR can be estimated by comparing the KoralW predictions with predictions of Excalibur,[12] which uses a different scheme for implementing the ISR. The disadvantage of comparing two independent Monte-Carlo predictions is that it requires large statistics. To reduce the statistical uncertainty of the comparison to 10% of the statistical uncertainty of the data, requires Monte-Carlo samples with 100 times the size of the data. A more powerful method involves the comparison of distributions derived from the same Monte-Carlo events, but use different event weights. As the distributions are highly correlated, these weights are close to unity, and the statistical uncertainty in the difference between the distributions is therefore greatly reduced. The event simulation with KoralW includes weights for each event, and it is therefore possible to reweight the distributions so that they correspond effectively to lower-order calculations. The comparison of the standard KoralW predictions with predictions corresponding to lower orders in α, in principle, overestimates the uncertainty, but the resulting error is still significantly smaller than the statistical uncertainty from the comparison of independent samples.

In the complete $\mathcal{O}(\alpha)$ QED calculation, the two pairs of fermions from the W bosons are not completely independent because of loop corrections. This correction can therefore influence the invariant mass spectrum of the fermion pairs.[14] The programs YfsWW [13] and RacoonWW [14] include these corrections in the double-pole approximation[15] for the CC03 diagrams. Distributions for YfsWW can be compared with those from KoralW with the help of event weights. Since the complete $\mathcal{O}(\alpha)$ QED corrections are only known for the CC03, and not for the full four-fermion matrix element, one can either use the difference between the two estimates from KoralW and YfsWW for the CC03 diagrams as a systematic error, or as an estimate of the $\mathcal{O}(\alpha)$ QED corrections, and correct the results obtained with the four-fermion matrix element by this amount. In the latter case, the systematic error has to be estimated either from the difference between YfsWW and RacoonWW, or by using YfsWW with different options, and switching on and off some parts of the higher orders. Since the double-pole approximation is only applicable for the CC03 diagrams, it is not sufficient to use just YfsWW for generating the Monte-Carlo samples.

In fact, inital W^+W^- analyses were based on Monte-Carlo samples calculated using only the CC03 diagrams. The systematic uncertainty from the missing interference with other four-fermion diagrams was taken as the full difference between the CC03 and the four-fermion prediction. This difference was again estimated from

KoralW events, using event weights to reweight the four-fermion matrix element to the CC03 matrix element. Since the effect of completely neglecting the interference with other four-fermion diagrams is typically < 30 MeV, no systematic error from higher-order uncertainties on this interference is assigned in the current analysis, which is based on the full four-fermion matrix element.

6.2. *Detector Effects*

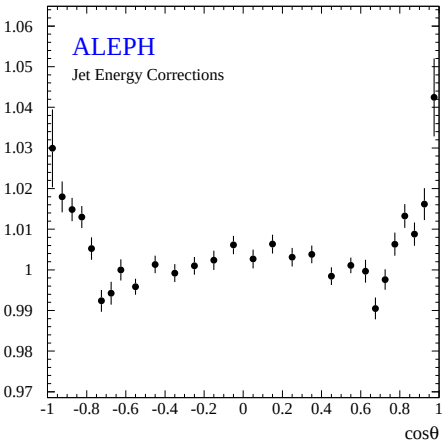

Fig. 43. The double ratio of $(E_{jet}/E_{beam})_{data}/(E_{jet}/E_{beam})_{MC}$ derived from a comparison of 1998 Z^0 data with Monte Carlo simulations.[59]

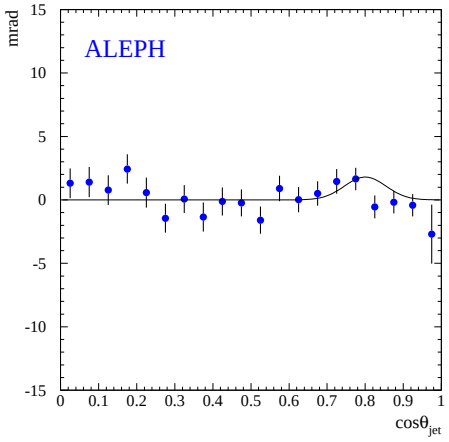

Fig. 44. Difference in the polar direction of 45 GeV jets between the measurement with charged tracks and with clusters in the electromagnetic calorimeter. The points show the results from the 1998 Z^0 calibration data, and the line shows the fit to the high statistics 1994 data sample.[59]

Monte-Carlo simulations used for determining the mass of the W include a full Geant-based detector simulation.[19] Well understood data sets are used to check how well the jet and lepton energies and directions are simulated in the Monte Carlo. Differences between data and the simulation are used to calculate correction factors. The uncertainties on these corrections are used to estimate the remaining systematic error from detector effects.

During each year of LEP-II operation, in addition to the high energy data, the LEP experiments also collected data at the Z^0 resonance. Since these data were collected with exactly the same detector configuration, it has been used to calibrate the detector response year by year. At the Z^0 resonance, decays into two jets produce events where both jets originate from primary partons, which have energies equal to the beam energy and are back to back. Comparing how well the measured and simulated jets fulfill this requirement, checks how well the jet energy

scale and the resolutions on jet energy and direction are simulated for jets of 45 GeV in energy. The statistics of the data are sufficient to perform this study as a function of the polar angle of the jets. Figure 43 shows an example from the ALEPH collaboration.[59] The energy scale for jets below 45 GeV can be checked when Z^0 decays produce three jets. Applying energy and momentum conservation, the energies of the three jets can be calculated from their directions and the measured jet masses, and compared with the direct measurement of jet energy. The precision on jet energy scale is compromised by uncertainties from hadronization that enter into the determination of the jet directions and masses. Nevertheless, these comparisons can be used to estimate a possible energy dependence of the jet-energy scale.

The jet-energy scale and its dependence on polar angle for energies energy above 45 GeV can be checked using two-jet events from higher-energy data collected above the W pair threshold. The energy scale for leptons, its resolution, and the angular resolution, can be determined in the same way as for jets, but using two-lepton events. The dependence on energy can be checked from events with a lepton pair and a photon. Two-lepton events in the highest-energy data, both with and without an additional photon, can be used to determine the energy scale for leptons for energies above 45 GeV.

The understanding of jet and lepton properties can also be checked by comparing measurements using different components of the detector. The jet direction can be determined either from charged tracks in the central tracking chamber, or from clusters in the electromagnetic calorimeter (mainly created by photons from π^0 decays – see Fig. 44). Electrons can be measured in the tracking chamber and in the electromagnetic calorimeter. The muon direction can be measured in the tracking device and the outer muon chambers. In addition, muons produce signals in the calorimeters expected for minimum ionizing particles (MIP) and these which can be used for further verification.

A systematic uncertainty of ≈ 10 MeV can be attributed to detector effects for the combined W-mass measurement at LEP.[62]

6.3. *Hadronization*

Hadronization is the process in which partons transform into hadrons that form massive jets observed in the detector. Since energy and momentum are conserved in hadronization, the invariant mass of all hadrons from W decay must equal the mass of the W boson, independent of the nature of the hadronization process. However, effects from associating particles to the wrong W boson and, more importantly, the detector response, depend on details of the hadronization. The systematic uncertainty on the measurement of the W mass is estimated by comparing different Monte-Carlo simulations and different sets of parameters used in these simulations. Each Monte Carlo contains phenomenological parameters that are adjusted, such that the high statistics data at LEP-I are described as well as possible. Unfortunately, none of the current models provide a set of parameters that describe all

aspects of the data simultaneously.

To determine which aspects of hadronization have the largest influence on the measurement of the W mass, it is informative to study the scaled hadronic mass for semileptonic W pair decays;

$$M = \sqrt{(E_1+E_2)^2-(\vec{\mathbf{p}}_1+\vec{\mathbf{p}}_2)^2}\cdot E_{beam}/(E_1+E_2)$$
$$= \sqrt{M_1^2+M_2^2+2E_1E_2+2|\vec{\mathbf{p}}_1||\vec{\mathbf{p}}_2|\cos\theta_{12}}\cdot E_{beam}/(E_1+E_2).$$

E_i, $\vec{\mathbf{p}}_i$ and M_i are the energies, momenta and masses of the individual jets, θ_{12} denotes the angle between them, and E_{beam} is the beam energy. The scaling factor $E_{beam}/(E_1+E_2)$ approximates the effect of energy conservation and the equal-mass constraint used in the kinematic fit. It effectively rescales the 4-momenta of the jets such that they have an energy corresponding to the beam energy. The effects of hadronization on the scaled hadronic mass are similar to those on the mass from a kinematic fit, but it provides an easier way to understand the impact of hadronization on the determination of the W mass. From the above equation, one can see that the scaled hadronic mass depends basically on the three quantities $(M_1^2+M_2^2)/(E_1+E_2)^2$, $E_1E_2/(E_1+E_2)^2$ and $\cos\theta_{12}$. All three depend on the nature of hadronization, but, as implied above, the effects will cancel exactly if the scaled hadronic mass is calculated directly from the hadrons simulated by the Monte-Carlo programs, before considering any detector effects. The effects of hadronization on the reconstructed mass can therefore be estimated better by studying the difference of these quantities before and after implementing detector simulation. Figure 45a)-c) shows these differences for two sets of Monte-Carlo parameters in JETSET,[16] as tuned by the OPAL collaboration. In the initial tuning,[63] the Monte-Carlo parameters were optimized primarily to provide a good description of inclusive quantities described by event shape variables such as thrust, differential jet rates, and jet masses. The more recent tuning includes exclusive quantities such as particle fractions and their energy spectra.[64] The differences between these two versions of JETSET provide a difference in the reconstructed W mass of 40-50 MeV, depending on the exact method of analysis. The greatest difference is in $(M_1^2+M_2^2)/(E_1+E_2)^2$, with a shift of 0.0006 in the mean value, corresponding to a mass shift of 40 MeV. The shifts observed in the two other variables correspond to mass shifts of ≤ 10 MeV in the W mass.

The two Monte-Carlo tunes predict significantly different detector corrections to jet masses. This can be attributed to their different baryon and kaon fractions. Events generated with the old tune contain on average 30% more baryons and 10% more charged kaons and K_L^0-mesons. As described in Section 1.5, jets are formed from charged tracks and from clusters in the electromagnetic and hadronic calorimeter. A pion mass is assumed for tracks, while a mass of zero is assumed for the pseudo-particles formed from calorimeter clusters. Neglecting the true particle masses, influences both the jet mass and energy. The effects on jet energy are corrected on average by the jet-energy calibration based on Z^0 data, and the impact

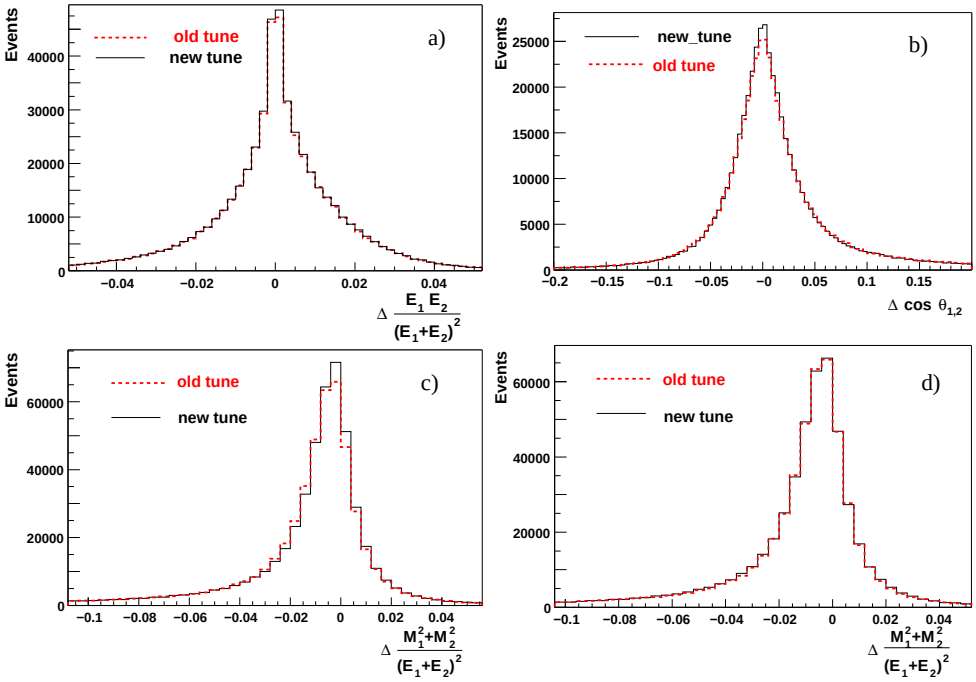

Fig. 45. Difference in the indicated variables, measured both without and with detector simulation. In a)-c), the prediction of the new JETSET tune is compared with that of the old one. In d), the prediction for the old JETSET tune is reweighted to the same baryon and kaon fraction as in the new tune.

on the reconstructed W mass is small due to the energy constraint in the kinematic fit. However, the effect on jet mass cannot be obtained from Z^0 data. This is because jets from the Z^0 decay are back to back, and it is possible to determine the imbalance in energy and momentum of the two jets assuming only energy and momentum conservation, but not whether the momentum scale is wrong. The latter can be determined for systems with known energy and momentum, but only when the total momentum does not vanish (e.g., the Z^0 in $Z\gamma$ event with photons measured in the detector).

Figure 46 shows the difference between mean value of$(M_1^2 + M_2^2)/(E_1 + E_2)^2$, without and with detector simulation, for semileptonic W decays, as a function of the number of baryons or charged kaons and K_L^0 in the event. Clearly, one must conclude that the detector bias on jet mass depends on the number of baryons and kaons in an event. In order to check whether the entire effect can be attributed to this difference, the distribution in $(M_1^2 + M_2^2)/(E_1 + E_2)^2$ for the old JETSET tune was re-calculated using event weights, creating the same baryon and kaon multiplicity as in the new tune. This reweighted distribution is compared to the distribution of the new tune in Fig 45d), and indicates that both Monte Carlos now show the same shift in the jet mass when they have the same baryon and kaon

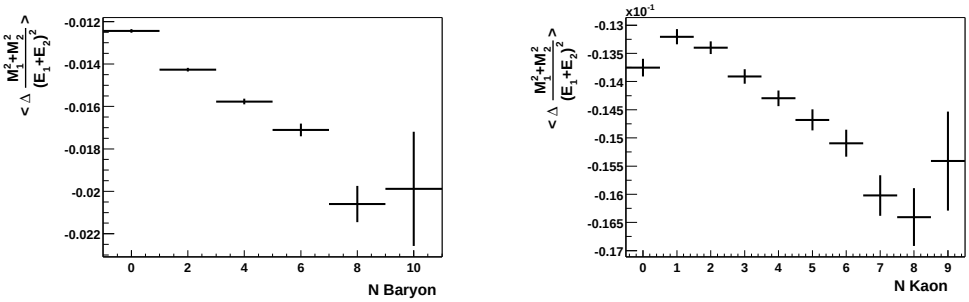

Fig. 46. Average difference between $(M_1^2+M_2^2)/(E_1+E_2)^2$ without and with detector simulation for semileptonic W decays, as function of the number of baryons (left), or charged kaons and K_L^0-mesons (right), in the event.

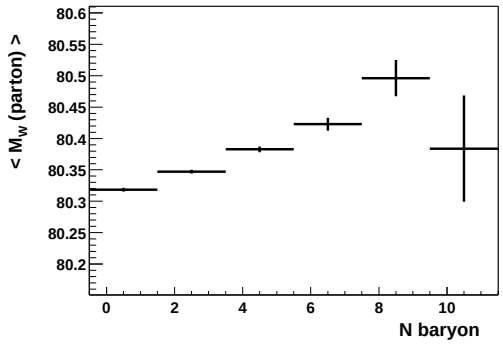

Fig. 47. Average W mass at parton level, for semileptonic W decays, as a function of the number of baryons in the event.

fractions.

When the reweighting technique is used to determine the W mass from a Monte Carlo sample with adjusted baryon and kaon fractions, the correlation of these fractions with quantities that should not be affected by the reweighting (e.g., properties of the W at parton level) have to be properly taken into account. Figure 47, which shows the average mass of the W boson at the parton level as function of the number of baryons per event, indicates the correlation between the two quantities. In events with a higher W mass, the production of baryons and kaons is more likely due to the larger phase space in the decay. To avoid a bias from such correlations, the weight factors affecting the average number of baryons and kaons in an event are normalized separately in bins of W mass and energy at the parton level. This normalization guarantees that the average weight for events in each bin of W mass and energy is the same, and that the parton mass and energy distributions are

Table 4. Shifts in W mass for different Monte Carlo models and tunes, without and with correction for different baryon, charged kaon, and K^0_L fractions.

	w/o rew.	with rew.	Change in Baryon frac.	Change in Kaon frac.
JT(old) - JT(new)	-50 ± 10	$+3 \pm 10$	1.32	1.10
HERWIG- JT(new)	-15 ± 10	-6 ± 10	0.92	1.08
ARIADNE 4.09 - JT(new)	-27 ± 10	$+3 \pm 10$	1.23	1.03
ARIADNE 4.11 - JT(new)	-17 ± 10	-4 ± 10	1.09	1.01
reweight JT(new)		-8 ± 10	1.10	1.00
reweight JT(new)		-10 ± 10	1.00	1.05

therefore not changed by kaon and baryon reweighting.

The uncertainty on hadronization can be estimated using data-sized subsamples in ensembles of the kind described in Section 5.4, and different Monte-Carlo generators. The results shown in Table 4 are based on Monte-Carlo samples from 10^6 W^+W^- pairs. The mass is extracted for semileptonic W-pair decays using a reweighting analysis. The reference distributions are determined from the new tune of JETSET by OPAL,[64] while the data-sized subsamples are taken for the old tune, a HERWIG tune, and two different ARIADNE tunes. The Table shows the results both with and without correcting the Monte-Carlo models for baryon and kaon multiplicity, and the ratio of these multiplicities to the reference values in the new JETSET tune. The two last lines show the effect of changing either the baryon or kaon fraction in the new tune. It can be seen from the Table that the differences between the Monte-Carlo simulations can be accommodated by their different baryon and kaon fractions. The uncertainty from multiplicity is estimated to a precision of ≈ 10 % and ≈ 5 % for baryons and kaons, respectively, and the remaining uncertainty due to the hadronization is smaller than 10 MeV.

6.4. *Mixed Lorentz-Boosted Z^0 Method*

In the estimation of systematic errors from detector effects and hadronization, many issues, such as the uncertainty on energy and direction of jets and leptons, and the difference between hadronization models, are considered separately. Since the uncertainty on most of these contributions is limited by Monte Carlo statistics, adding the uncertainties in quadrature leads to a total error that could be reduced if such effects could be considered simultaneously. This would also have the advantage of gaining a better treatment of the correlation between errors. The ansatz of the mixed Lorentz-boosted Z^0 (MLBZ) method[65] is based on a treatment of Z^0 events in a way that would provide a direct estimate of the uncertainty in the measured W mass from detector-resolution and hadronization effects, purely through a comparison of data with simulated events.

Events with features similar to hadronic W-pair decays are constructed from two Z^0 events. First, the 4-momenta of all measured particles in a Z^0 event are Lorentz boosted in one direction by the Lorentz factor $\gamma = E_{b,W}/m_W$, where γ is the average boost expected for a W boson with a mass of $m_W = 80.35$ GeV/c^2 at a

beam energy $E_{b,W}$. The boosted event is then combined with a second event treated in exactly the same way, except that the Lorentz boost is performed in the opposite direction. In order to optimize the available statistics, each Z^0 event is combined with several other Z^0 events. The correlations introduced between such events due to multiple use of the same Z^0 event are taken into account in the estimate of statistical uncertainty of the method. The newly created events are then passed through a standard mass analysis, assuming a center-of-mass energy $\sqrt{s} = 2\gamma E_{b,Z}$ in the constrained fit, where $E_{b,Z}$ is the beam energy for the Z^0 data ($2E_{b,Z} \approx M_{Z^0}$). Since the technique used to determine the mass is largely invariant under a rescaling of all masses and energies, any shift in the mass of MLBZ-events determined from simulated Z^0 events (M^{sim}_{MLBZ}) compared to the mass determined from Z^0-data (M^{data}_{MLBZ}) provides a measure of the shift expected in the measurement of the mass of the W boson:

$$\Delta M_{\mathrm{W}}^{MLBZ} = (M^{data}_{MLBZ} - M^{sim}_{MLBZ}) \cdot \frac{M_{\mathrm{W}}}{M^0_{\mathrm{Z}}}$$

$\Delta M_{\mathrm{W}}^{MLBZ}$ therefore estimates the systematic errors on the W mass for an imperfect detector-simulation and effercts from an imperfect simulation of the hadronization. The two most important biases in the reconstruction of the mass in MLBZ events are:

- A positive shift of the mass due to ISR photons that are lost along the beam pipe and not taken into account in the kinematic fit.
- A negative bias due to the smearing of the direction of the momentum vectors of the jets from Z^0 decay. The true direction of the momenta are always back to back, and any smearing of the reconstructed direction will always lead to a reduced opening angle between the two jets and therefore to a reduced invariant mass.

These biases can be canceled out by comparing the reconstructed mass from MLBZ-events calculated form Z^0-data and from simulated Z^0 events.

Since the events are correlated through multiple use in combinations of two Z^0 events in one MLBZ event, care has to be taken in the estimation of the statistical accuracy. Both the RMS of statistically independent samples and the "Jackknife" method,[66] have been used to estimate the statistical precision of the method as about $300/\sqrt{n_{Z^0}}$ MeV for a Z^0 sample with n_{Z^0} events. For example, this corresponds to an uncertainty of about 3 MeV for the 1997 DELPHI data.[65]

There are several limitations to the MLBZ method, mainly due to the difference between W and Z^0 decays, the different event topologies of Z^0 and W-pair decays, and the fact that two seperate events are mixed. In particular,

- MLBZ events cannot be used to study any bias from initial-state radiation, since there is far less ISR at the Z^0 pole.
- Effects of final state interactions (FSI) between decay products of the two W bosons cannot be examined.

- The results from MLBZ events might be influenced by different flavor composition of W and Z^0 decays. The influence of b-quark decays can be estimated by studying the mass bias as a function of a b-tag probability in Z^0 events (due to the relatively long life time of B hadrons, the fraction of b quarks in a sample can be changed by changing criteria on tracks to originate from the primary vertex).
- The MLBZ method is sensitive mainly to a jet energy scale of 45 GeV.
- Effects from detector response on particle density, such as double-track resolution, etc., can only be examined if the particles originate from the same W or Z^0.
- The back-to-back geometry often leads often to an over estimation of uncertainties that are sensitive to this symmetry, such as acceptance near the beam pipe, or at the edges of the central and forward detectors.
- The back-to-back topology of Z^0 decays also reduces sharply the sensitivity to single-jet mass effects that are important for understanding the uncertainty in hadronization. Qualitatively, momentum and energy conservation in Z^0 events can be used only to determine the energy scale, because rescaling of the momentum would not influence the constraint that the total momentum should be zero. This can be examined more quantitatively if one approximates the mass from the constrained fit by the scaled hadronic mass:

$$m_{scale} = m_{inv} \cdot \frac{E_{cm}/2}{E_1 + E_2} = \sqrt{(E_1 + E_2) - (\vec{p_1} + \vec{p_2})} \cdot \frac{E_{cm}/2}{E_1 + E_2}.$$

where E_i and $\vec{p_i}$ are the energies and momenta of the two jets forming the W or Z^0 boson, and E_{cm} is the center-of-mass energy in the system used for the constrained fit. (In the approximation that both W bosons from a W-pair have the same mass, $E_{cm}/2$ equals the W energy.) When the change in the center-of-mass energy is taken into account, this quantity is nearly invariant under a Lorentz boost, because both E_{cm} and $(E_1 + E_2)$ are increased by the same γ factor (neglecting the fact that $|\vec{p_1} + \vec{p_2}| \neq 0$, because of detector resolution effects), and m_{inv} is therefore invariant under Lorentz transformations. We can consequently estimate the bias on m_{scale} prior to implementing the Lorentz boost. We can parametrize the difference of the measured jet momenta relative to those in a perfect detector as $\vec{p_1} + \vec{p_2} - (\vec{p_1}^{\,true} + \vec{p_2}^{\,true}) = \Delta\vec{p}_{res} + \Delta\vec{p}_M$, where $\Delta\vec{p}_{res}$ is due to the resolution of the momentum measurement, and $\Delta\vec{p}_M$ is due to a bias in the reconstruction of the mass of single jets, and the biases in $|p/E|$ of the jets. Using this parametrization, the average bias from the momentum

measurement is:

$$\begin{aligned} < m^2_{scale} - m^2_{true} > &= < (\vec{p_1}^{\,true} + \vec{p_2}^{\,true})^2 - (\vec{p_1} + \vec{p_2})^2 > \\ &= - < (\vec{p_1}^{\,true} + \vec{p_2}^{\,true}) \cdot \Delta\vec{p}_M > - \\ &\quad < (\vec{p_1}^{\,true} + \vec{p_2}^{\,true} + \vec{p}_M) \cdot \Delta\vec{p}_{res} > - \\ &\quad < (|\Delta\vec{p}_M|^2 > - < (|\Delta\vec{p}_{res}|^2 > . \end{aligned}$$

The last term is the bias of the scaled mass towards lower values due to momentum resolution. In the case of the Z^0 boson, the first term vanishes because of momentum conservation ($\vec{p_1^{true}} + \vec{p_2}^{\,true} = 0$). For W pair events, $\vec{p_1^{true}} + \vec{p_2}^{\,true}$ is different from 0. Furthermore, $\Delta\vec{p}_M$ is due to a mismeasurement of the size of the momenta, and its direction is therefore strongly correlated with the directions of $\vec{p_1}^{\,true}$ and $\vec{p_2}^{\,true}$, leading to a non vanishing contribution to the bias in the W mass from a bias in individual jet masses.

The MLBZ method provides an interesting cross check for the estimation of uncertainty from detector effects and hadronization. But, in order to fully exploit it in the evaluation of these errors, all above-mentioned points have to be taken into full account.

6.5. *Beam Energy*

The kinematic fit constrains the total energy of the W pair to a center-of-mass energy assumed to be twice the beam energy. If the beam energy assumed in the kinematic fit is larger then the true beam energy by a factor $(E_{beam} + \Delta E_{beam})/E_{beam}$, all jet and lepton energies reconstructed by the kinematic fit will be larger by this factor relative to a kinematic fit using the correct beam energy. The reconstructed W mass is therefore also larger by this factor, leading to a shift on the W mass of:

$$\Delta M_{\mathrm{W}} = \frac{M_{\mathrm{W}}}{E_{beam}} \Delta E_{beam}$$

The beam energies were determined by the LEP Energy Working Group with a precision of 20 to 25 MeV,[67] as described below.

6.5.1. *Determination of the LEP Beam Energy*

By far, the most precise method for determining the beam energy at LEP is based on resonant depolarization.[68] At LEP-I energies, the precision in the beam energy using this method is < 1 MeV. This method is based on determining the spin tune, ν, which is proportional to the beam energy E_{beam}:[67]

$$\nu = \frac{(g_e - 2)}{2} \frac{E_{beam}}{m_e c^2}$$

where $(g_e - 2)$ is the anomalous magnetic moment of the electron, and m_e is the electron mass. Depolarization effects increase sharply with beam energy, leading to

an insufficient build up of transverse polarization at center-of-mass energies used in runs at LEP-II. The measurements of beam energy at LEP-II are therefore based on an estimate of the total integrated magnetic field (B) along the beam trajectory, which is proportional to the beam energy:[67]

$$E_{beam} = \frac{e}{2\pi c} \int_{\mathrm{LEP}} B dl$$

The integrated field is estimated from the continuous measurement of 16 NMR probes situated in several of the 3200 LEP bending dipoles. Each of the NMR probes samples the field in only a small region of the magnet.

Energy measurements based on NMR probes can be calibrated in the range of 40-55 GeV through the precise measurement of beam energy using resonant depolarization. With this calibration, the beam energy can be determined with each of the probes. These measurements, taken over all runs in a given year, yield spreads among the different NMR probes with an RMS of $\sigma_{NMR} = 30$ to 50 MeV, leading to a contribution to the systematic uncertainty in absolute energy of $\sigma_{NMR}/\sqrt{16} =$ 8 to 13 MeV.

The extrapolation of the calibrated energy from the the 40 GeV to 55 GeV range to center-of-mass energies used for physics runs was checked using flux-loop measurements, as follows. Each dipole magnet is instrumented with a flux loop, which can be used to measure the change in magnetic field as the magnet is ramped up. The measurements are performed during dedicated magnet cycles, outside of the normal runs. The flux loops sample 98% of the field in each of the main bending dipoles, excluding fringe fields at the ends of the magnets. This corresponds to 96% of the total bending field, because certain special magnets are not instrumented with such flux loops. The changes in magnetic field are calculated and compared with the NMR measurements, but are not used to correct the results from NMR. The difference between the two measurements is used only to estimate a systematic uncertainty from the extrapolation of the NMR measurements to the energies of interest. This uncertainty was 20 MeV for the year 1997, and 15 MeV for the following years.

For the year 2000, another important source of systematic uncertainty had to be investigated because of the impementation of bending-field spreading (BFS). For any fixed RF acceleration voltage, the power loss from synchrotron radiation depends on the structure of the bending field. During t 2000, approximately 100 previously unconnected corrector magnets were powered in order to exploit this dependence for boosting the beam energy by 0.18 GeV. The increase in energy from the BFS was calibrated in test runs with the help of a beam spectrometer,[69] by testing how much the RF frequency had to be adjusted in order to achieve the same bending without BFS as with the BFS. The systematic uncertainty of this calibration was estimated to be 13 MeV. The beam spectrometer was used to obtain the bending angle in a laminated steel dipole magnet using six beam-position monitors, each of which measured the charge induced by the beam on

four electrodes. The beam position was determined from the relative sizes of the induced charges, which were measured with a precision of $2 \cdot 10^{-5}$ to achieve a required precision in position of $1\mu m$.

The total uncertainty on the beam energy estimated by the LEP Energy Working Group[67] for individual years is between 20 and 25 MeV, with a year-to-year correlation of 82%.

6.5.2. *Beam-Energy Measurement using Radiative Fermion-Pairs*

The cross section for radiative fermion-pair events $e^+e^- \rightarrow f\bar{f}\gamma$ has a maximum when the invariant masses of the fermion pair equals the Z^0 mass. When the di-fermion mass is reconstructed using the constraint of energy conservation, its value depends on the ratio of assumed to true beam energy. Using the known Z^0 mass, the reconstructed mass can therefore also be used to determine the beam energy. This kind of analysis uses techniques similar to those used in the determination of the mass of the W, and can be inverted to provide an additional cross check on the systematics from hadronization and detector uncertainties. The masses of leptonically-decaying Z^0 bosons are related to the directions of the leptons relative to the photon, as follows:[70]

$$\frac{s'}{s} = \frac{\sin\theta_1 + \sin\theta_2 - |\sin(\theta_1+\theta_2)|}{\sin\theta_1 + \sin\theta_2 + |\sin(\theta_1+\theta_2)|},$$

where $\sqrt{s}$ is the center-of-mass-energy of the event, $\sqrt{s'}$ the invariant mass of the lepton pair, and θ_1 and θ_2 the angles between the leptons and the photon. When the event contains an observed energetic photon, its direction can be used in the analysis, otherwise, an unobserved photon is assumed to be emitted along the beam pipe. Muon pairs comprise the most sensitive lepton channel. In the case of electron pairs, additional background from t-channel processes must be taken into account, and for τ pairs there is a substantial loss in efficiency.

The dominant systematic error in this energy measurement arises from the uncertainty in the polar angles of the leptons. Using a wrong ratio of the length to width of the detector for determining the polar angles leads to biases in beam energy. This "aspect ratio" cannot be checked with Z^0-calibration data because a wrong value still yields back-to-back leptons. The uncertainty is therefore estimated by comparing results from different detector components (the tracking system, the calorimeter, and the muon detector) with each other.

In hadronic $f\bar{f}\gamma$ events, the two fermions are reconstructed as jets by forcing all observed particles, except isolated photons, into two jets. The beam energy can be determined in a manner similar to that used in the lepton analysis (from the directions of the jets relative to an isolated photon or the beam axis). The mass of the jet mass, however, cannot be neglected. In this case s'/s is given by:

$$\frac{s'}{s} = \frac{\sin\theta_1 + \sin\theta_2 + |\sin(\theta_1+\theta_2)| \left(1 - \frac{2(|p_1|+|p_2|+|p_\gamma|)}{\sqrt{s}}\right)}{\sin\theta_1 + \sin\theta_2 + |\sin(\theta_1+\theta_2)|}.$$

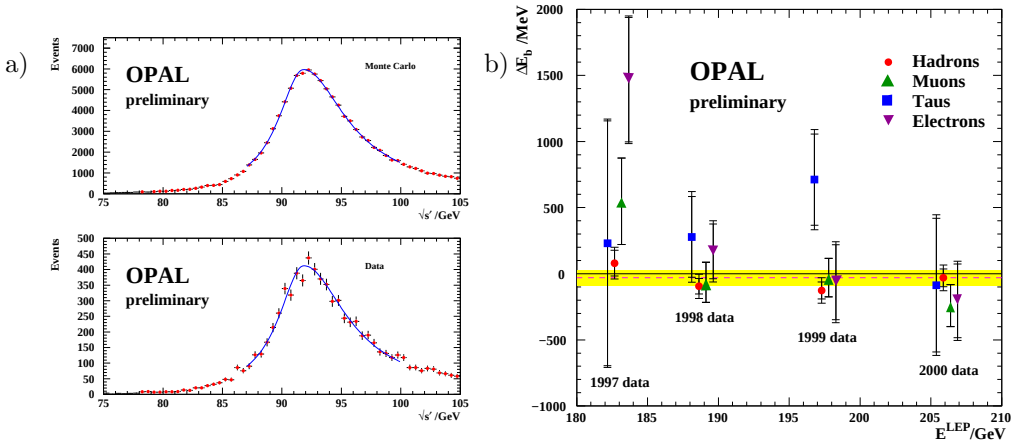

Fig. 48. a) Invariant mass of the $q\bar{q}$ system in $e^+e^- \to q\bar{q}\gamma$ Monte-Carlo events and data at $\sqrt{s} = 206$ GeV. The curves are the fitted functions used to determine the beam energy. b) Difference between the measured beam energy and the one predicted by the LEP Energy Working Group (ΔE_b). For clarity, the muon points are displaced rightwards by 0.5 GeV, the τ points leftwards by 0.5 GeV, and the electron points rightwards by 1 GeV. The dashed line indicates the mean ΔE_b, with its ± 1 standard derivation band given by the shaded region.

The sum of the momenta can be approximated as:[71]

$$|p_1| + |p_2| + |p_\gamma| = \sqrt{s} - \sum_{jet} \frac{1}{2} \frac{m_j^2}{E_j} + \mathcal{O}(\frac{m_j^4}{E_j^3}).$$

In this approach, the jet direction can be determined either by all particles, or from charged tracks, or just from the calorimeter information. Alternatively, the $q\bar{q}$ invariant mass can be determined from a kinematic fit, using energy and momentum conservation, similar to that implemented in the W-mass measurement. The beam energy can then be determined by fitting an analytic function to the mass distribution. Figure 48 a) shows the mass distributions for Monte-Carlo events and data at $\sqrt{s} = 206$ GeV from the OPAL collaboration.[70] The data are well described by the fitted function. For the preliminary OPAL analyses, the largest systematic uncertainty in this channel arises from differences in hadronization models. These yield different baryon and kaon fractions, which can bias mass reconstruction, as discussed in Section 6.3. The effect on the $q\bar{q}$ invariant mass in radiative events is even larger then for W pairs, because of the larger Lorentz factors. Other major sources of systematic error are from uncertainty on the measurement of the jet energy and direction. Figure 48 b) shows the difference between the OPAL measurement of the beam energy and the prediction from the LEP Energy Working Group. The average of all channels over the years is[70]

$$\Delta E_{beam} = 31 \pm 41(stat.) \pm 36(syst.) \text{ MeV}$$

The L3 collaboration expresses their results for the hadronic channel in terms of a

measurement of the Z^0 mass:[71]

$$m_Z = 91.226 \pm 0.034(stat.) \pm 0.072(syst.) \text{ GeV}$$

Both results show no significant deviation from expectation.

6.6. *Color Reconnection*

The lifetime of the W boson is smaller than typical time scales for parton hadronization. The decay products of two hadronically decaying W bosons can therefore have significant space-time overlap. In principle, the two W bosons do not hadronize independently, and can exchange gluons during the hadronization process. Consequently, any particles produced during fragmentation cannot be associated unambiguously with any one of the W bosons. The exchange of colored gluons that affects the color flow between the partons is called color reconnection. In order to estimate possible effects of this color reconnection, one requires a modification in standard models of hadronization.

The models of Sjöstrand and Khoze (SK models)[72] are based on the Pythia Monte-Carlo generator (see also Section 1.4). Calculations indicate that the probability of gluon exchange during the perturbatively-described parton-shower process is small. The color reconnection in the SK models is therefore based on a modification of string fragmentation. As described in Section 1.4, a string connects all partons forming a color singlet: it starts at a quark, ends at an anti-quark, and has kinks at gluons vertices. In the case of color reconnection, the string configurations are changed such that partons from both W bosons can belong to the same string. In the SK-I model, strings are assumed to have finite width, and this affects the phase space overlap between any two strings. If this is large enough, the strings are reconnected at the point of largest space-time overlap. The width of the string is a parameter of the model that can be used to produce an arbitrary overall reconnection probability. In the SK-II models, strings are assumed to be infinitesimally narrow, and color reconnection occurs the first time two strings cross. This affects primarily the middle of the string. Particles produced at this point tend to have low energy, and are far from the main jets, which are dominated by the high energy hadrons formed at the ends of the strings, and which reflect the direction of the original quarks that initiate the parton shower.

In the Herwig Monte Carlo, color reconnection is implemented in the cluster fragmentation.[73] If color reconnection is enabled, gluons from different W bosons are allowed to form a cluster. New associations of partons into a cluster are considered if they lead to a smaller space-time extent of the cluster. When such an association exists, it is realized with a probability of 1/9, reflecting the probability that the two partons form a color singlet.

In the Ariadne (AR) model, the implementation of color reconnection takes place in the inherent simulation of the QCD shower.[74] The perturbative shower is described by radiation of gluons from a color dipole. Higher-order effects are

implemented through the requirement that a gluon be radiated only with smaller transverse momentum than the previous radiation. When the option of color reconnection is switched on, the dipole that radiates a gluon can be formed by partons from the same or different W bosons. The decision as to which partons form dipoles is based on the minimization of the string length λ, as defined by:[75]

$$\lambda = \sum_{1}^{n-1} \ln(p_i + p_{i+1})^2 / m_0^2.$$

where the string consists of n partons with 4-momenta p_i (with neighboring partons in the string forming dipoles), and m_0 is a hadronic mass scale of ≈ 1 GeV. In this model, partons close in momentum space are more likely to be color connected. The minimization of the string length λ introduces not only color reconnection between the two W bosons, but it also changes the assignment of partons to color dipoles within a color singlet (a W or Z^0). In models without color reconnection, this assignment is based purely on the order of gluon emission in the dipole cascade. The AR3 model, which considers all gluons in the simulation of color reconnection, is theoretically disfavored because gluons radiated with energies greater than Γ_W are perturbative, and therefore radiated incoherently by the two initial color dipoles from separate W bosons.[72] In the AR2 model,[74] only gluons with energy less then $\Gamma_W \approx 2$ GeV are allowed to influence the opposite W. As mentioned previously, the modeling of color reconnection in ARIADNE also contains contributions to events that contain only one hadronically decaying W or Z^0. It is certainly inconsistent to apply fragmentation parameters to a color-reconnection model when these were derived from models without any color reconnection applied fitted to high statistics Z^0 data. The cleanest way to minimize confusion between color reconnection and hadronization effects (for different tunes of Monte Carlos) is to compare the AR2 model to a model where color reconnection is allowed for partons that originate from the same W or Z^0, but not allowed for partons from different W-bosons (as in, e.g., the AR1 model). By construction, both Ariadne models are identical for Z^0 decays.

The rearranging of strings and clusters due to color reconnection, affects mainly the low energy particles that are emitted far from the jet axis. The analyses that attempt to constrain color-reconnection models, or try to reduce the impact of color reconnection on the determination of the W mass, concentrate therefor on such particles.

6.7. *Reducing the Influence of Color Reconnection on the Determination of the Mass of the* W

The scaled di-jet mass can also be used to examine the influences of color reconnection on the extracted W mass. As discussed in Section 6.3, the measurement of the W mass is sensitive to the opening angle between the individual jets and to the jet masses. Figure 49 a) shows the difference in the opening angle of the two

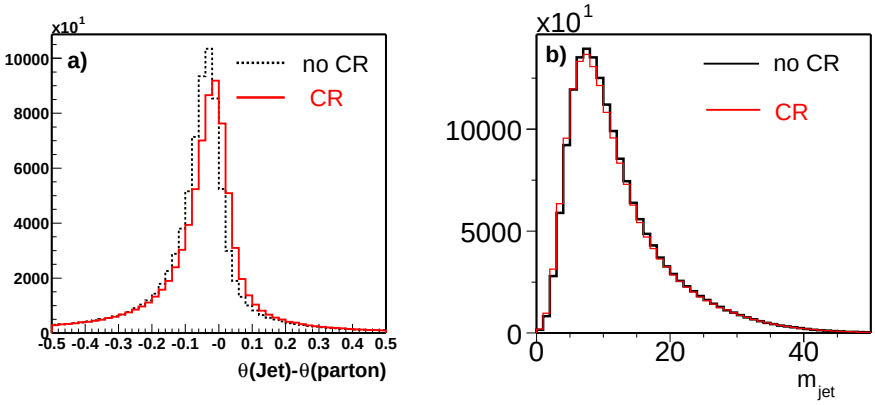

Fig. 49. Comparison between the SK-I model with full color reconnection and PYTHIA without color reconnection for: a) the difference in the opening angle in the W $\rightarrow q\bar{q}$ decay, and b) the jet mass' when calculated using jets and the original partons.

jets belonging to the same W boson, calculated either from the information in the detector or from the initial quark-antiquark pair. The jets acquire mass in the process of hadronization, but, assuming no cross-talk between the two W-bosons, and because of energy and momentum conservation, the hadronization process should not affect the W mass. The contribution of the individual jet masses to the invariant mass of the pair must therefore be compensated by a smaller angle between the two jets relative to the angle between the original quark-antiquark pair. In addition to this effect, the figure shows the difference in the angle between the SK-I model with full color reconnection, and the one without color reconnection. These differences in the opening angles lead to a change of 350 MeV in the scaled di-jet mass. The effect of color reconnection on the individual jet mass, shown in Fig. 49 b), is relatively small, and would contribute to a change of only about 25 MeV. The main effect of the color reconnection relevant to the measurement of the W-boson mass is therefore a change in jet direction.

Three strategies were tried to reduce the impact of color reconnection on jet direction. First, either particles with a momentum larger than p_{cut} were used to calculate the jet directions, or those within a cone with a half opening angle of ρ around the jet axis. In a third approach, the jet direction was determined from the vector sum $\sum \mathbf{p}|\mathbf{p}|^{\kappa}$ over all particles in a jet, where each particle momentum is weighted by an extra factor $|\mathbf{p}|^{\kappa}$. Positive κ emphasizes high-momentum particles, and negative κ low-momentum particles. The three approaches are compared with the standard analysis in Fig. 50. The values of p_{cut}, ρ and κ were chosen such that the statistical uncertainty from the the determination of the jet direction was of similar in the three analyses. The figure shows the mass difference between a Monte Carlo without color reconnection and the SK-I model, as a function of the color-reconnection probability. All three approaches reduce substantially the mass bias

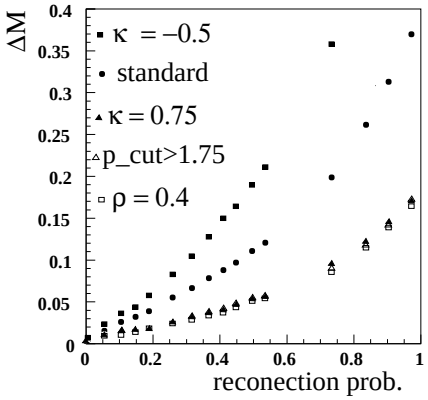

Fig. 50. Mass bias as a function of color reconnection probability for the SK-I model.

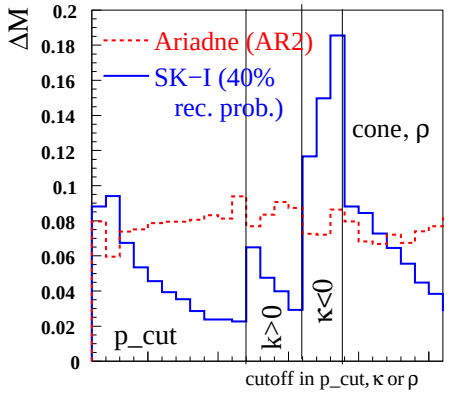

Fig. 51. Comparison of mass bias for the ARIADNE (AR2) and PYTHIA (SK-I) model.

from color reconnection, and, as expected, the bias increases for negative values of κ. Figure 51 shows the mass bias for the SK-I and AR2 models, for different values of p_{cut}, ρ and κ. In the SK-I model, the mass bias from color reconnection decreases with larger cutoffs. The figure also shows that the mass bias can be increased relative to the standard analysis by increasing the influence of low-momentum particles on jet direction (i.e., by using negative κ values). In the ARIADNE model, the mass bias is not affected through modifications in the calculation of the jet direction. This difference in behavior might be due to the fact that in the AR2 model, the color reconnection affects the gluon radiation in the QCD shower. (In the SK models, only string fragmentation is affected by color reconnection) Because of the 2 GeV requirement on gluon energy, it was expected that only low-momentum particles would be influenced in AR2 by color reconnection, which is clearly not the case.

6.7.1. *Limits on Color Reconnection Models*

The W mass is not the only observable that is influenced by effects from color reconnection. Without color reconnection, the particle multiplicity of hadronically-decaying W-pairs should, naively, be exactly twice that of hadronically-decaying W bosons in semileptonic decays. However, this does not follow when color reconnection is present. Measuring the difference between the multiplicity in hadronic W-pair decays and twice that in semileptonic decays, can provide a measure of color reconnection. Most of the systematic uncertainty in the measurement of multiplicity can be avoided in the difference measurement, with the main contribution being due to different event selections and different backgrounds in the two channels.

Because of color reconnection, more particles are expected to be emitted between jets from different W bosons. Therefore, models can be tested by comparing the particle flow in the region between jets from the same W with the particle flow between jets from different W bosons. Because the four jets in a hadronic W-pair

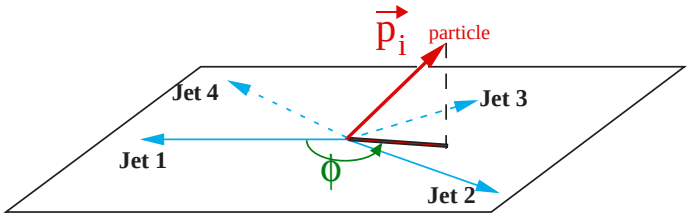

Fig. 52. Illustration of the method used to construct distributions of particle flow.

decay are in general not in one plane, and since the average angles between the jets from the same and from different W bosons are different, there is much flexibility for defining the regions between jets to be used in the analysis.

The L3 collaboration applies quite strict requirements for their events, so as to guarantee well-defined separated event topologies.[76] The efficiency for complete event selection is on average 12%, and the probability to pick the correct jet pairing is 91%. The definition of particle flow is illustrated in Fig. 52. A plane is defined by the most energetic jet (jet-1) and the jet belonging to the same W (jet-2). The azimuthal angle between jet 1 and the projection of all particle and jet momenta onto that plane, is defined by the sense of rotation from jet-1 (towards jet-2). The fact that the angles between jets differ from one event to another, and that the events are not planar, is parametrized by a rescaled angle, as follows. A particle i for which the above-defined projection falls between jet-j and jet-k is reprojected onto the plane spanned by those two jets. The angle Φ_i between jet-j and this projection is divided by the space angle ϕ_{jk} between jet-j and jet-k. This is termed the rescaled angle $\Phi^i_{resc} = \Phi_i/\phi_{jk}$.

In order to characterize the particle flow, each particle enters the Φ_{resc} distribution with unit weight. For energy flow, the weight equals the energy of the particle. Figure 53 compares the particle flow for PYTHIA without color reconnection and the SK-I model with full color reconnection. In order to show the four regions of flow in one diagram, the rescaled angle for particles in the region between jet-2 and jet-3 (region C) is increased by 1, for particles between jet-3 and 4 (region B) by 2, and for particles between jet-4 and 1 (region D) by 3. We see that the Monte-Carlo simulation with color reconnection predicts fewer particles in regions A and B (between jets from the same W), and more particles in the regions C and D (between jets from different W bosons). By measuring the ratio of particle flow between jets from the same and different W bosons, the dependence on absolute flow in the inter-jet region can be minimized, while maintaining sensitivity to color reconnection. Figure 54 compares the L3 measurement for particle and energy flow with different Monte-Carlo predictions.[76]

The particle flow analysis of the OPAL Collaboration is based on less stringent criteria for event topology,[77] which provide an overall efficiency for W-pair all-jet events of 42%. Comparing this analysis to a more restricted one similar to the analysis of L3,[76] shows an improvement in the sensitivity to color reconnection

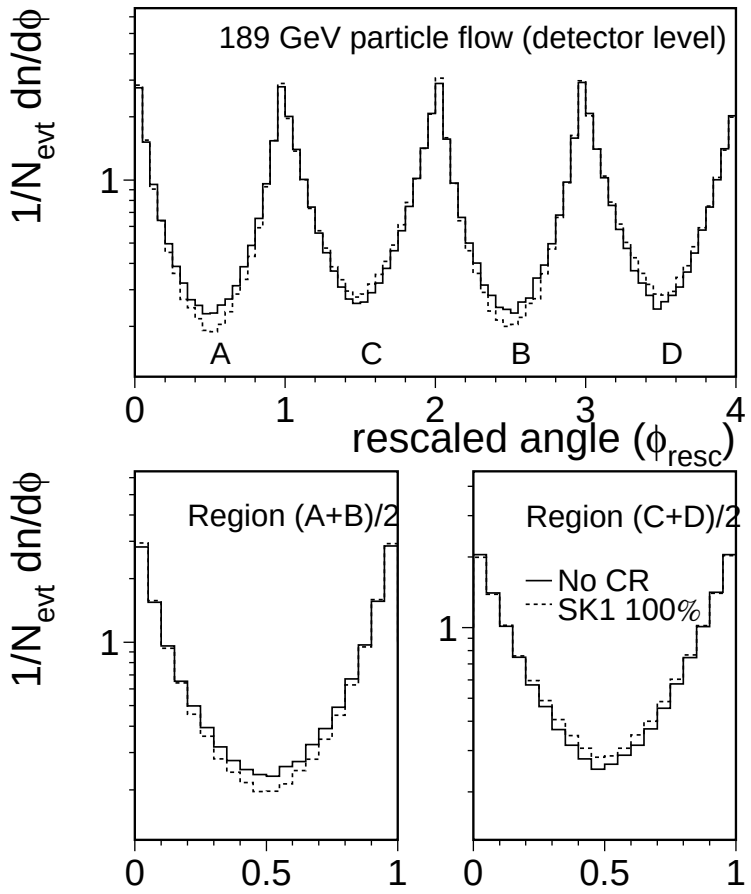

Fig. 53. Distribution in particle flow predicted for $\sqrt{s} = 189$ GeV.

models of about 15%-30%. It should be pointed out that the more restrictive OPAL analysis is distinct from the L3 analysis, as it uses the OPAL jet pairing, jet ordering, and the result of a kinematic fit for defining jet directions. Weighting has been tried for the particle flow using a factor $\ln(1/x_p)$, where x_p is the particle momentum divided by that of the beam. Although this enhances the contribution from low-momentum particles, which should in principle make the analysis more sensitive to color reconnection effects, it dose not provide any significant improvement in sensitivity.

6.8. *Bose-Einstein Correlations*

The production of identical bosons (e.g., pions) close together in phase space can be affected by Bose-Einstein correlations, even when the two bosons originate from

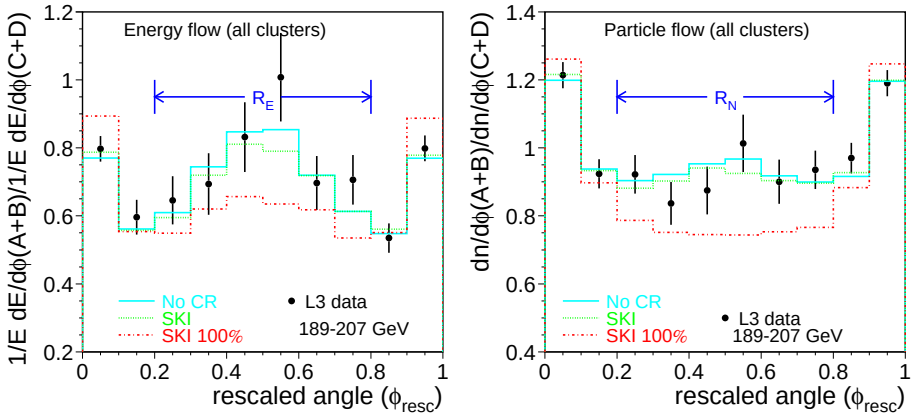

Fig. 54. Ratio of flow in the regions between jets for the same W (A and B), to the flow in the region between jets from different W bosons (C and D)

different W decays. Any observed enhancement would suggest that the hadronization of the two W bosons from hadronic W-pair decays is not independent. This, in turn, could influence the reconstructed W mass.

6.8.1. *Bose-Einstein Correlations within* Z^0 *and* W *Bosons*

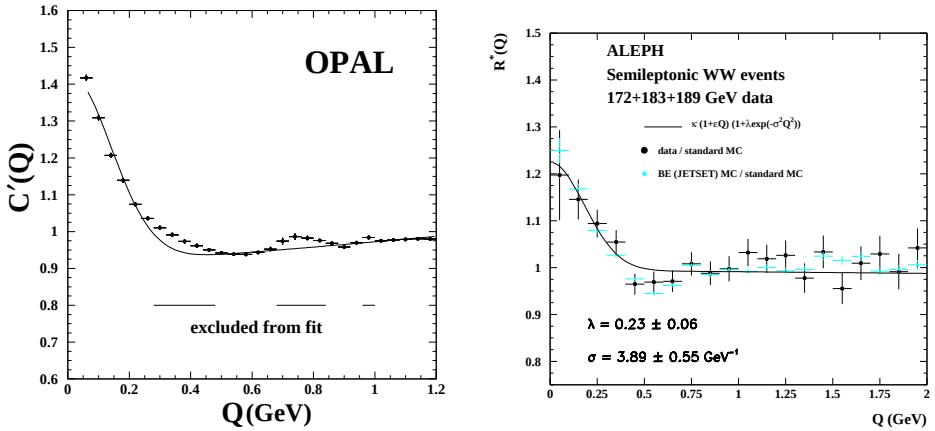

Fig. 55. Observation of Bose-Einstein correlations in Z^0 events,[79] and W-pair events containing only one hadronic W-decay.[80] The distribution was obtained by comparing like-sign boson pairs with opposite-sign pairs. The correlation from resonance decays to particles of opposite charge has not been fully corrected, and such regions have therefore been excluded from the fit.

Figure 55 shows the well-established Bose-Einstein correlations observed within

both Z^0 and W boson decays. They can be observed through two-particle correlations that can be parametrized as:[78]

$$f_2(Q) = \frac{\rho(p_1, p_2)}{\rho(p_1)\rho(p_2)} = (1 + f_\pi(Q)\lambda e^{-Q^2/R^2})(1 + \delta Q + \epsilon Q^2).$$

where p_1 and p_2 are the 4 momenta of the two particles, $Q^2 = -(p_1 - p_2)^2$, $\rho(p_i)$ and $\rho(p_1, p_2)$ are the single and two-particle density functions, and $f_\pi(Q)$ is the probability that the two observed charged tracks are pions. The parameter λ describes the strength of the correlation, and R can be interpreted as the size of the source for the correlated particles. The factor $1 + \delta Q + \epsilon Q^2$, with free parameters δ and ϵ, reflects long-range correlations (e.g., correlation due to charge and momentum conservation, and constraints from phase space).

In a full quantum-mechanical description of hadronization, Bose-Einstein correlation can be incorporated by symmetrizing the overall wave function. Since such a description is not available, models are used to accommodate any Bose-Einstein correlations. There are basically two approaches used in Monte-Carlo simulations: In a global approach, events are weighted in a way that yields the desired correlation functions after the reweighting. The weight for each event can be defined as the product of the $f_2(Q)$ values for all pairs of identical particles. In the local approach, the desired two-particle correlation function is generated by modifying the momentum of the particles and thereby pulling identical particles closer together in phase space.

At a first glance, the global event weighting is more appealing, because changing the probability that an event is produced with a given particle correlation is what would be expected from symmetrizing the wave function. This ansatz, however, has two major problems. Technically, because of the high multiplicities, some of the event weights can get very large, and produce large fluctuations. Moreover, global event weights in general violate the factorization hypothesis, which requires that properties determined by the perturbative parts of the interaction, such as the width of the Z^0, the b fraction, and the three-jet rate, are not affected by hadronization. This hypothes has been well tested, in that the distributions in the above observables agree with theoretical predictions.

The problem of factorization can be circumvented by implementing a veto algorithm applied only to the hadronization phase of the simulation. This ansatz[81] is based on the PYTHIA program (see Section 1.4), in which quarks and gluons are simulated first by a perturbative QCD shower, and then hadronized via a string model. The selection procedure takes each simulated event with a probability proportional to the product of the $f_2(Q)$ values for all pairs of identical particles in an event, however, if the event is rejected by the veto algorithm, then without changing the quark and gluon configuration from its perturbative simulation, the simulation of the hadronization is repeated. In this way, observables that depend only on the perturbative process are not affected by the rejection algorithm. Only the particles produced in the primary interactions are used in the calculation of weights for

the rejection algorithm. This keeps the number of identical particles small and the weights of manageable size.

In the model of Kartvelishvili and Kvatadze (K&K model),[82] motivated by a string model, the event weights are based on the following ansatz for the matrix element:[83]

$$M_{12} = exp[(i\kappa - b/2)A_{12}]$$

where κ is the string tension, b a breaking probability, and A_{12} a space-time area of the string containing the particle 1 and 2. Symmetrizing this matrix element, $(A_{12} \neq A_{21})$ leads to a weight:

$$w = 1 + \sum_{perm} \frac{\cos(\kappa(A_{12} - A_{21}))}{\cosh(\frac{b}{2}(A_{12} - A_{21}))} = 1 + \sum_{perm} \frac{\cos(RQ)}{\cosh(\xi RQ)}$$

where we have substituted $\kappa(A_{12} - A_{21}) \rightarrow RQ$ and $\frac{b}{2}(A_{12} - A_{21}) \rightarrow \xi RQ$. This functional form produces weights that are smaller than unity for some values of Q (see Fig 56). The parameter ξ can be tuned such that the average weight equals

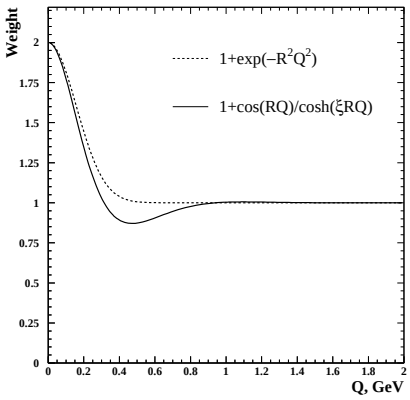

Fig. 56. Weight function (w) for global reweighting.

unity, and this keeps the width of the Z^0 from changing, and keeps the weights reasonably small. An advantage of this model is that it can be applied a posteriori to fully simulated events.

Factorization in the local approach is preserved by construction, because the underlying parton structure of an event is not influenced by the local disturbance of the momenta. The small value of ≈ 1 fm for R indicates furthermore that the effect of Bose-Einstein correlation is localized to only parts of a string, but that ends of the strings fragment nearly independently of each other. In the local approach of Lönnblad and Sjöstrand,[84] the value of Q for a pair of identical bosons with masses

m is changed by δQ, as defined by:

$$\int_0^Q \frac{q^2 dq}{\sqrt{q^2+4m^2}} = \int_0^{Q+\delta Q} f_2(Q) \frac{q^2 dq}{\sqrt{q^2+4m^2}}.$$

This change cannot be achieved in a way that satisfies both energy and momentum conservation. In order to conserve momentum, and to change the configuration as little as possible, the momenta of the two particles are altered by equal amounts in the direction defined by their momentum difference: $\delta \mathbf{p}_1 = -\delta \mathbf{p}_2 = c(\mathbf{p}_1 - \mathbf{p}_2)$; the factor c is chosen to obtain a change of Q by amount δQ. This procedure leads to typical shifts of several hundred MeV in total energy, for Z^0 events. Different schemes can be used to ensure energy conservation. In the original model (BE_0), the momenta of all particles are rescaled by a common factor to yield energy conservation. This rescaling has only minor impact on most other observables, but it introduces a negative bias in the reconstructed W mass in hadronic W-pair decays.

To avoid this bias, other schemes have been developed, in which energy conservation is achieved without a global rescaling of all particle momenta. In the BE_3 and BE_{32} schemes, the functional form of $f_2(Q)$ is modified in a way that $f_2(Q)$ gets smaller than 1 for certain values of Q. In these schemes, $f_2(Q)$ contains a free parameter, which is determined in each event in such a way that the energy shift from pairs with $f_2(Q) > 1$ is compensated by those from pairs with $f_2(Q) < 1$. In the BE_m and BE_λ schemes, for each pair of identical particles, a pair of non-identical particles with configuration close to the original pair is also selected. The opening angle of this pair is changed such that the resulting energy shift compensates exactly the energy shift from the pair of identical particles. The two schemes differ in their definition of how a pair of non-identical particles is selected. The implementation of Bose-Einstein correlations as a momentum transfer between two identical particles with small Q^2 looks technically as a final-state interaction. Nevertheless, this implementation does not imply that the underlying process has its origin in such an interaction.

6.8.2. *Bose-Einstein Correlations between Particles from Different* W *Bosons.*

As we mentined, it is not possible to determine a priori whether any two particles in hadronically decaying W-pair events originated from the same or from different W bosons. A model must therefore be formulated to test whether the observed correlation in hadronic W-pair decays is due only to Bose-Einstein correlations between particles from the same W, or whether there is an additional contribution from a correlation between different W bosons. This can be done by comparing the two-particle density function in all-hadronic and single-hadronic W-pair decays, by checking the validity of the relation:

$$\rho^{WW}(1,2) = 2\rho^{W}(1,2) + \rho^{WW}_{mix}$$

where $\rho^{WW}(1,2)$, $\rho^{W}(1,2)$, and ρ^{WW}_{mix} represent, respectively, the two-particle densities from hadronic W-pair decays, the hadronic part of "semileptonic" W-pair decays, and two "semileptonic" events that are combined to represent all-hadronic W-pairs. The last term is needed to describe any contributions to two-particle density for particles arising from different W bosons.

The mixed events are constructed by adding the hadronic parts of two "semileptonic" events, after applying appropriate rotations and boosts in order to reflect the desired kinematics. Since not all detector effects are invariant under boosts and rotation, it is important to select pairs for which the required transformations cause the smallest possible bias.

The observed particle correlations must also be corrected for background. This is important because of the significant contributions from $e^+e^- \to \mathrm{Z}^0/\gamma \to q\bar{q}$ events. The hadronic Z^0/γ decays that pass the W-pair selection have a two-particle density distribution that is sufficiently different from that of hadronic W-pairs, and that must be taken into account. The validity of the above relation can be checked by examining the difference:

$$\Delta\rho(Q) = \rho^{WW}(1,2) - 2\rho^{W}(1,2) - \rho^{WW}_{mix}$$

or checking the ratio

$$D(Q) = \frac{\rho^{WW}(1,2)}{2\rho^{W}(1,2) + \rho^{WW}_{mix}}.$$

To parametrize any discrepancy between data and Monte-Carlo models, we define the integral:

$$J \equiv \int_0^{Q_{max}} \Delta\rho dQ$$

In the L3 measurement,[85] $Q_{max} = 0.68$ is chosen as the point where predictions for the Monte-Carlo with and without Bose-Einstein correlations differ by less than one standard deviation. Figure 57 shows a comparison of the L3 data with the LUBOYE (BE_{32}) Monte-Carlo[84] both with and without Bose-Einstein correlations. The data clearly disfavor Bose-Einstein correlations of same strength between particles from different W bosons as for paritcles within the same W.

6.9. *Combining of LEP Results*

In order to combine the separate mass measurements into one LEP result, the correlation in the systematic uncertainties between different channels, years of data taking, and between experiments, must be taken into account. The detector systematics and the uncertainties from limited Monte-Carlo statistics are the only errors that are assumed to be uncorrelated between experiments. The four LEP experiments claim significantly different systematic uncertainties from final state interactions.[86,87,88,89] Nevertheless, studies of Monte Carlo samples with identical events passed through all the detector simulations suggest that the experiments

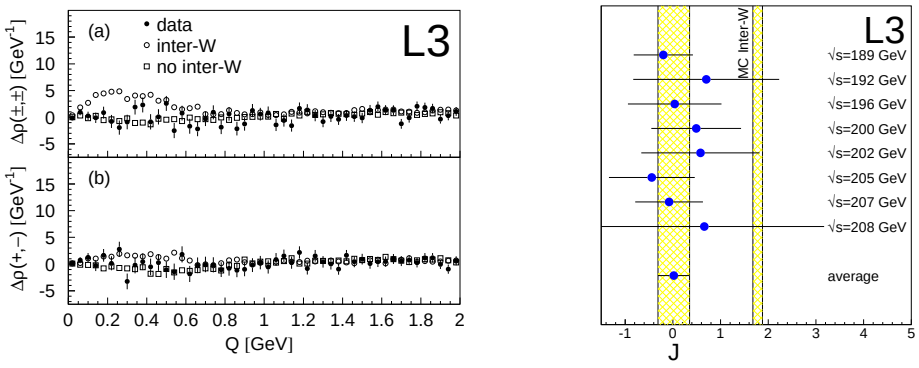

Fig. 57. Comparison of $\Delta\rho$ and J for L3 data with Monte-Carlo models both with and without Bose-Einstein correlations between particles from different W bosons.[85]

have the similar sensitivity to final-state effects, and that the differences are due primarily to different choices of model parameters used to estimate the uncertainty. In combining the results, the same systematic errors from FSI are used for all four experiments. Similar studies are in preparation to gauge the hadronization uncertainties. The uncertainty from hadronization and detector effects on the measurement of jet properties are considered to be fully correlated between the hadronic and semileptonic W-pair decays. The uncertainty from beam energy is fully correlated between channels and experiments. The year-by-year correlation is taken from the estimates of the LEP Beam Energy Group.[67] Table 5 lists the systematic errors on the preliminary determination of the combined mass of the W boson.[62]

7. Determination of the W Mass from Purely Leptonic W-Pair Decays

An event, in which both W bosons decay leptonically contains two unobserved neutrinos. It is therefore not possible to completely reconstruct the kinematics of such an event. However, on a statistical basis, the observed charged leptons carry information about the W-boson mass, that is, their momenta depend on the mass of the W-boson. In fact, positions of edges of kinematic distributions, reflecting limits of phase space, can be used to measure the W mass. The simplest variable is the energy of a single charged lepton, which can be expressed as the following function of the W mass:

$$E_l = \frac{\sqrt{s}}{4} + \cos\theta_l^* \sqrt{\frac{s}{16} - \frac{M_{\mathrm{W}}^2}{4}}.$$

where s is the square of the center-of-mass energy, and θ_l^* is the angle between the lepton direction measured in the W rest frame and the direction of the W in the laboratory frame ("helicity" frame). The maximum and minimum in the energy

Table 5. Decomposition in uncertainties for the combined LEP W-mass results. Detector systematics include uncertainties in jet and lepton energy scales and resolution. The 'Other' category refers to errors, all of which are uncorrelated between experiments, arising from: simulation statistics, background estimation, four-fermion treatment, fitting, method and event selection. The error decomposition in the $qql\nu$ and $qqqq$ channels refers to separate fits to the two channels. The last line indicates the statistical error for a combination that minimizes the statistical error and not the total error.

Source	Systematic Error on M_{W} (MeV)		
	$qql\nu$	$qqqq$	Combined
ISR/FSR	8	8	8
Detector Systematics	12	8	11
Hadronization	19	18	18
LEP Beam Energy	17	17	17
Color Reconnection	–	90	9
Bose-Einstein Correlations	–	35	3
Other	4	5	4
Total Systematic	29	101	30
Statistical	33	36	30
Total	44	107	42
Statistical in absence of Systematics	32	29	22

spectrum occurs at $|\cos\theta_l^*| = 1$, where the lepton is emitted along or opposite the direction direction of the W. These values clearly depend on the W mass.

The OPAL collaboration uses another "edge" variable sensitive to the W mass.[90] Energy and momentum conservation and the assumption that both W bosons have the same mass yield only five constraints. The kinematics of the reaction is therefore underconstraind. But the assumption that the neutrino momentum vectors lie in the plane defined by the momenta of the charged leptons, defines two solutions for neutrino momenta, and the event can therefore be reconstructed. Using this kind of reconstruction, a "mass" of the W can be expressed as a function of the momenta of the charged leptons, as follows:

$$M_{\pm}^2 = \frac{2}{|\mathbf{p}_l + \mathbf{p}_{\bar{l}}|^2}\Bigg((P\mathbf{p}_l - N\mathbf{p}_{\bar{l}})\cdot(\mathbf{p}_l + \mathbf{p}_{\bar{l}}) \pm$$

$$\sqrt{|\mathbf{p}_l \times \mathbf{p}_{\bar{l}}|^2\,[|(\mathbf{p}_l + \mathbf{p}_{\bar{l}})|^2(E_{beam} - E_l)^2 - (P+N)^2]}\Bigg)$$

where P and N are given by:

$$P = E_{beam}E_l - E_l^2 + \frac{1}{2}m_l^2 \qquad N = -E_{beam}E_{\bar{l}} - \mathbf{p}_l \cdot \mathbf{p}_{\bar{l}} + \frac{1}{2}m_{\bar{l}}^2.$$

E_{beam} denotes the beam energy, and $\mathbf{p}_l$, $\mathbf{p}_{\bar{l}}$, E_l, $E_{\bar{l}}$, m_l, and $m_{\bar{l}}$ are, respectively, the momenta, energies, and masses of the charged lepton and antilepton. Of course, in general, the two neutrinos are not emitted in the same plane as the two charged leptons, and the reconstructed mass values are therefore not always close to the W mass. Nevertheless, the larger of the two solutions has a distribution that is

in general beyond the W mass, and has a lower limit (from events where the two neutrinos are nearly in the same plane as the charged leptons) at the mass of the W boson. In the following, this solution will be referred to as pseudo-mass.

Measurements of the W mass that rely on lepton energy or on the pseudo-mass have only small correlations because these distributions correspond to information from different regions of the phase space. For the case of lepton energy, mainly events in which a lepton is emitted along the W direction affect the mass determination. For the pseudo-mass, events in which the neutrinos and charged leptons are nearly in the same plane contribute sharp information to the mass measurement. Both the pseudo-mass and the energy spectrum rely on a precise measurement of lepton energy, which is not possible for τ-leptons because of the additional neutrino in each τ decay. In events, where one of the W bosons decays into a τ, only the energy spectrum of the other lepton is used.

The statistical uncertainty of these dilepton mass determinations is larger than for hadronic or semileptonic channels, because only $\approx 10\%$ of the W-pairs decay leptonically (≈ 5 % decay into electrons and muons), and because only events near the edges of phase space contribute useful information to the mass determination. The ALEPH collaboration uses the lepton energy spectrum in their analysis,[59] while the OPAL collaboration uses both the lepton energy spectrum and the pseudo-mass.[90]

7.1. *Mass Determination*

Both the reweighting technique (see Section 5.2) and the comparison with an analytic function (see section 5.1) can be used to determine the W mass from the lepton energy and the pseudo-mass. Compared to the hadronic and semileptonic channel, the reweighting technique has two disadvantages: First, the distributions do not have clear maxima at specific values, but are broad spectra with edge cutoffs. Consequently, only a small fraction of the events contribute to the region that is important for determining the mass. In addition, the larger statistical error requires a reweighting over a range of the order of the width of the W boson. This increases the statistical uncertainties on the reweighted distributions, and necessitates the use of very large Monte-Carlo samples for different input W masses to get stable results. The need for large Monte-Carlo samples is reduced if the W mass is determined by comparing the lepton energy and pseudo-mass distributions with analytic functions. The lepton energy E_l can be parametrized as:

$$f = \frac{1}{e^{\frac{-(E_l - P_1)}{P_2}} + 1} \frac{1}{e^{\frac{E_l - P_3}{P_4}} + 1} (P_5 + P_6 E_l),$$

where P_1 and P_3 are given by the position of the rising and falling edges of the energy spectrum, P_2 and P_4 reflect the steepnesses of the edges, which depend on the lepton energy resolution, P_6 describes the rise of the spectrum with energy, and parameter P_5 is determined for each set of values of the other parameters by normalizing the function f to unit area or to the number of events in the data.

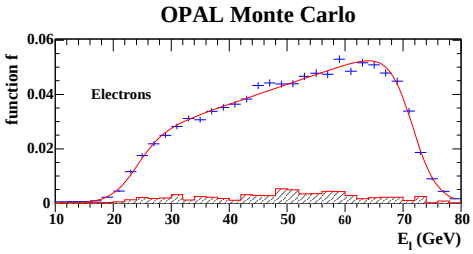

Fig. 58. Fit of the electron energy spectrum for Monte Carlo events at $\sqrt{s} = 189$ GeV and $M_{\mathrm{W}} = 80.33$ GeV. The hashed region indicates the background.

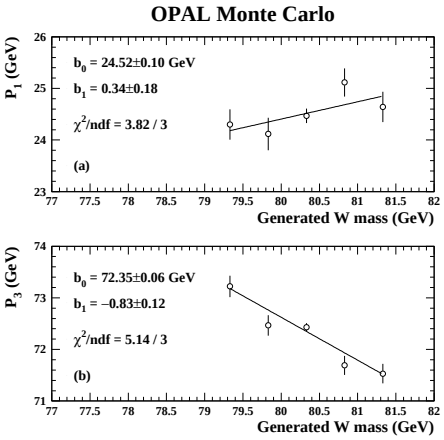

Fig. 59. Linear fit [$R = b_0 + b_1 \times (M_{\mathrm{W}} - 80.33\mathrm{GeV})$] of the coefficients P_1 in (a) and P_3 in (b).

Figure 58 shows a fit of the electron energy spectrum to a Monte-Carlo sample at $\sqrt{s} = 189$ GeV and $M_{\mathrm{W}} = 80.33$ GeV/c. Figure 59 shows that in the relevant mass range the parameters P_1 and P_3 depend linearly on the W-boson mass. The other parameters P_2, P_4 and P_6 show no significant mass dependence.

The pseudo-mass distribution can be parametrized with the function

$$f' = \frac{P_1}{e^{\frac{-(x-P_2)}{P_3}} + 1} + P_4,$$

where P_2 is given by the position of the edge in the pseudo-mass distribution, while P_3 reflects the steepness of the edge. The constant term P_4 is needed to describe events with low pseudo-mass that have mismeasured lepton momenta. The parameter P_1 can be determined from the normalization of the function f' to unit area or to the number of events in the data. Figure 60 shows a fit of the pseudo-mass distribution for electron-electron events ($\mathrm{W}^+W^- \to e^+\nu e^-\bar{\nu}$) for a Monte-Carlo sample at $\sqrt{s} = 189$ GeV and $M_{\mathrm{W}} = 80.33$ GeV. Figure 61 shows that the parameter P_2 depends linearly on the W mass. The other parameters show no significant mass dependence.

Since the energy resolution of the OPAL detector is significantly better for electrons than for muons, the lepton energies are fitted separately. For the case of the pseudo-mass, ee, $e\mu$ and $\mu\mu$ final states are all treated separately. The W mass is then determined from a simultaneous fit to the two lepton-energy spectra and the three pseudo-mass distributions at each center-of-mass energy. The parameters that do not depend on the W mass are fixed to the values determined by Monte-Carlo. The parameters sensitive to W mass are parametrized as linear functions

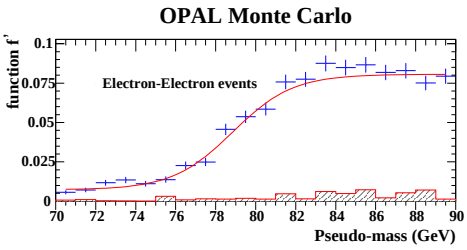

Fig. 60. Fit of the pseudo-mass distribution from electron-electron Monte Carlo events at $\sqrt{s}$ = 189 GeV and M_{W} = 80.33 GeV. The hashed region indicates the background.

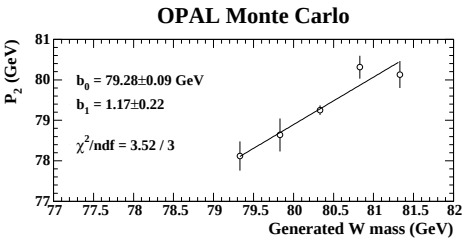

Fig. 61. Linear fit of the coefficient P_2 to $b_0 + b_1 \times (M_{\mathrm{W}} - 80.33\mathrm{GeV})$.

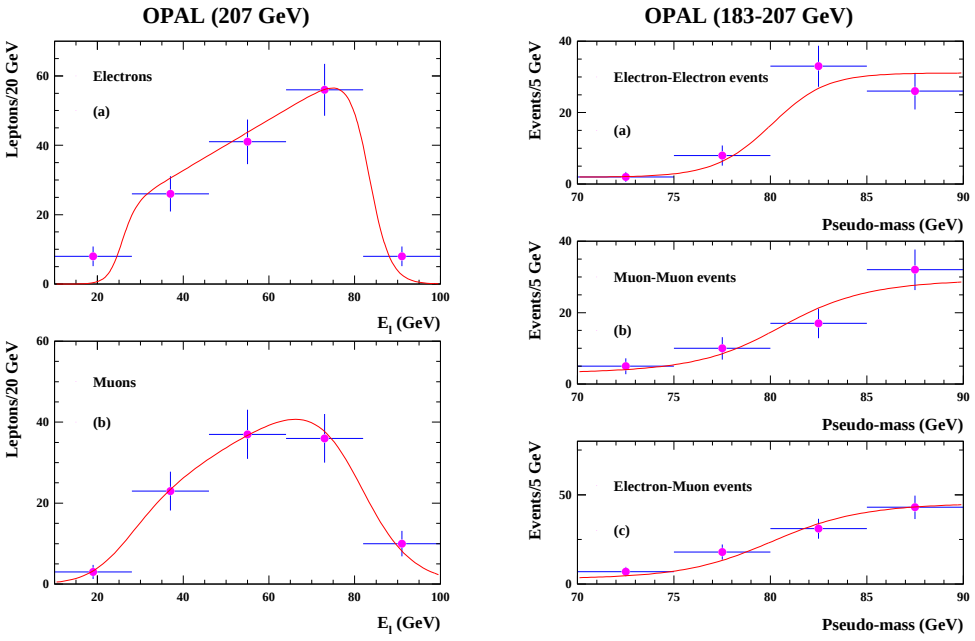

Fig. 62. Fit to the OPAL data for the lepton energy spectrum and the pseudo-mass.

of M_{W} using Monte-Carlo samples at different W input masses, as illustrated in Figures 58b and c, and 60b. Figure 62 shows the fit to data for the lepton energy and pseudo-mass at $\sqrt{s} = 207$ GeV. For illustration purposes, the pseudo-mass distribution is for data combined from all center-of-mass energies, and compared with the corresponding sum of the fitted functions at different center-of-mass energies.

The figure suggests sharper edges in distributions for electrons relative to those for muons, reflecting the better energy resolution for electrons.

To determine the degree of correlation between the mass measurements using the pseudo-mass and the lepton energy, separate fits were performed to the energy spectrum and to the pseudo-mass for a large set of data-sized Monte-Carlo samples. A correlation coefficient of $11 \pm 1\%$ was determined from the distribution of the result for the lepton energy versus results for the pseudo-mass. This was confirmed by the pull of the common fit for lepton energy and pseudo-mass. After correcting the statistical error by the factor of 1.11 from this the correlation, the width of the pull distribution became 1.00 ± 0.02, thereby confirming the internal consistency of the procedure.

7.2. *Results*

The systematic errors for the W mass in the fully leptonic channels are estimated in a way similar to that discussed in Section 6. The result from the OPAL collaboration, analyzing the complete LEP-II data set, is:[90]

$$M_{\mathrm{W}}(l\nu l\nu) = 80.41 \pm 0.41 \pm 0.13 \text{ GeV}.$$

The first error is statistical and the second systematic. The dominant source for the systematic errors are the uncertainties in the lepton energy scale and in the resolution. These are limited by the available statistics from the Z^0 calibration runs. The measurement in the fully leptonic channel has no contribution from uncertainties from hadronization; also the error due to the uncertainty in beam energy is smaller than for semileptonic events because of the different dependence of the upper and lower edges of the energy spectrum, and the edge of the pseudo-mass, on beam energy, which for dileptons provide partial cancellations. Future high-luminosity experiments should therefore be able to reduce the systematic uncertainty to a level below that in semileptonic W pair decays.

The uncertainty on the measurement of the W mass in the fully leptonic channel is large compared to the other channels. Nevertheless, its inclusion improves the overall precision by about 1% corresponding to an additional luminosity of 2%. More importantly, the analysis is complementary to those used in the other channels, and therefore serves as a cross check. Improvements to the W-mass measurement will likely come from measurements at hadron colliders (TeVatron and LHC). These are more sensitive to leptonic W decays, and the interesting comparison of W mass in different decay channels can probably be carried out only at electron-positron colliders.

8. The Mass and Width of the W boson

Table 6. Preliminary W mass measurements from direct reconstruction ($\sqrt{s}$ = 172 − 209 GeV).[86,87,88,89,91] The first error is statistical and the second systematic. Results are given for the semileptonic, the fully-hadronic channels, and their combination. The $W^+W^- \to q\bar{q}\ell\bar{\nu}_\ell$ results from the ALEPH and OPAL collaborations include mass information from the $W^+W^- \to \ell\nu_\ell\ell\bar{\nu}_\ell$ channel.

Experiment	$W^+W^- \to q\bar{q}\ell\bar{\nu}_\ell$ M_W GeV	$W^+W^- \to q\bar{q}q\bar{q}$ M_W GeV	Combined M_W GeV
ALEPH	80.377 ± 0.062	80.431 ± 0.117	80.385 ± 0.059
DELPHI	80.414 ± 0.089	80.374 ± 0.119	80.402 ± 0.075
L3	80.314 ± 0.087	80.485 ± 0.127	80.367 ± 0.078
OPAL	80.516 ± 0.073	80.407 ± 0.120	80.495 ± 0.067

8.1. *Results*

The preliminary results of the direct reconstruction of the W mass in all four LEP experiments are given in Table 6.[86,87,88,89,91] Figure 63 shows the values obtained for the W mass and its width. Figure 64 shows results separately for the hadronic and semileptonic W-pair channels. The preliminary combined result for the four LEP experiments and all channels, including the threshold measurements of Ref.[92], is:[62,91]

$$M_W = 80.412 \pm 0.029(\text{stat.}) \pm 0.031(\text{syst.})\text{GeV}.$$

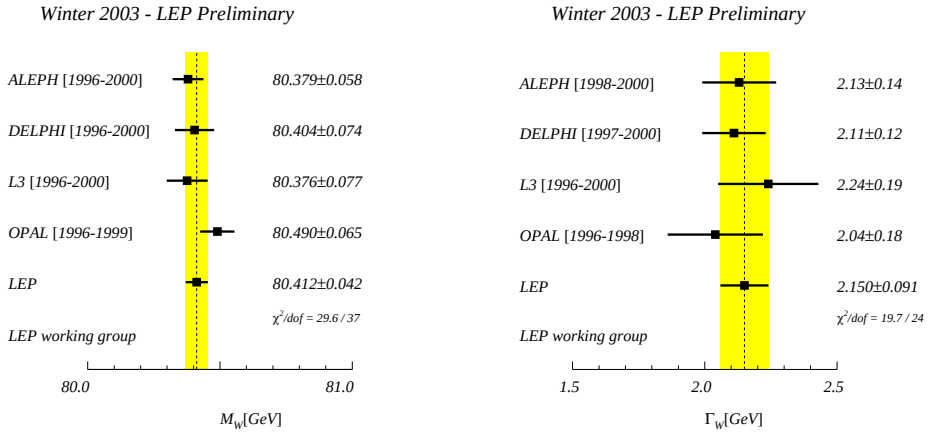

Fig. 63. The combined preliminary results for the measurements of the W mass and W width obtained by the four LEP collaborations.[91] The combined values take into account correlations between experiments and years of running, and hence, in general, do not give the same central value as a simple average. In the LEP combination of the $W^+W^- \to q\bar{q}q\bar{q}$ results, common values of errors are used for the color reconnection and Bose-Einstein correlation. The individual and combined M_W values include the results from the measurements of the W^+W^- cross sections at threshold.

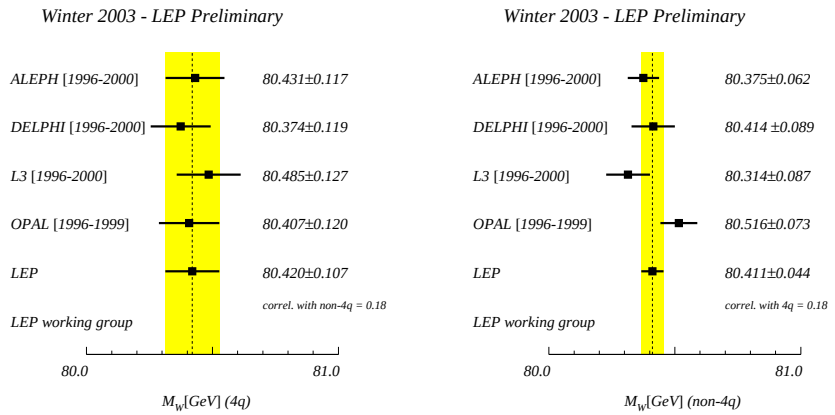

Fig. 64. Preliminary measurements of W-mass in semileptonic and hadronic channels obtained by the four LEP collaborations.[91] The combined values take into account correlations between experiments, years of running, and correlations between the two channels. In the LEP combination of the $W^+W^-\to q\overline{q}q\overline{q}$ results, common values of errors are used for color reconnection and Bose-Einstein correlation. The ALEPH and L3 $W^+W^-\to q\overline{q}\ell\overline{\nu}_\ell$ and $W^+W^-\to q\overline{q}q\overline{q}$ results are correlated since they are obtained from a fit to both channels that take account of inter-channel correlations.

As a cross check, the difference in the W mass determined from hadronic and semileptonic W-pair decays is:[62,91]

$$\Delta M_{\rm W}(q\overline{q}q\overline{q} - q\overline{q}\ell\overline{\nu}_\ell) = +22 \pm 43 \text{ MeV}.$$

A significant value for $\Delta M_{\rm W}$ could indicate that final-state interaction effects are biasing the measurement of $M_{\rm W}$ determined from $W^+W^-\to q\overline{q}q\overline{q}$ events. Since $\Delta M_{\rm W}$ is primarily of interest as a check on the possible effects of final-state interactions, the errors from color reconnection and Bose-Einstein correlation are ignored in this determination.

8.2. *Implications for the Standard Model*

The properties of the Z^0 boson measured at LEP-I and SLD can be used to predict the W mass. Figure 65 compares the direct measurements from LEP-II and the TeVatron [94] with indirect predictions from the ratio of neutral-current to charged-current reactions in neutrino-nucleon scattering from NuTeV,[95] and with predictions from fits to precision electroweak data.[4] The direct measurements of $M_{\rm W}$ now have similar uncertainty as the predictions from fits to the Standard Model. Figure 66 compares the direct measurements of the mass of the top quark[93] and of the W boson with the prediction of the Standard Model, and with a fit to electroweak precision measurements. The gray bands show the dependence of the W mass on the top and Higgs masses in the Standard Model. (As a result of loop corrections in the W propagator, $M_{\rm W}$ depends quadratically on the top mass and

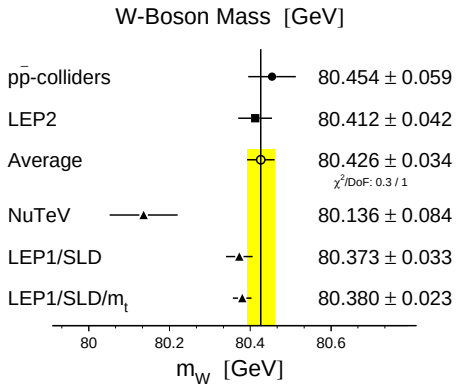

Fig. 65. Comparison of direct measurements of M_{W} at LEP-II and the TeVatron with indirect measurements.[91]

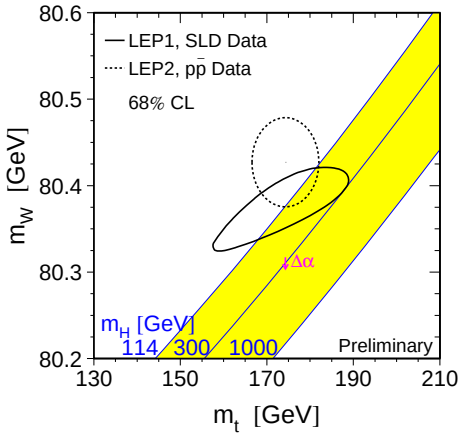

Fig. 66. Comparison of direct measurements of M_{W} and m_t with the results of a Standard Model fit to electroweak data.[91] The gray bands show the prediction for different Higgs masses.

logarithmically on the Higgs mass.) The dependence is shown for three values of Higgs mass, with the value of $m_H = 114$ GeV corresponding to the 95 % lower bound on m_H obtained from the direct search for the Higgs boson.[96] Similarly, the properties of the Z^0 boson depend on the Higgs and top-quark masses, and this can be used to determine the W and the top-quark mass without reference to the direct mass measurements. The fact that the two measurements agree within their uncertainties constitutes a particulary stringent test of the Standard Model at the level of quantum-loop corrections.

The impact of the mass and width of the W boson on the Higgs mass is illustrated in Fig. 67, where the LEP measurements are compared to the predictions of the Standard Model as a function of Higgs mass. The value of the W mass suggests a light Higgs, while the width is not sufficiently precise to influence fits to the Standard Model.

9. Summary and Outlook

9.1. *Summary*

From 1996 to 2000, the LEP accelerator operated at center-of-mass energies above the production threshold for W-boson pairs. One of the main goals was the precision determination of the W mass. The successful operation of the LEP accelerator and detectors, together with the great efforts to understand the source of systematic uncertainties in the measurement of the mass of the W boson, made it possible to reach this goal. The preliminary result from the combination of all LEP experiments

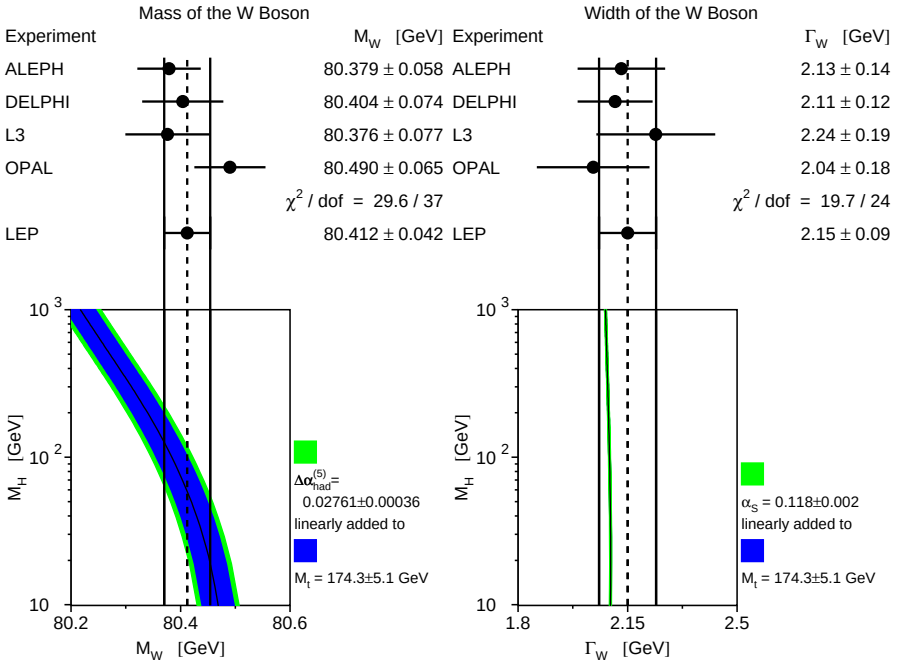

Fig. 67. Dependence of the W mass and width on Higgs mass.

and all channels is:[62,91]

$$M_{\mathrm{W}} = 80.412 \pm 0.029(\mathrm{stat.}) \pm 0.031(\mathrm{syst.})\mathrm{GeV}.$$

he precision of this measurement is comparable with the precision of its indirect prediction from electroweak fits to data measured at the Z^0 resonance by the experiments at LEP and SLD. The fact that the direct measurements of the W and top-quark masses agree with the Standard Model is an important test of electroweak theory at the level of quantum-loop corrections.

The kinematic reconstruction of four-fermion events in the region of phase space dominated by W-pair production provides the key ingredient to the precise determination of the mass of the W boson. The mass resolution is improved greatly by forcing energy and momentum conservation in the kinematic reconstruction of the final state. When both W bosons decay hadronically, the mass extraction can be improved by treating events with hard-gluon radiation as having five instead of four jets.

LEP experiments use different approaches for determining the W mass from the information content of each event. One approach is to fit the reconstructed mass spectrum with an analytic function, and then extract the W mass from the parameters of the fit, with any additional bias corrections estimated from Monte-Carlo simulations. In a second approach, the results from the kinematic fits for each event are compared to Monte-Carlo-generated reference distributions, which can be

recalculated for arbitrary W masses through a reweighting procedure. In a third approach, event likelihoods are determined from results of a kinematic fit through the convolution of a matrix element for the process with a resolution function, and the W mass is extracted from a maximum likelihood fit that is based on the mass-dependence of the event likelihoods.

To bring the systematic uncertainties of the mass measurements to levels comparable to the statistical errors, required consideration of many detailed issues, among which are that: The results of kinematic fits to final states have explicit dependence on center-of-mass energy, with the consequence that the uncertainty on beam energy contributes to the systematic error on the W-boson mass; the detector response to jets and leptons be studied using control samples of Z^0 events collected in parallel with the WW events, but at e^+e^- energies near the Z^0 resonance; the systematic uncertainties from fragmentation of partons into hadrons be estimated from comparisons of different Monte-Carlo models, and these models tuned to describe previous high-statistics Z^0 data. (One important aspect of the hadronization uncertainty is the sensitivity of the W mass to the fraction of baryons and kaons produced in parton fragmentation).

For events where both W bosons decay hadronically, the effects of interactions and interference between the two hadronic systems (Bose-Einstein correlations and color reconnection) are not as yet fully understood, but can affect significantly the systematic uncertainty on the W mass in these final states. As a consequence, these events contribute less than 10% to the final combination of mass results, despite the fact that their statistical precision is comparable to that of the semileptonic W-pair decays.

The measurement of the total and differential four-fermion cross sections clearly demonstrates the presence of the WWZ and $WW\gamma$ gauge-boson couplings. From the agreement of these measurements with the Standard Model, it is possible to set limits on various anomalous contributions to the couplings, which are in general in the range of a few percent. Neutral gauge-boson couplings are studied using final states dominated by Z^0 pair production (at center-of-mass energies above the threshold for Z^0 pairs). Final states involving photons are used to study quartic gauge boson couplings.

9.2. *Outlook*

In the future, both hadron-collider experiments, and any next generation linear electron-positron collider, will be able to contribute to the improvement of the precision on the W mass.

It is not possible, for various reasons, to fully reconstruct W events in hadronic collisions, but primarily this is because the interactions are between quarks and gluons contained within the colliding hadrons. Consequently, neither the center-of-mass energy nor the momentum parallel to the beam direction of the hard interaction are known a priori. Also, future hadron colliders will be operated at luminosities

at which many overlapping and unrelated primary interactions will be recorded at the same time. In addition, the reconstruction of hadronic W-boson decays is exceptionally challenging because of the presence of huge background from strong-interaction processes at hadron colliders. The W mass at hadron colliders must therefore be determined from the momenta of charged leptons in leptonic W decays and from the imbalance in momentum in the plane perpendicular to the beam (missing transverse momentum).

The current value of the mass of the W boson from the TeVatron proton-antiproton collider is $M_{\mathrm{W}} = 80.456 \pm 0.059$ GeV, and is limited both by the statistical and systematic uncertainties in the determination of the lepton energy and the missing transverse momentum.[94] Both the lepton energy and the missing transverse momentum can be calibrated using leptonic Z^0 decays. The uncertainty of these calibrations is currently dominated by the statistics of Z^0 events.

After a major upgrade of the TeVatron accelerator and detectors, a new data-taking period started in Spring 2001. The integrated luminosity is expected to increase by a factor of ≈ 100 in the next ≈ 6 years. This increase will reduce both the statistical and the systematic uncertainty currently limited by the statistical uncertainty of the calibration samples. Uncertainties from parton density functions (PDF), higher-order QCD corrections, and non-uniformities of the electromagnetic calorimeter, however, will not scale with integrated luminosity. The total uncertainty expected to be achieved on the W mass is ≈ 30 MeV.[97]

The proton-proton collider LHC is expected to start taking data in ≈ 2007. At the LHC, the rates for W and Z^0 bosons will be so high that the statistical uncertainties of the measurement (or from the calibration samples) will be negligible. Even with these large samples of Z^0 bosons, the dominant errors on the measurement of the W mass will be from the energy and momentum of electrons and muons. It will be quite challenging to calibrate the detectors to the level needed to reach a total error of 20 MeV.[98]

At any future linear electron-positron collider, the highest precision for the W-boson mass should be reached by a scan of the W-pair production cross section near threshold.[99] With an integrated luminosity of 100 fb^{-1}, the W mass can be determined with an experimental precision of ≈ 6 MeV, assuming the same efficiency and purity reached at LEP, and assuming a total error of 0.25% on the luminosity. A full four-fermion calculation of the cross section as a function of the W mass (with radiative corrections) will be required to reach this ultimate level of accuracy.

10. Acknowledgments

This kind of review is clearly not possible to undertake without the support of many colleagues. I am grateful to the members of the LEP W Working Group and the members of the four LEP collaborations working on W physics for their inputs. I would like to thank Tim Christiansen, Jörg Dubbert, Günter Duckeck and Tom

Ferbel for helpful discussion and advice in preparing this document. I also want to express my gratitude to Dorothee Schaile for leading our group at LMU in a way that created an atmosphere that stimulated creative contributions and a free exchange of ideas, and I thank her for encouragement and for her support of my scientific and academic development, which made my work in the field of W physics at LEP and this review possible.

References

1. S.L. Glashow, Nucl. Phys. **B22** (1961) 579;
   A. Salam and J.C. Ward, Phys. Rev. Lett. **13** (1994) 168;
   S. Weinberg, Phys. Rev. Lett. **19** (1967) 1264.
2. G. Arnison *et al.*, UA1 Collaboration, Phys. Lett. **B122** (1983) 103; Phys. Lett. **B126** (1983) 398;
   M. Banner *et al.*, UA2 Collaboration, Phys. Lett. **B122** (1983) 476; Phys. Lett. **B129** (1983) 130.
3. W. Beenakker *et al.*, *"WW Cross-Sections and Distributions"*, in "Physics at LEP-II", eds. G. Altarelli *et al.*, CERN 96-01,79.
4. The LEP Collaborations ALEPH, DELPHI, L3, OPAL, the Electroweak Working Group and the SLD Heavy Flavor Group. *"A Combination of Preliminary Electroweak Measurements and Constraints on the Standard Model."* LEPEWWG/2002-1, 8.5.2002.
5. S. Meyers, *"The LEP Collider"*, CERN 91-08 (1991).
6. D. Decamp *et al.*, ALEPH Collaboration, Nucl. Instr. and Meth. **A360** (1995) 481.
7. P. Aarnio *et al.*, DELPHI Collaboration, Nucl. Instr. and Meth. **A303** (1991) 233.
8. B. Adeva *et al.*, Nucl. Instr. and Meth. **A289** (1990) 35.
9. H. Ahmet *et al.*, OPAL Collaboration, Nucl. Instr. and Meth. **A305** (1991) 275.
10. Program KORALW V1.33, M. Skrzypek *et al.*, Comp. Phys. Comm. **94** (1996) 216; M. Skrzypek *et al.*, Phys. Lett. **B372** (1996) 289.
11. Program GRC4F V2.0 and V2.2, J. Fujimoto *et al.*, Comp. Phys. Comm. **100** (1997) 128.
12. Program EXCALIBUR, F.A. Berends, R. Pittau and R. Kleiss, Comp. Phys. Comm. **85** (1995) 437.
13. S. Jadach,W. Placek, M. Skrzypek, B.F.L. Ward, Phys. Rev. **D54** (1996) 5434.
    S. Jadach,W. Placek, M. Skrzypek, B.F.L. Ward, Z. Wąs, Phys. Lett. **B417** (1998) 326; Phys. Rev. **D61** (2000) 113010; Comp. Phys. Comm. **140** (2001) 432.
14. A. Denner, S. Dittmaier, M. Roth and D. Wackeroth, Nucl. Phys. **B560** (1999) 33; Nucl. Phys. **B587** (2000) 67; Phys. Rev. **B475** (2000) 127.
15. R. G. Stuart, Nucl. Phys. **B498** (1997) 28.
16. T. Sjöstrand, Comp. Phys. Comm. **82** (1994) 74.
17. Program HERWIG, G. Marchesini *et al.*, Comp. Phys. Comm. **67** (1992) 465.
18. L. Lönnblad, Comp. Phys. Comm. **71** (1992) 15.
19. R. Brun, GEANT 3 Users Guide. VERN/DD/EE 84-1, CERN, 1984.
20. JADE Collaboration, S. Bethke *et al.*, Phys. Lett. **B213** (1988) 235.
21. S. Catani *et al.*, Phys. Lett. **B269** (1991) 432.
22. The LEP Collaborations ALEPH, DELPHI, L3, OPAL, the Electroweak Working Group. *"LEP W-pair Z-pair and Single* W *Cross Section Results for the Summer 2001 Conferences"*, LEPEWWG/XSEC/2001-3, 14.8.20001.
23. M. W. Grünewald, G. Passarino *et al.*, *"Four Fermion Production in Electron Positron Collisions"*, in *"Reports of the Working Groups on Precision Calculations for LEP2 Physics"*, CERN 2000-009, hep-ph-0005309.
24. S. Jadach,W. Placek, B.F.L. Ward, Phys. Rev. **D56** (1997) 6939.
25. G. Passarino in [23].
26. L3 Collaboration, *"Preliminary Results on the Measurements of W-Pair Cross Sections in e+e- Interactions at sqrt(s)=205-208* GeV *and W-Decay Branching Fractions"*, L3 Note 2638.
27. Z. Kunszt *et al.*, *"QCD"*, in *"Physics at LEP-I"*, eds. G. Altarelli *et al.*, CERN 89-08 Vol.1 373.

28. S. Catani and M.H. Seymour, Phys. Lett. **B378** (1996) 287.
29. G. Abbiendi *et al.*, OPAL Collaboration, *"W^+W^- Production Cross Section and* W *Branching Fractions in e^+e^- Collisions at 189* GeV*"*, Phys. Lett. **B493** (2000) 249.
30. Particle Data Group, D.E. Groom *et al.*, Eur. Phys. J. **C15** (2000) 1.
31. The LEP Collaborations ALEPH, DELPHI, L3, OPAL and the LEP TGC Working Group. *"A Combination of Preliminary Results on Triple Gauge Boson Couplings Measured by the LEP Experiments"*, LEPEWWG/TGC/2002-1, 19.5.2002.
32. G. Gounaris *et al.*, *"Triple Gauge Boson Couplings"*, in *"Physics at LEP-II"*, eds. G. Altarelli *et al.*, CERN 96-01 Vol.1 525.
33. H. Aronson, Phys. Rev. **186** (1969) 1434.
34. G. Abbiendi *et al.*,OPAL Collaboration, Eur. Phys. J. **C19** (2001) 1.
35. A. De Rujula, M.B. Gavela, P Hernandez and E. Masso, Nucl. Phys. **B384** (1992) 3. K. Hagiwara, S. Ishihara, R. Szalapski and D. Zeppenfeld, Phys. Lett. **B283** (1992) 354; Phys. Rev. **D48** (1993) 2182.
36. K. Abe *et al.*, SLD Collaboration, Phys. Rev. Lett. **84** (2000) 5945.
37. M. Diehl and O. Nachtmann, Zeit. Phys. **C62** (1994) 397.
38. G.K. Fanourakis, D. Fassouliotis and S.E. Tzamarias, Nucl. Instr. and Meth. **A412** (1998) 465; Nucl. Instr. and Meth. **A414** (1998) 399.
39. ALEPH Collaboration, *"Measurement of Triple Gauge-Boson Couplings at LEP energies up to 208* GeV*"*, ALEPH 2001-027 CONF 2001-021.
40. A. Heister *et al.*, ALEPH Collaboration, Eur. Phys. J. **C3** (2001) 423.
41. P. Abreu *et al.*, DELPHI Collaboration, Phys. Lett. **B502** (2001) 9.
42. M. Acciarri *et al.*, L3 Collaboration, Phys. Lett. **B467** (1999) 171.
43. L3 Collaboration, *"Measurement of TGCs"*, L3 Note 2732.
44. W. Beenakker *et al.*, Nucl. Phys. **B304** (1988) 463;
    J. Fleicher, F. Jegerlehner, M. Zralek, Zeit. Phys. **C42** (1989) 409;
    J. Fleicher *et al.*, Nucl. Phys. **B378** (1992) 443;
    E. Argyres *et al.*, Nucl. Phys. **B391** (1993) 23;
    J. Papavassiliou, K. Philippides, Phys. Rev. **D48** (1993) 4255.
45. A. Arhrib, J.-L. Kneur and G. Moultaka, CERN-TH/95-344 (hep-hp/9512437).
46. P. Molnár, M. Grünewald, Phys. Lett. **B461** (1999) 149.
47. F.M. Renard, Nucl. Phys. **B196** (1982) 93;
    K. Hagiwara, R.D. Peccie, D. Zeppenfeld and K. Hikasa, Nucl. Phys. **B282** (1987) 253;
    K. Hagiwara, A. Baroso, F. Bodjemena, J. Cole and N. Dombey, Zeit. Phys. **C28** (1985) 149.
48. E. Boos, H.J. He, W. Kilian, A. Pukhov, C.P. Yuan and P.M. Zerwas, *"Strongly Interacting Vector Bosons at TeV e^+e^- Linear Colliders"*, DESY-96-256, hep-ph/9708310.
49. A.S. Belyaev, O.J.P. Eboli, M.C. Gonzales-Garcia, J.K. Mizukoshi, S.F. Novaes and I. Zacharov, Phys. Rev. **D59** (1999) 015022.
50. G. Abbiendi *et al.*, OPAL Collaboration, Phys. Lett. **B471** (1999) 293.
51. M.Acciarri *et al.*, L3 Collaboration, Phys. Lett. **B478** (2000) 39, Phys. Lett. **B490** (2000) 187.
    P. Achard *et al.*,L3 Collaboration, Phys. Lett. **B527** (2002) 29, Phys. Lett. **B540** (2002) 43.
52. O.J.P. Eboli, M.C. Gonzales-Garcia and S.F. Novaes, Nucl. Phys. **B411** (1994) 381. A. Brunnstein, O.J.P. Eboli and M.C. Gonzales-Garcia, Phys. Lett. **B375** (1996) 233.
53. J.P. Berge, F.T. Solmitz and H.D.Taft, Review of Scientific Instruments **A32** (1961) 538.
54. G. Abbiendi *et al.*, OPAL Collaboration, Phys. Lett. **B507** (2001) 29.

55. OPAL Collaboration, *"Measurement of the Mass of the W Boson in e^+e^- annihilations at 192-202* GeV*"*, OPAL Physics Note PN422.
56. M. Acciarri *et al.*, L3 Collaboration, Phys. Lett. **B454** (1999) 386.
57. P. Abreu *et al.*, DELPHI Collaboration, Phys. Lett. **B462** (1999) 410.
58. P. Abreu *et al.*, DELPHI Collaboration, Phys. Lett. **B511** (2001) 159.
59. R.Barate *et al.*, ALEPH collaboration, Eur. Phys. J. **C17** (2000) 241.
60. T. Christiansen, *"Influence of 5-Jet Events on the Measurement of the Mass of the W Boson in e^+e^- Collisions"*, Diploma thesis, LMU München, September 2000.
61. J. Dubbert, *"Measurement of the* W *Boson Mass in the* $W^+W^- \to q\bar{q}l\bar{\nu}$ *Channel with the OPAL Detector at LEP"*, PhD thesis, LMU München, November 2000.
62. The LEP Collaborations ALEPH, DELPHI, L3, OPAL and the LEP W Working Group. *"Combined Preliminary Results on the Mass and Width of the* W *Boson Measured by the LEP Experiments"*, LEPEWWG.MASS/2002-02.
63. P. Acton *et al.*, OPAL Collaboration, Zeit. Phys. **C58** (1993) 387.
64. G. Alexander *et al.*, OPAL Collaboration, Zeit. Phys. **C69** (1996) 543.
65. N. Kjaer and M. Mulders, DELPHI 2000-51 CONF 366.
66. B. Efron, *"Computers and the Theory Statistics"*, SIAM Rev. 31(1979) 460.
67. LEP Energy Working Group, *"Evaluation of the LEP Center-of-Mass Energy for Data taken in 2000"*, LEP Energy Working Group 01/01,12 March 2001
LEP Energy Working Group, A. Blondel *et al.*, Eur. Phys. J. **C11** (1999) 573.
68. R. Assmann *et al.*, LEP Energy Working Group, Eur. Phys. J. **C6** (1999) 187.
69. E. Barbero, B. Dehning, J. Prochnow, J. Bergoz, K. Unser, J. Matheson and E. Torrence, *"Accuracy of the LEP Spectrometer Beam Orbit Monitors"*, CERN-SL-2001-022-BI, *Prepared for 5th European Workshop on Diagnostics and Beam Instrumentation, Grenoble, France, 13-15 May 2001.*
70. OPAL Collaboration, *"Determination of the LEP Beam Energy using Radiative Fermion-Pair Events"*, OPAL Physics Note PN493 and PN476.
71. L3 Collaboration, *"Measurement of the Z Boson Mass using Z Decays in $e^+e^- \to Z\gamma$ events at LEP-2 Energies"*, L3 Note 2733.
72. T. Sjöstrand and V.A. Khoze, Zeit. Phys. **C62** (1994) 281; Phys. Rev. Lett. **72** (1994) 28.
73. G. Corcella *et al.*, J. High Energy Phys. JHEP 1(2001)010.
74. L. Löndbad, Zeit. Phys. **C70** (1996) 107.
75. G. Gustafson, J. Häkkinen, Zeit. Phys. **C64** (1994) 659.
76. L3 Collaboration,*"Search for Color Reconnection Effects in $e^+e^- \to WW \to$ Hadrons through Particle-Flow Studies at $\sqrt{s}$=189-208* GeV *"* , L3 Note 2683.
77. OPAL Collaboration, *"Color Reconnection Studies in $e^+e^- \to W^+W^-$ at $\sqrt{s} = 189$* GeV *using Inter-Jet Multiplicity"*, OPAL Physics Note PN448.
OPAL Collaboration, *"Color Reconnection Studies in $e^+e^- \to W^+W^-$ at $\sqrt{s}$ =189-208* GeV *using Particle Flow"*, OPAL Physics Note PN506.
O. Sahr, *"Color Reconnection in hadronischen W-Paar Zerfällen"*, PhD thesis, LMU München, January 2001.
78. G. Goldhaber *et al.*, Phys. Rev. Lett. **3** (1959) 181; Phys. Rev. **120** (1960) 300.
79. G. Abbiendi *et al.*, OPAL Collaboration, Eur. Phys. J. **C16** (2000) 423.
80. B. Pietrzyk *et al.*, ALEPH Collaboration, Phys. Lett. **B478** (2000) 50.
81. Š. Todorova-Nová and J. Rameš, hep-ph/9710280.
82. V. Kartvelishvili, R. Kvatadze, Phys. Lett. **B514** (2001) 7.
V. Kartvelishvili, R. Kvatadze, R. Moller, Phys. Lett. **B408** (1997) 331.
83. Bo Anderson *et al.*, Phys. Lett. **B169** (1986) 364.
84. L. Lönnblad and T. Sjöstrand, Eur. Phys. J. **C2** (1998) 165.

85. L3 Collaboration, *"Bose-Einstein Correlations in* $e^+e^- \rightarrow W^+W^-$ *Events at* $\sqrt{s}$*=189-208* GeV*"*, L3 Note 2674.
86. R. Barate *et al.*, ALEPH Collaboration, Phys. Lett. **B453** (1999) 121.
R. Barate *et al.*, ALEPH Collaboration, Eur. Phys. J. **C17** (2000) 241.
ALEPH Collaboration, *"Measurement of the* W *Mass and Width in* e^+e^- *Collisions at* $\sqrt{s} \sim 192 - 208$ GeV*"*, ALEPH note 2001-020 CONF 2001-017.
87. P. Abreu *et al.*, DELPHI Collaboration,Eur. Phys. J. **C2** (1998) 581.
P. Abreu *et al.*, DELPHI Collaboration,Phys. Lett. **B462** (1999) 410.
P. Abreu *et al.*, DELPHI Collaboration,Phys. Lett. **B511** (2001) 159.
DELPHI Collaboration, *Measurement of the Mass and Width of the* W *Boson in* e^+e^- *Collisions at* $\sqrt{s} = 192 - 209$ GeV, DELPHI 2001-103 CONF 531.
88. M. Acciarri, *et al.*, L3 Collaboration, Phys. Lett. **B407** (1997) 419.
M. Acciarri, *et al.*, L3 Collaboration, Phys. Lett. **B454** (1999) 386.
L3 Collaboration, *"Preliminary Results on the Measurement of Mass and Width of the* W *Boson at LEP"*, L3 Note 2377.
L3 Collaboration, *"Preliminary Results on the Measurement of Mass and Width of the* W *Boson at LEP"*, L3 Note 2575.
L3 Collaboration, *"Preliminary Results on the Measurement of Mass and Width of the* W *Boson at LEP"*, L3 Note 2637.
89. K. Ackerstaff *et al.*, OPAL Collaboration, Eur. Phys. J. **C1** (1998) 395.
G. Abbiendi *et al.*, OPAL Collaboration, Phys. Lett. **B453** (1999) 138.
G. Abbiendi *et al.*, OPAL Collaboration, Phys. Lett. **B507** (2001) 29.
OPAL Collaboration, *"Measurement of the Mass of the* W *Boson in* e^+e^- *annihilations at 192-202 GeV"*, OPAL Physics Note PN422.
OPAL Collaboration, *"Determination of the* W *Mass in the Fully Leptonic Channel using an unbinned Maximum Likelihood Fit"*, OPAL Physics Note PN480.
90. G. Abbiendi *et al.*, OPAL Collaboration, CERN-EP-2002-022, Submitted to Eur. Phys. J.
P. Méndez-Lorenzo, *"Measurement of the* W *Boson Mass in the* $e^+e^- \rightarrow W^+W^- \rightarrow \ell\nu_\ell\ell\overline{\nu}_\ell$ *Channel with the OPAL Detector at LEP"*, PhD thesis, LMU München, May 2001.
91. A. Venturi, *"*W *Mass and EWK Fits at LEP"*, Presented at 17th rencontres de physique de la Vallee d'Aoste (La Thuile) 9-15th March 2003
92. R. Barate *et al.*,ALEPH Collaboration, Phys. Lett. **B401** (1997) 347.
K. Ackerstaff *et al.*, OPAL Collaboration, Phys. Lett. **B389** (1996) 416.
P. Abreu *et al.*, DELPHI Collaboration, Phys. Lett. **B397** (1997) 158.
M. Acciarri, *et al.*, L3 Collaboration, Phys. Lett. **B398** (1997) 223.
93. L. Demortier, R. Hall, R. Hughes, B. Klima, R. Roser and M. Strovink, The Top Averaging Group Collaboration, *"Combining the top quark mass results for Run 1 from CDF and DØ"*, FERMILAB-TM-2084.
94. Tevatron Electroweak Working Group and the CDF and DØ Collaborations, *"Combination of CDF and DØ Results on* W *Boson Mass and Width"*, FERMILAB-FN-716.
95. G. P. Zeller *et al.*, NuTeV Collaboration, Phys. Rev. Lett. **88** (2002) 091802.
96. The LEP Collaborations ALEPH, DELPHI, L3, OPAL and the LEP Working Group for Higgs Boson Searches. *"Search for the Standard Model Higgs Bo."* LEPEWWG/2002-1, 8.5.2002.
97. *"Future Electro Weak Physics at the Fermilab Tevatron: Report of the TeV-2000 Study Group"*, ed. D. Amidei and R. Brock, FERMILAB-PUB-96-082.
98. ATLAS Collaborations, *"Atlas Detector and Physics Performance Technical Design Report"*, CERN/LHCC 99-14

99. G. Wilson, *"Precision Measurement of the* W *Mass with a Polarized Threshold Scan at a Linear Collider,"* LC-PHSM-2001-009.